NASA TECHNICAL MEMORANDUM

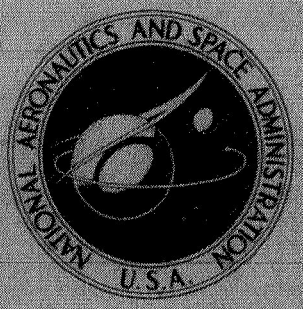

NASA TM X-1995

NASA TM X-1995

TRANSONIC AERODYNAMIC CHARACTERISTICS OF A MEDIUM HYPERSONIC L/D REENTRY SPACECRAFT WITH A VARIABLE GEOMETRY WING

by John P. Decker

Langley Research Center
Langley Station, Hampton, Va.

NATIONAL AERONAUTICS AND SPACE ADMINISTRATION • WASHINGTON, D. C. • APRIL 1970

1. Report No. NASA TM X-1995	2. Government Accession No.	3. Recipient's Catalog No.
4. Title and Subtitle TRANSONIC AERODYNAMIC CHARACTERISTICS OF A MEDIUM HYPERSONIC L/D REENTRY SPACECRAFT WITH A VARIABLE GEOMETRY WING		5. Report Date April 1970 6. Performing Organization Code
7. Author(s) John P. Decker		8. Performing Organization Report No. L-6939 10. Work Unit No. 124-64-01-03-23
9. Performing Organization Name and Address NASA Langley Research Center Hampton, Va. 23365		11. Contract or Grant No. 13. Type of Report and Period Covered Technical Memorandum
12. Sponsoring Agency Name and Address National Aeronautics and Space Administration Washington, D.C. 20546		14. Sponsoring Agency Code
15. Supplementary Notes		

16. Abstract

A wind-tunnel investigation was conducted at Mach numbers from 0.40 to 1.20 to determine the basic longitudinal and lateral-directional aerodynamic characteristics of a variable geometry spacecraft having a hypersonic lift-drag ratio near 2. The configuration represents one approach to improve the subsonic lift-drag ratio of a lifting body by the incorporation of severe afterbody boattailing to decrease the base drag and by the addition of an internally stowed variable-sweep rigid wing. The model was tested with the wings deployed to 20^0, 65^0, 75^0, and 90^0 (stowed) at angles of attack from about -6^0 to 16^0 and at angles of sideslip of 0^0 and 5^0.

17. Key Words Suggested by Author(s) Variable geometry spacecraft Lifting bodies	18. Distribution Statement Unclassified – Unlimited		
19. Security Classif. (of this report) Unclassified	20. Security Classif. (of this page) Unclassified	21. No. of Pages 87	22. Price* $3.00

*For sale by the Clearinghouse for Federal Scientific and Technical Information
Springfield, Virginia 22151

TRANSONIC AERODYNAMIC CHARACTERISTICS OF A MEDIUM HYPERSONIC L/D REENTRY SPACECRAFT WITH A VARIABLE GEOMETRY WING

By John P. Decker
Langley Research Center

SUMMARY

A wind-tunnel investigation was conducted at Mach numbers from 0.40 to 1.20 to determine the basic longitudinal and lateral-directional aerodynamic characteristics of a variable geometry spacecraft having a hypersonic lift-drag ratio near 2. The configuration investigated represents one approach to improve the subsonic lift-drag ratio of a lifting body by incorporation of severe afterbody boattailing to decrease base drag and by the addition of an internally stowed variable-sweep rigid wing.

The results of the investigation indicated that deploying the wings to 20°, 65°, or 75° increased the static longitudinal stability of the basic spacecraft at test Mach numbers from 0.40 to 1.20. The model with the wings stowed or deployed required a large negative deflection of the elevons to trim at any reasonable lift coefficient as a result of a negative pitching moment at zero lift that caused a substantial loss in maximum lift-drag ratio. The model with the wings deployed to 20° had pitch-up near the lift coefficient for maximum lift-drag ratio at Mach numbers of 0.40 and 0.60.

The model with the wings deployed to 20° had positive effective dihedral throughout the angle-of-attack range at Mach numbers of 0.40 and 0.60 whereas sweeping the wings to 75° provided the model with positive effective dihedral at Mach numbers above 0.60. The static directional stability of the model with the wings deployed to 20° or 75° was deficient over large sections of the angle-of-attack range at all test Mach numbers.

INTRODUCTION

The National Aeronautics and Space Administration is presently conducting investigations on several types of variable geometry spacecraft having hypersonic lift-drag capability from 1 to about 3. One such vehicle having a hypersonic lift-drag ratio near 2 has been investigated in the Langley 8-foot transonic pressure tunnel to determine basic longitudinal and lateral-directional aerodynamic characteristics at transonic speeds.

The configuration investigated represents one approach to improving the subsonic lift-drag ratio of a lifting body by incorporation of severe afterbody boattailing to decrease the base drag and by the addition of an internally stowed variable-sweep rigid wing. Aerodynamic control surfaces, located at the trailing edge on the top and bottom surface of the body, may function in unison at subsonic speeds to minimize base drag, or independently at higher speeds under conditions where base drag is of less significance. The wing, of rectangular planform and stowed inside of the spacecraft just above the lower surface heat shield, was sized to maximize the useful wing area in subsonic flight. At subsonic speeds the wing would be deployed to a low sweep position, whereas at transonic speeds the wing could be deployed in a high sweep position to improve the static longitudinal stability if necessary. This present configuration design philosophy was derived primarily from the baseline vehicle described in reference 1.

The spacecraft was tested with the wings deployed to 20°, 65°, 75°, and 90° (stowed) at Mach numbers from 0.40 to 1.20, at angles of attack from about -6° to 16°, and at angles of sideslip of 0° and 5°.

SYMBOLS

The aerodynamic coefficients presented herein are referred to the body axes system with the exception of the lift and drag coefficients which are referred to the stability axes system. The moment reference center was located at 50 percent of the body length along the model reference line. (See fig. 1.) All coefficients are based on the planform area, length, and span of the body alone.

b body span, 16.683 cm (6.568 in.)

C_D drag coefficient, $\frac{\text{Drag}}{qS}$

C_L lift coefficient, $\frac{\text{Lift}}{qS}$

C_l rolling-moment coefficient, $\frac{\text{Rolling moment}}{qSb}$

C_{l_β} effective dihedral parameter, $\frac{\Delta C_l}{\Delta \beta}$, per deg

C_m pitching-moment coefficient, $\frac{\text{Pitching moment}}{qS\ell}$

$C_{m,o}$ pitching-moment coefficient at $C_L = 0^o$

C_n yawing-moment coefficient, $\frac{\text{Yawing moment}}{qSb}$

C_{n_β} yawing-moment parameter, $\frac{\Delta C_n}{\Delta \beta}$, per deg

C_Y side-force coefficient, $\frac{\text{Side force}}{qS}$

C_{Y_β} side-force parameter, $\frac{\Delta C_Y}{\Delta \beta}$, per deg

L/D lift-drag ratio

$(L/D)_{max}$ maximum lift-drag ratio

l body length, 0.6568 m (2.155 ft)

M free-stream Mach number

q free-stream dynamic pressure

R Reynolds number based on body length

S body projected planform area, 0.08542 m^2 (0.91944 ft^2)

α angle of attack referenced to body axis (see fig. 1), deg

β angle of sideslip, deg

$\delta_{e,l}$ lower elevon deflection (fig. 1), positive for trailing edge down, deg

$\delta_{e,u}$ upper elevon deflection (fig. 1), positive for trailing edge down, deg.

Λ wing leading-edge sweep angle, deg

APPARATUS AND METHODS

Model

Details of the model are shown in figure 1 and geometry characteristics are shown in table I. The basic spacecraft had cross-sectional shape progressions as indicated in figure 1 and was provided with two outboard-mounted vertical tails which had a cant angle of 13° and a toe-in angle of 11.5°. The spacecraft had upper surface afterbody boattailing of about 12° and was provided with upper and lower elevons located at the trailing edge of the spacecraft.

The model was also provided with a deployable low wing which had a constant chord and an incidence angle of 5° when at a 0° sweep position. The airfoil was a modified NACA 64_3-618 section. The wing was tested at sweep angles of 20°, 65°, 75°, and 90° (stowed). Some photographs of the model are shown as figure 2.

Tests

The tests were conducted in the Langley 8-foot transonic pressure tunnel at Mach numbers from 0.40 to 1.20 at angles of attack from about -6° to 16°, and at angles of sideslip of 0° and 5°. The stagnation dewpoint temperature was maintained sufficiently low to avoid condensation effects at all test Mach numbers. The variation of the test Reynolds number, based on the body length, with Mach number is as shown in figure 3.

All tests of the model were performed with a 0.05-inch-wide (0.13-cm) band of No. 120 (0.0049 in. or 0.0124 cm) carborundum grit located 0.80 inch (2.03 cm) streamwise behind the nose and vertical tails and 0.60 inch (1.52 cm) streamwise behind the wing leading edge. A Reynolds number study was not conducted in the present investigation; however, a fluorescent-oil technique (ref. 2) was used to insure that grit size selected tripped the flow to turbulent conditions. For some of the runs, the entire lower surface of the body was covered with a uniform coating of No. 80 (0.0083 in. or 0.0211 cm) carborundum grit to obtain some information on the effects of ablation surface roughness.

Model Support, Measurements, and Corrections

The model was sting supported and the aerodynamic forces and moments were measured by an internally mounted six-component strain-gage balance. When the lower elevon was deflected to -15°, part of the sting forward of the base was exposed to the airstream. (See fig. 4(a).) To obtain some information on the potential sting interference effects when the lower elevon was in this position, a fairing over the exposed part of the sting, forward of the base, was attached to the lower elevon. (See fig. 4(b).)

Balance chamber and base pressures were measured by means of static orifices located in the balance chamber and at the base of the model. No base drag corrections were made to the data. No sting interference corrections were applied to the data. Angles of attack and sideslip were corrected for balance and sting deflection due to aerodynamic load. No corrections were made for tunnel flow misalinement; however, for lifting body models of this size, past experience has indicated that the tunnel flow misalinement is negligible.

PRESENTATION OF RESULTS

The results of this investigation were presented in the following figures:

DISCUSSION

The configuration of the present investigation represents one approach by means of significant afterbody boattailing and variable-sweep wings toward achievement of a high subsonic L/D. The present investigation was undertaken primarily to define the transonic aerodynamic characteristics; however, data were also obtained at subsonic speeds to identify some of the lower speed characteristics associated with the design approach.

Longitudinal Aerodynamic Characteristics

The data obtained for the lower elevon deflected -15° and with the lower elevon fairing on and off are presented in figure 5. (See fig. 4 for fairing details.) Also shown in this figure are data for a configuration with the lower elevon fairing on and with the upper elevon span extended to the side of the vertical tails, which increased the upper elevon area by 15 percent. The results shown in this figure indicate that there must be some sting interference when the lower elevon is deflected to -15°. The interference effects caused a displacement of the data curves and a resulting change in $C_{m,o}$ which would affect the trim characteristics of the configuration and consequently the trimmed $(L/D)_{max}$.

Figures 6 and 7 indicate that deploying the wings to 20°, 65°, or 75° increased the static longitudinal stability of the basic spacecraft at all Mach numbers. At Mach numbers at or below 0.60, untrimmed $(L/D)_{max}$ is substantially increased by deploying the wings to $\Lambda = 20^{\circ}$ whereas at Mach numbers above 0.60, the wings swept to 65° or 75° give the maximum untrimmed L/D. Figures 6 and 7 show that for all configurations with the wings deployed, the model displayed pitch-up or pitch-up tendencies at the higher lift coefficients at almost all Mach numbers.

The model with the wings deployed or stowed and with the elevons set at 0° has a large negative $C_{m,o}$. (See figs. 6 and 8.) Figure 8 includes data at other elevon settings with the wings deployed to $\Lambda = 20^{\circ}$ and indicates that a large negative deflection of both upper and lower elevons would be required to trim at moderate lift coefficients and would result in a substantial loss in $(L/D)_{max}$. The loss in $(L/D)_{max}$ is twofold. First, if the lower elevon is deflected to a large negative angle, flow separation would be expected to occur on the lower elevon surface thereby increasing the drag. Secondly, deflection of the upper elevon increases the base area and consequently the base drag. Hence, the loss in $(L/D)_{max}$ indicated in figure 8 due to deflection of the lower and upper elevons appears to be reasonable. However, a complete analysis of the drag increments due to elevon deflections would be required to determine the actual trimmed $(L/D)_{max}$. Such an analysis is beyond the scope of this paper. Figure 8 also indicates that for the model with the wings deployed to $\Lambda = 20^{\circ}$ and at Mach numbers at or below 0.60, the maximum

C_L measured did not exceed 0.60 and this value was for conditions considerably out of trim. Furthermore, pitch-up is indicated at lift coefficients near the lift coefficient for $(L/D)_{max}$.

Figure 10 presents the longitudinal results for a configuration in which an attempt has been made to quantify the effects of ablation roughness by applying a uniform distribution of carborundum over the entire lower surface of the body even though the method of scaling such roughness is not known. The data show that the distributed roughness produced only small changes in the longitudinal data.

Lateral-Directional Aerodynamic Characteristics

Figure 14 indicates that the model with the wings swept to $\Lambda = 20^{\circ}$ had negative effective dihedral $\left(+C_{l_\beta}\right)$ at Mach numbers of 0.80 and 0.90 and at angles of attack less than about 3°. At Mach numbers of 0.40 and 0.60, large changes in C_{l_β} are indicated at positive angles of attack because of flow separation on the wing. The static directional stability parameter C_{n_β} is shown to decrease with increasing angle of attack and C_{n_β} becomes negative at the larger angles of attack for all Mach numbers between 0.40 and 0.90.

Sweeping the wings to 75° provides the model with positive effective dihedral $\left(-C_{l_\beta}\right)$ throughout the angle-of-attack range and at Mach numbers between 0.60 to 1.20. (See fig. 15.) However, the static directional stability parameter becomes negative or zero over a large portion of the angle-of-attack range at Mach numbers from 0.90 to 1.20.

Results to quantify the effects of ablation surface roughness on the lateral-directional aerodynamic characteristics and parameters are presented in figures 13 and 16, respectively. The data of figure 13 indicate that there are indeed some differences in the aerodynamic coefficients with the model smooth or rough. However, except near the highest test angles of attack, all the trends of the data at either 0° or 5° sideslip are close. The differences in rolling-moment coefficient (fig. 13) and hence C_{l_β} (fig. 16) shown at the higher angles of attack are associated with the flow separation on the wings rather than changes in the flow on the body due to the presence of the roughness.

SUMMARY OF RESULTS

Wind-tunnel tests to determine the basic aerodynamic characteristics of a variable-geometry spacecraft at transonic speeds have indicated the following results:

1. Deploying the wings to 20°, 65°, or 75° increased the static longitudinal stability of the basic spacecraft at all test Mach numbers from 0.40 to 1.20.

2. The model with the wings stowed or deployed requires a large negative deflection of the elevons to trim at any reasonable lift coefficient as a result of a negative pitching moment at zero lift; as a result, there is a substantial loss in maximum lift-drag ratio.

3. The model with the wings deployed to 20° has pitch-up near the lift coefficient for maximum lift-drag ratio at Mach numbers of 0.40 and 0.60.

4. The model with the wings deployed to 20° had positive effective dihedral throughout the angle-of-attack range at Mach numbers of 0.40 and 0.60 whereas sweeping the wings to 75° provided the model with positive effective dihedral at Mach numbers above 0.60.

5. The static directional stability of the model with the wings deployed to 20° or 75° was deficient over large portions of the angle-of-attack range at all test Mach numbers.

6. Results to quantify the effects of ablation surface roughness on the longitudinal and lateral-directional aerodynamic characteristics by applying a uniform distribution of carborundum grit over the entire lower surface of the body showed that the distributed roughness produced only small changes in the aerodynamic data; however, the method of scaling such roughness is not known at this time.

Langley Research Center,
National Aeronautics and Space Administration,
Langley Station, Hampton, Va., January 30, 1970.

REFERENCES

1. Lynch, Robert A.: The First Manned Lifting Entry Vehicle Configuration. AIAA Pap. No. 66-959, Nov.-Dec. 1966.

2. Loving, Donald L.; and Katzoff, S.: The Fluorescent-Oil Film Method and Other Techniques for Boundary-Layer Flow Visualization. NASA MEMO 3-17-59L, 1959.

TABLE I.- GEOMETRIC CHARACTERISTICS OF MODEL

Body reference dimensions:		
Length, cm (in.)	65.684	(25.860)
Span, cm (in.)	16.683	(6.568)
Area, cm^2 (in^2)	854.185	(132.399)
Body:		
Length, cm (in.)	65.684	(25.860)
Plan area (without fins), cm^2 (in^2)	854.185	(132.399)
Width (without fins), cm (in.)	16.683	(6.568)
Outboard vertical fin:		
Airfoil	Slab	
Area (true, per fin), cm^2 (in^2)	69.742	(10.810)
Dihedral (angle with respect to vertical), deg	13.0	
Incidence (leading edge toed in), deg	11.5	
Leading-edge sweep (projected side view), deg	60.5	
Root chord (theoretical), cm (in.)	16.078	(6.330)
Tip chord (theoretical), cm (in.)	4.470	(1.760)
Span (root to tip chord), cm (in.)	9.652	(3.800)
Upper flap:		
Area (reference), cm^2 (in^2)	85.806	(13.300)
Chord (reference), cm (in.)	6.706	(2.640)
Span (reference), cm (in.)	12.802	(5.040)
Hinge-line sweep, deg	0	
Lower flap:		
Area (reference), cm^2 (in^2)	85.806	(13.300)
Chord (reference), cm (in.)	6.706	(2.640)
Span (reference), cm (in.)	12.802	(5.040)
Hinge-line sweep, deg	0	
Wing:		
Airfoil	Modified 64_3-618	
Planform shape	Rectangular	
Incidence angle ($\Lambda = 0^o$), deg	5	
Exposed area, cm^2 (in^2), at –		
$\Lambda = 20^o$	239.690	(37.152)
$\Lambda = 65^o$	173.264	(26.856)
$\Lambda = 75^o$	94.761	(14.688)
Elevon base areas, cm^2 (in^2), for –		
$\delta_{e,l} = 0^o$; $\delta_{e,u} = 0^o$	39.484	(6.120)
$\delta_{e,l} = -15^o$; $\delta_{e,u} = 0^o$	20.129	(3.120)
$\delta_{e,l} = -15^o$; $\delta_{e,u} = -10^o$	35.871	(5.560)
$\delta_{e,l} = -15^o$ (faired); $\delta_{e,u} = -25^o$	58.839	(9.120)

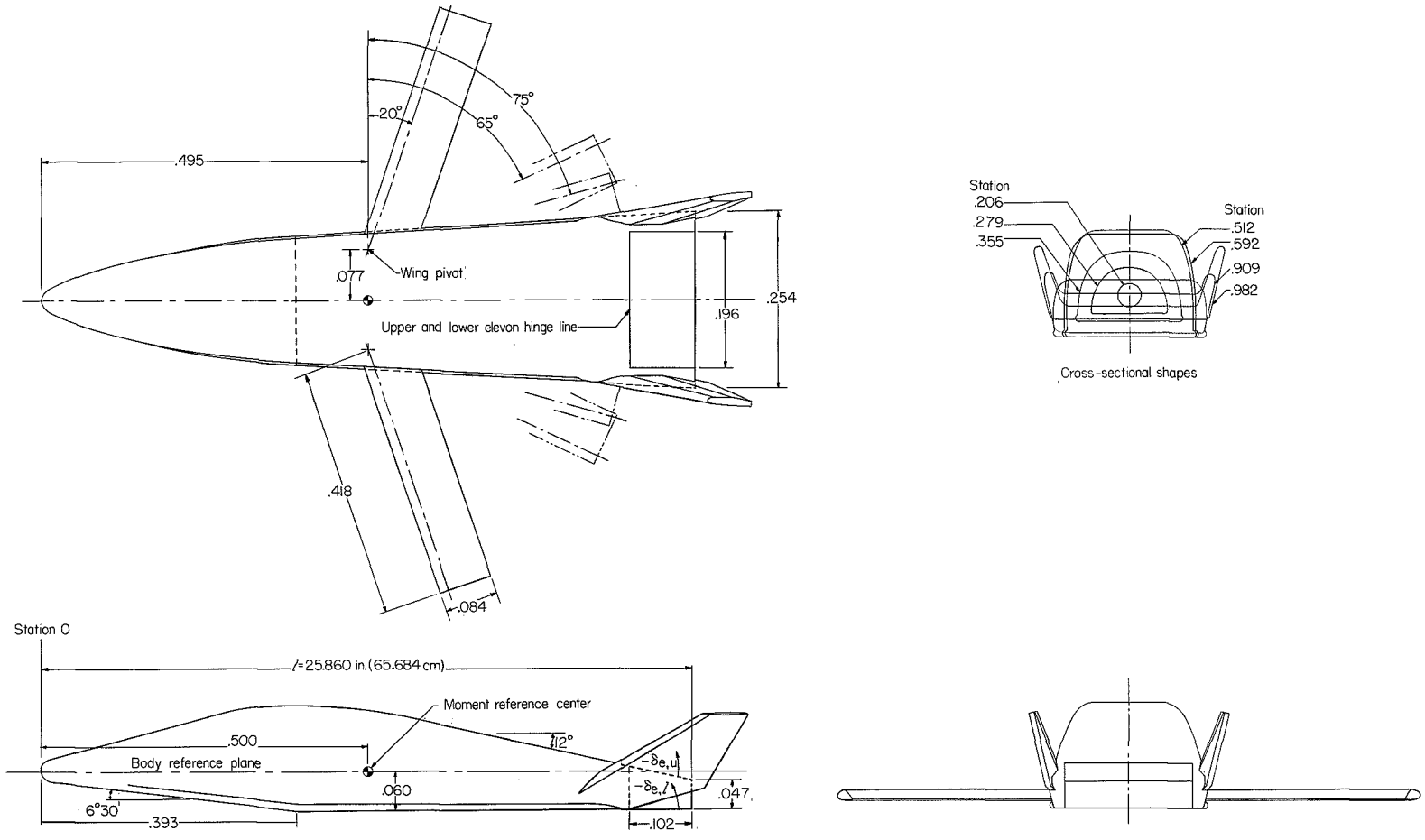

Figure 1.- Details of model. All linear dimensions are based on body length l = 25.86 in. (65.68 cm).

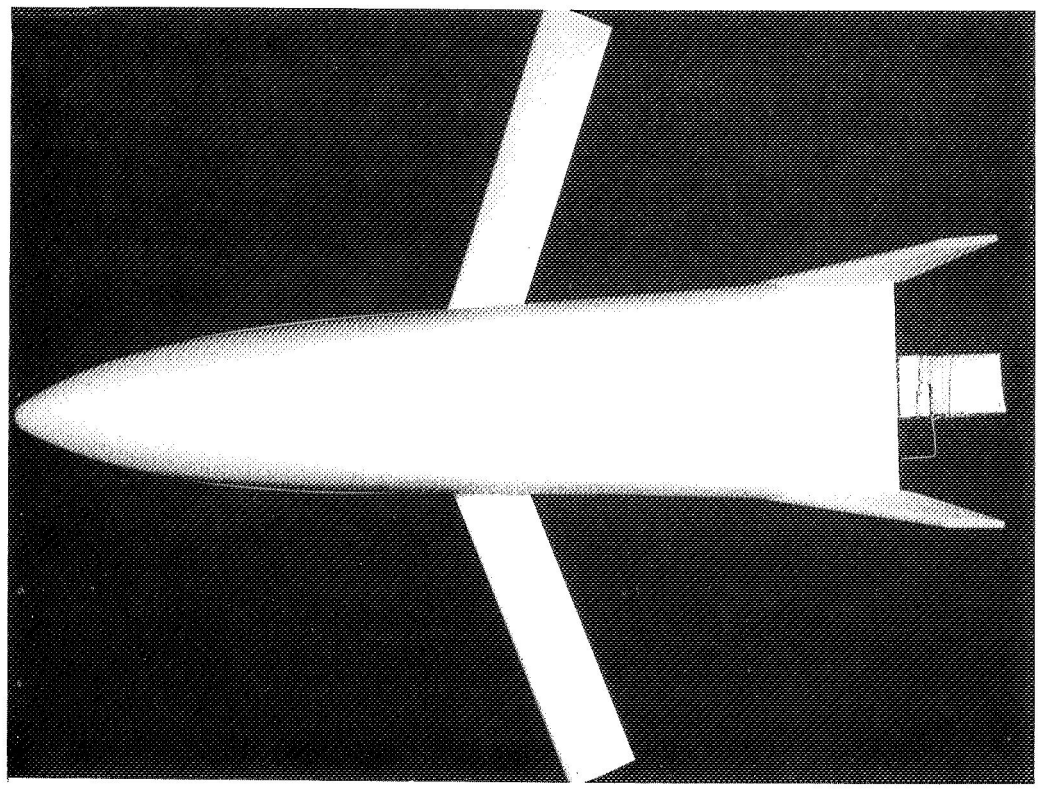

(a) Top view. L-68-3342

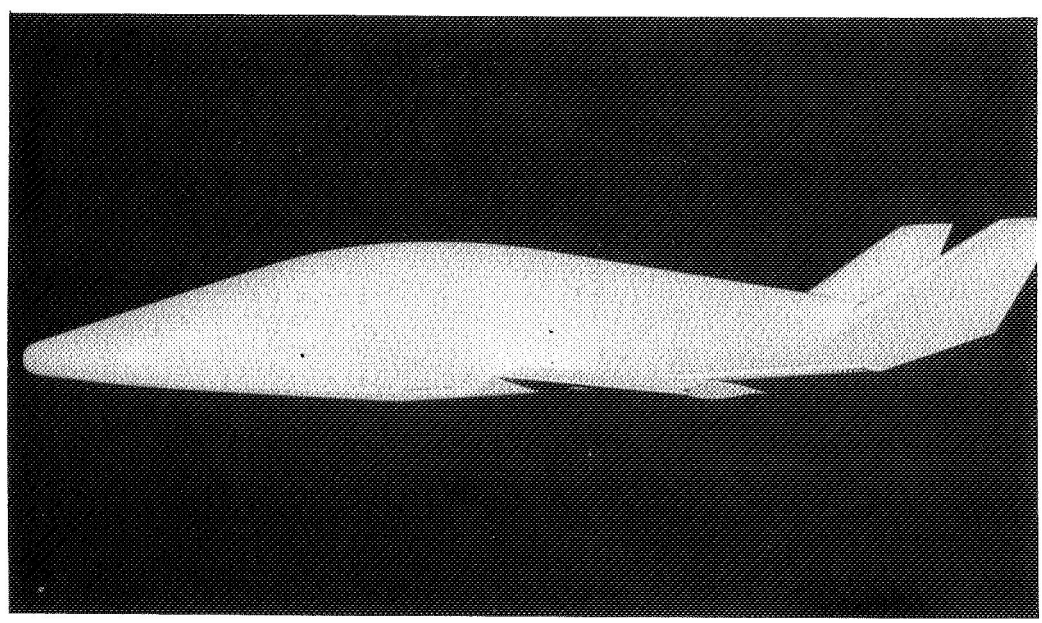

(b) Side view. L-68-3341

Figure 2.- Photographs of model.

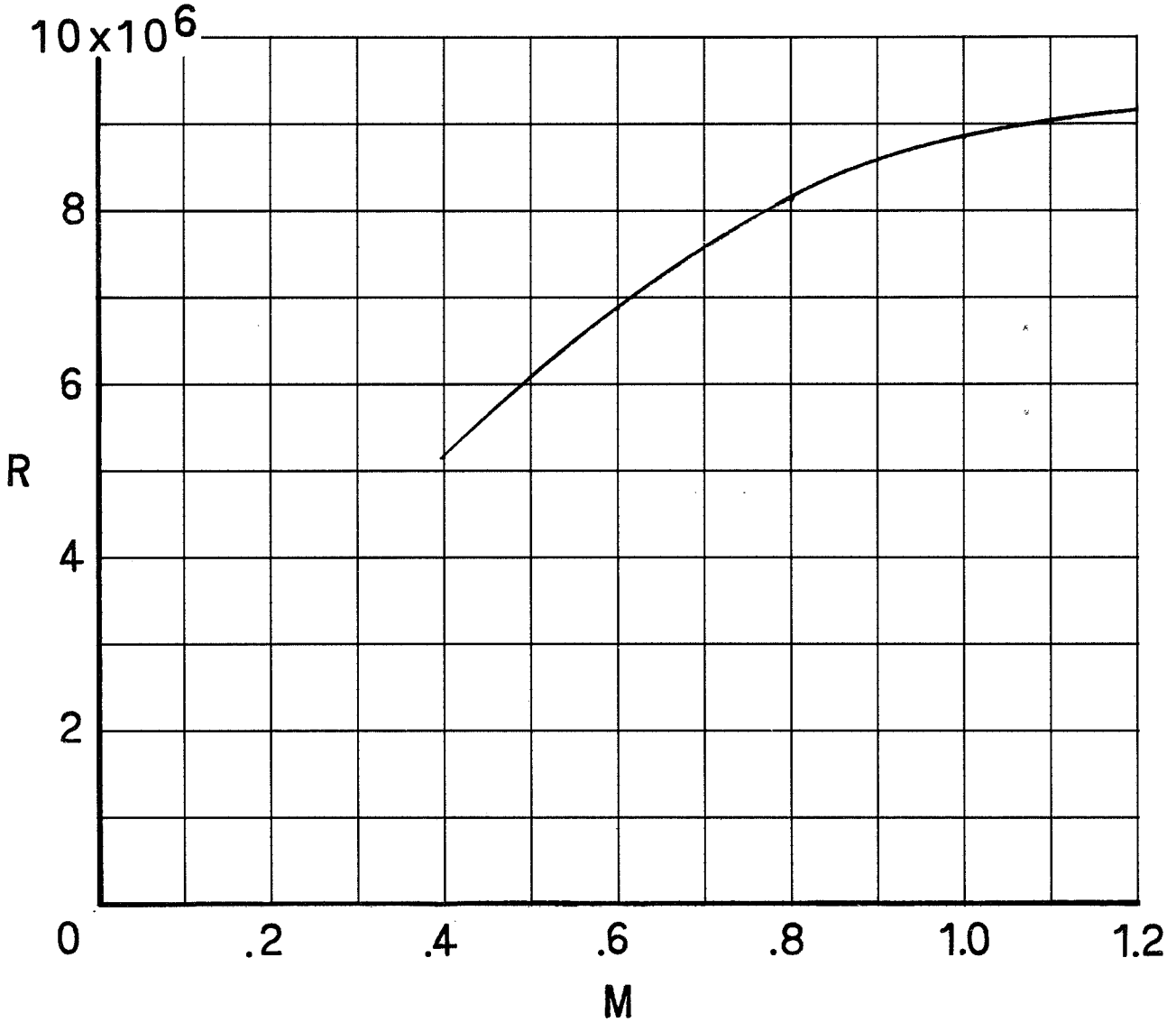

Figure 3.- Variation of test Reynolds number with Mach number.

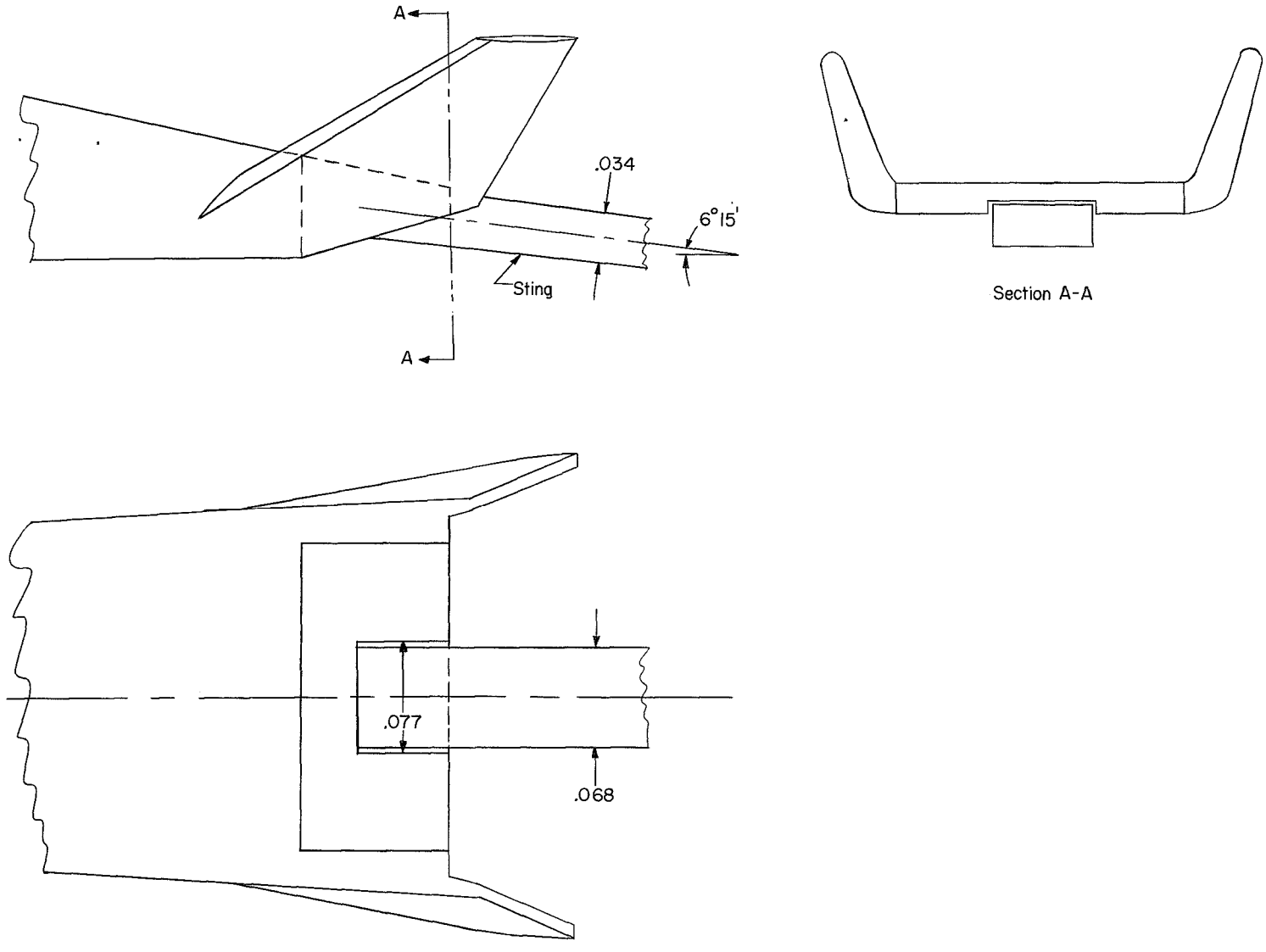

(a) Unfaired lower elevon.

Figure 4.- Modifications to body for sting support when lower elevon is deflected to -15^0. All linear dimensions based on body length l = 25.86 in. (65.68 cm).

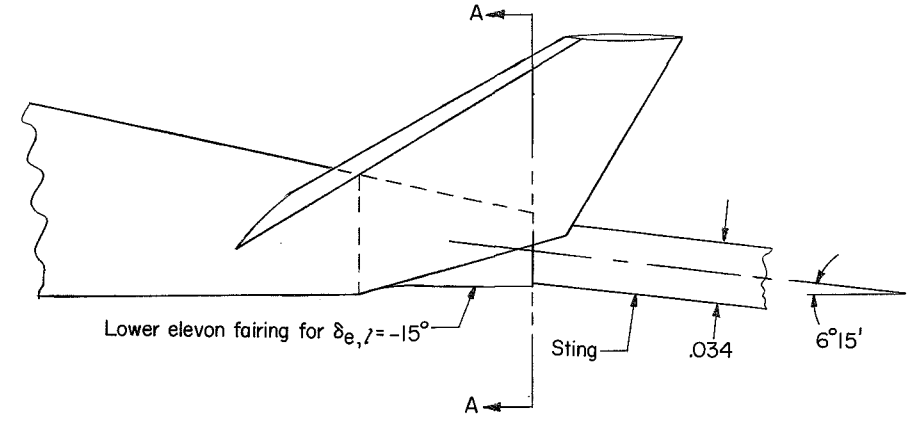

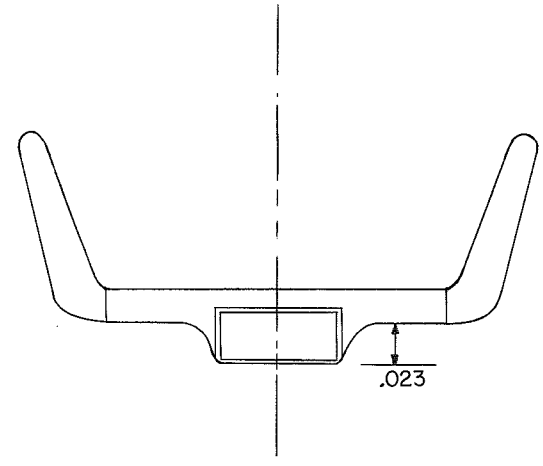

Section A-A

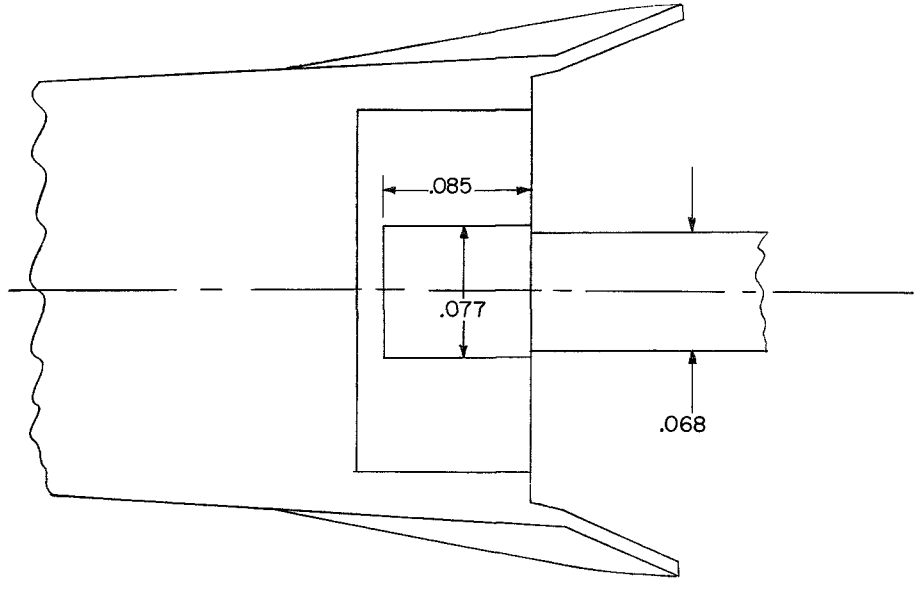

(b) Faired lower elevon.

Figure 4.- Concluded.

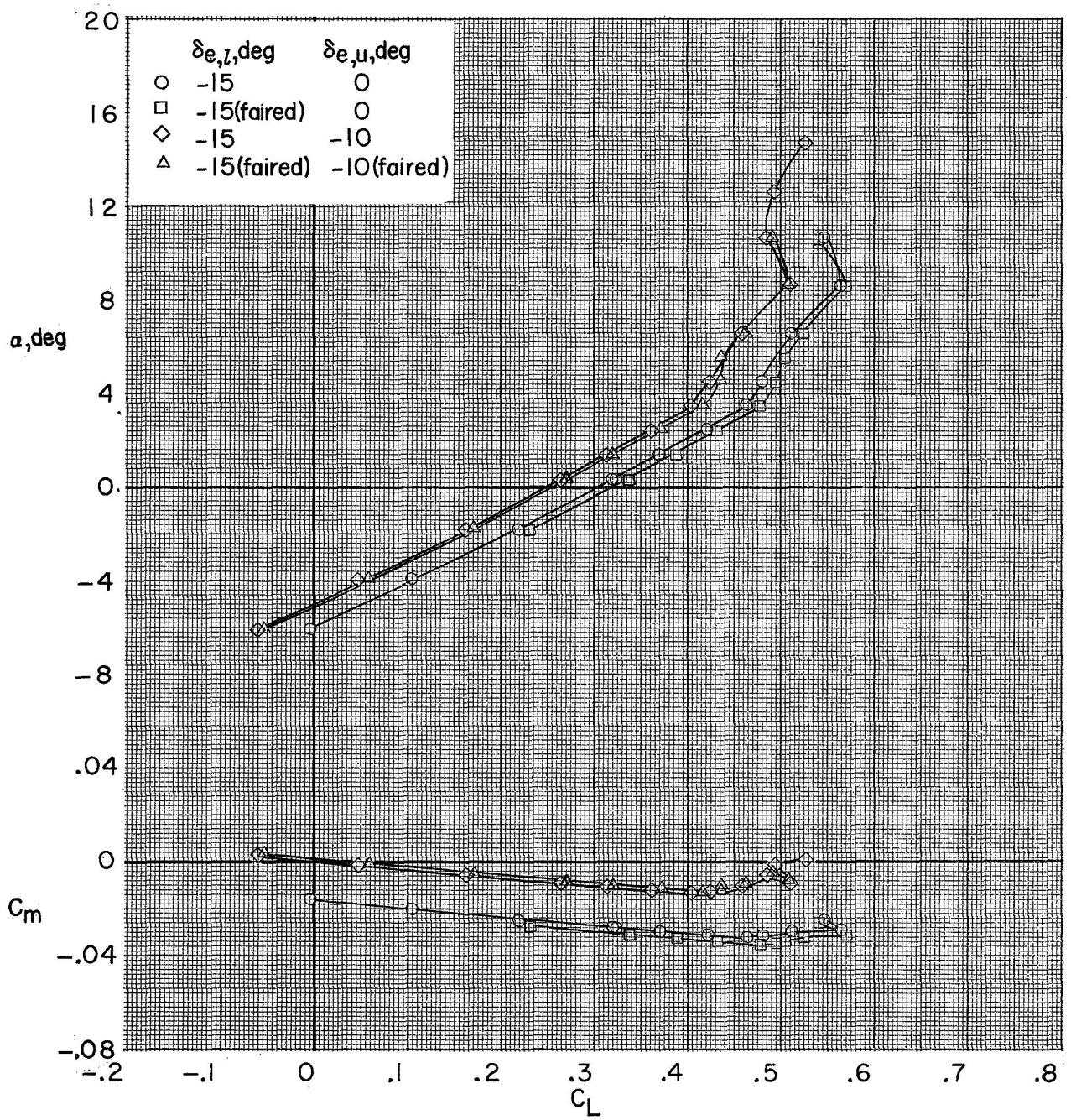

(a) M = 0.40.

Figure 5.- Effect of elevon fairings on the longitudinal aerodynamic characteristics of the model with wings deployed to $\Lambda = 20^{0}$.

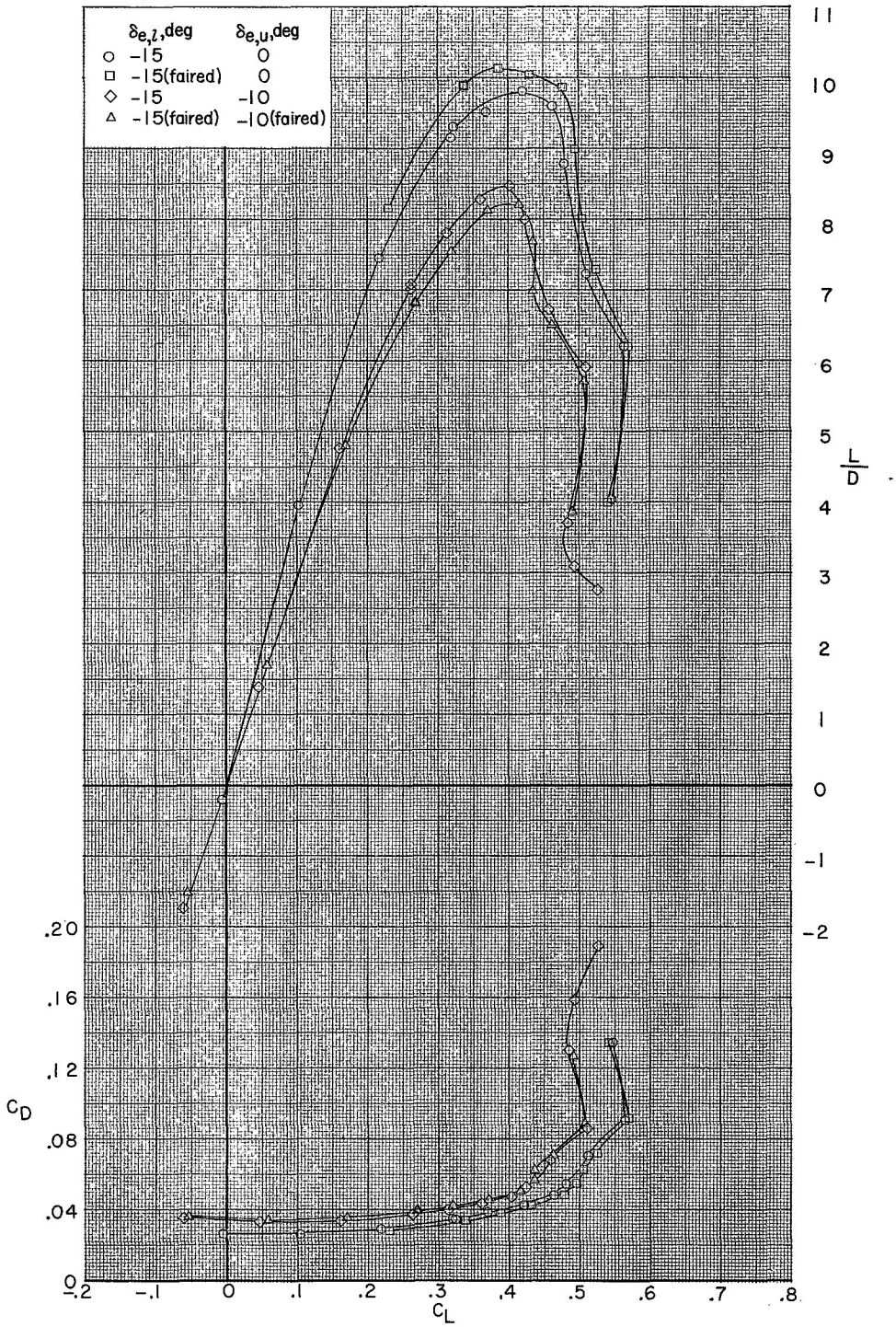

(a) Concluded.

Figure 5.- Continued.

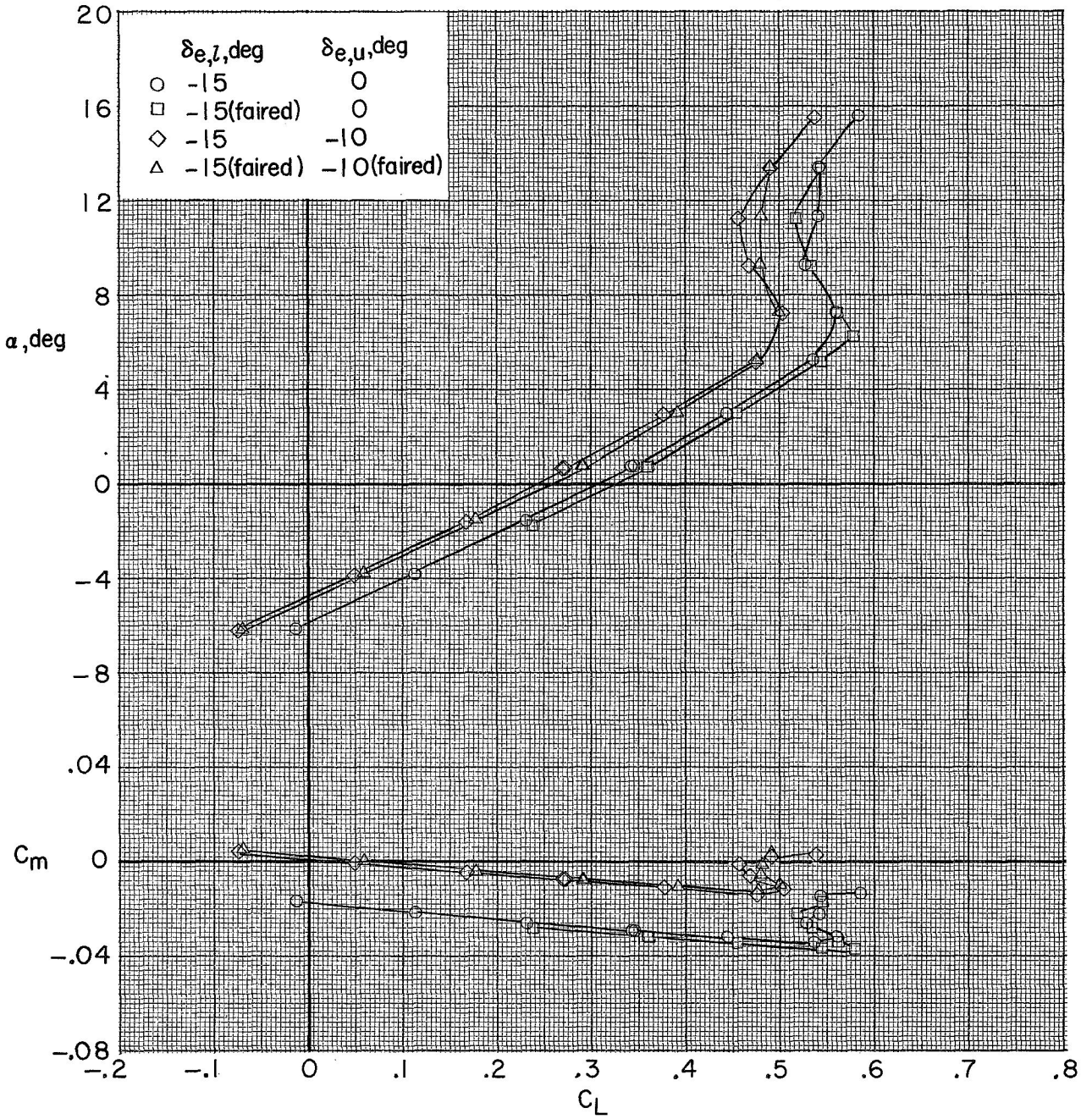

(b) M = 0.60.

Figure 5.- Continued.

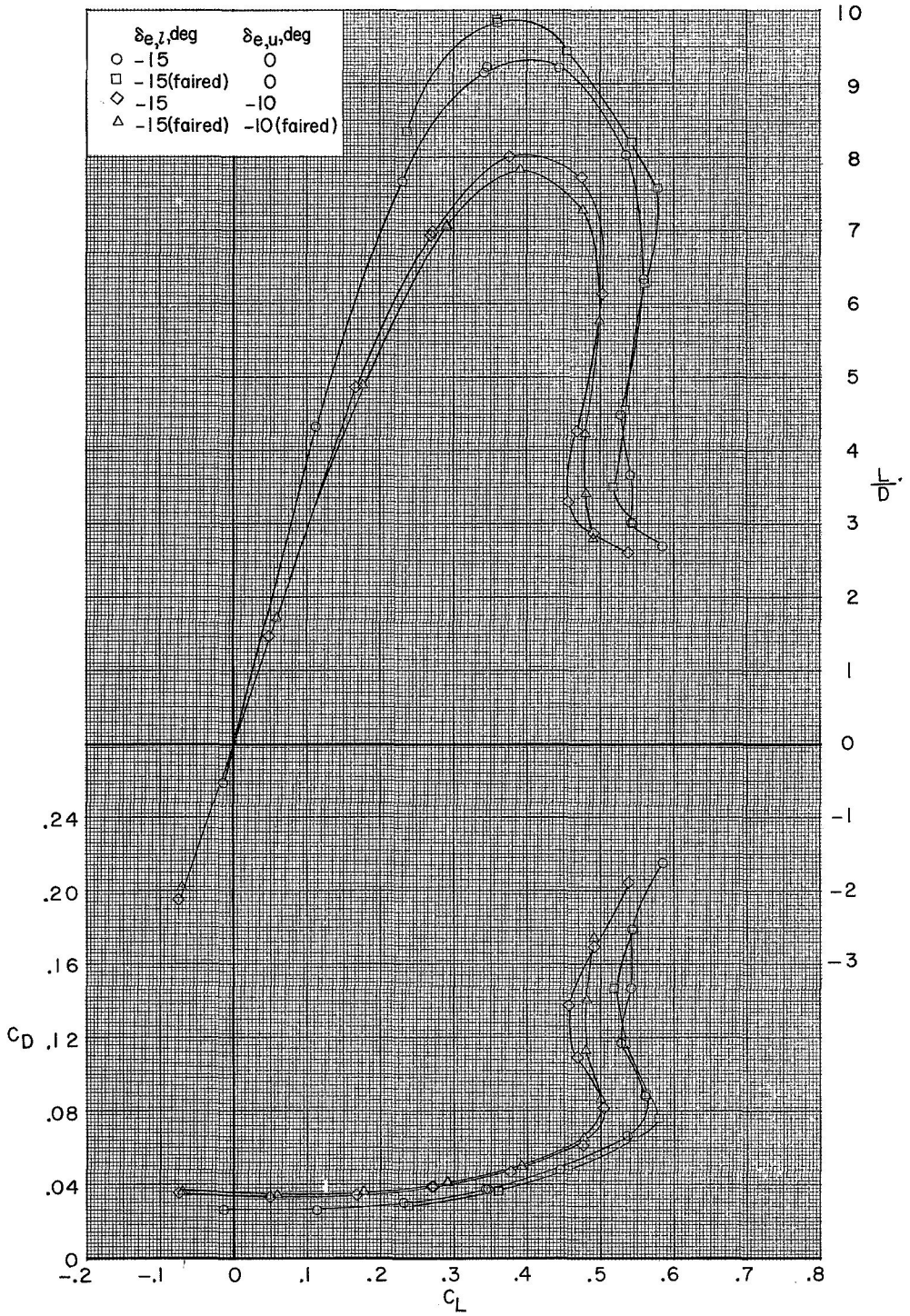

(b) Concluded.

Figure 5.- Continued.

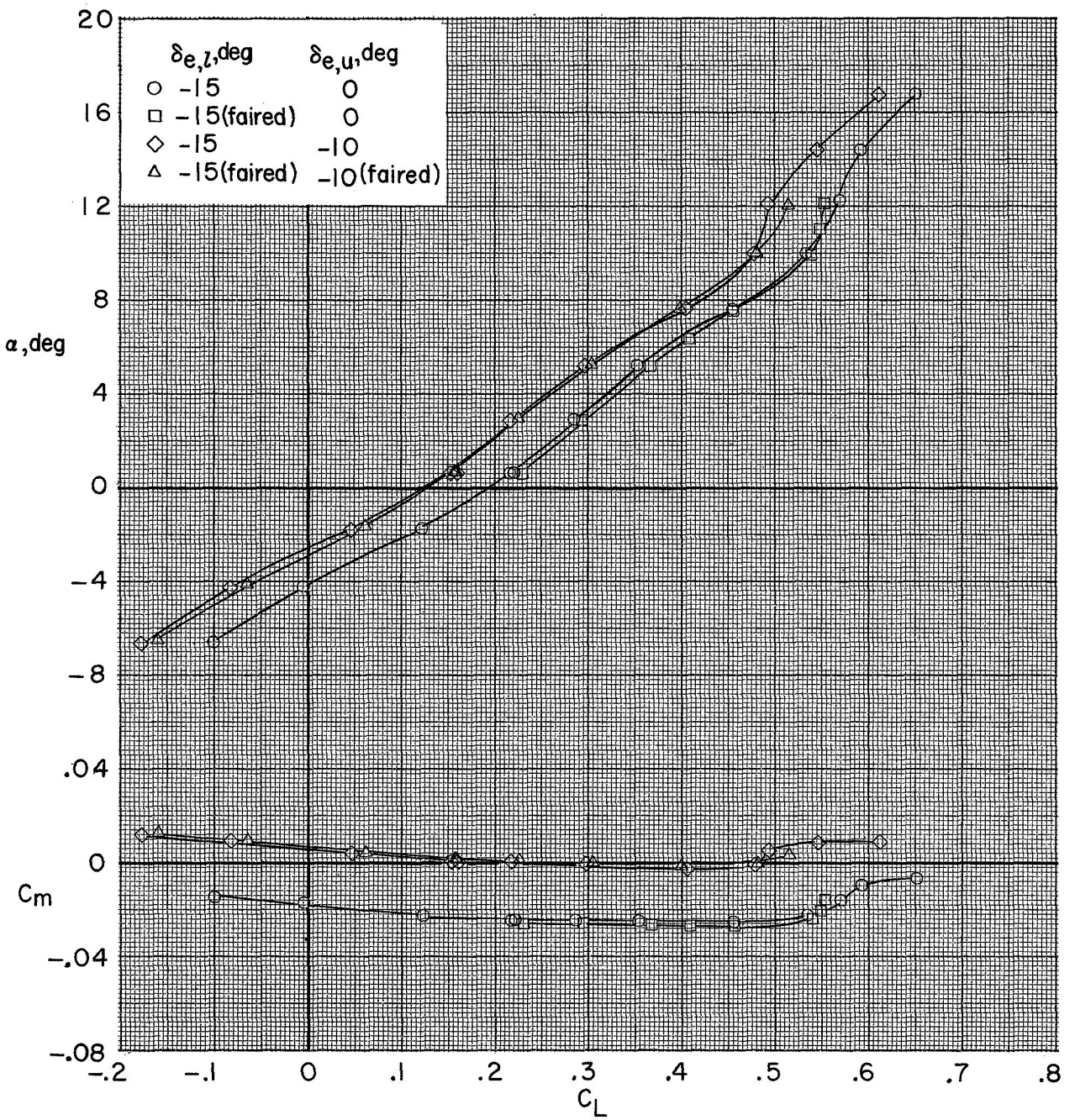

(c) M = 0.80.

Figure 5.- Continued.

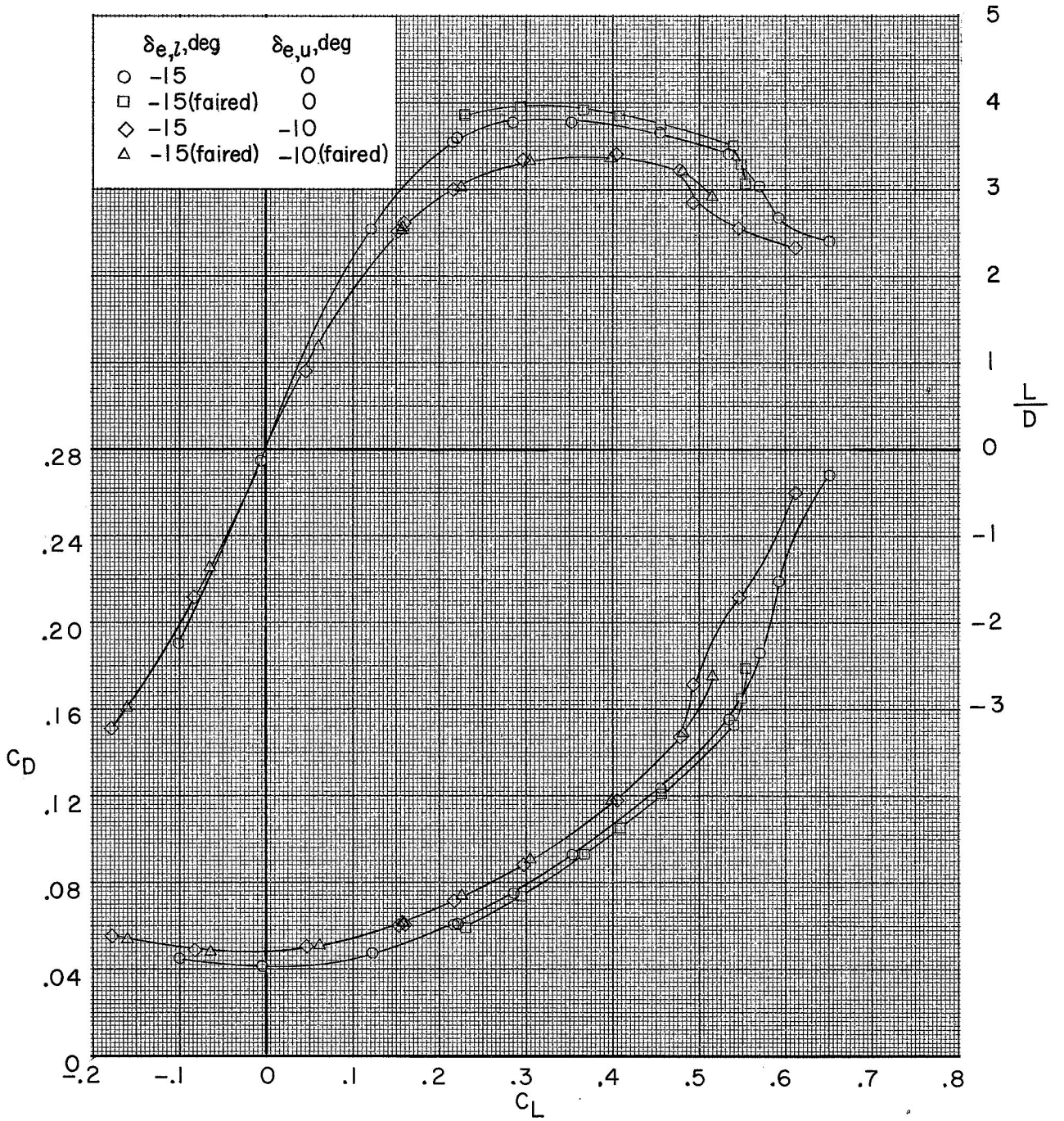

(c) Concluded.

Figure 5.- Continued.

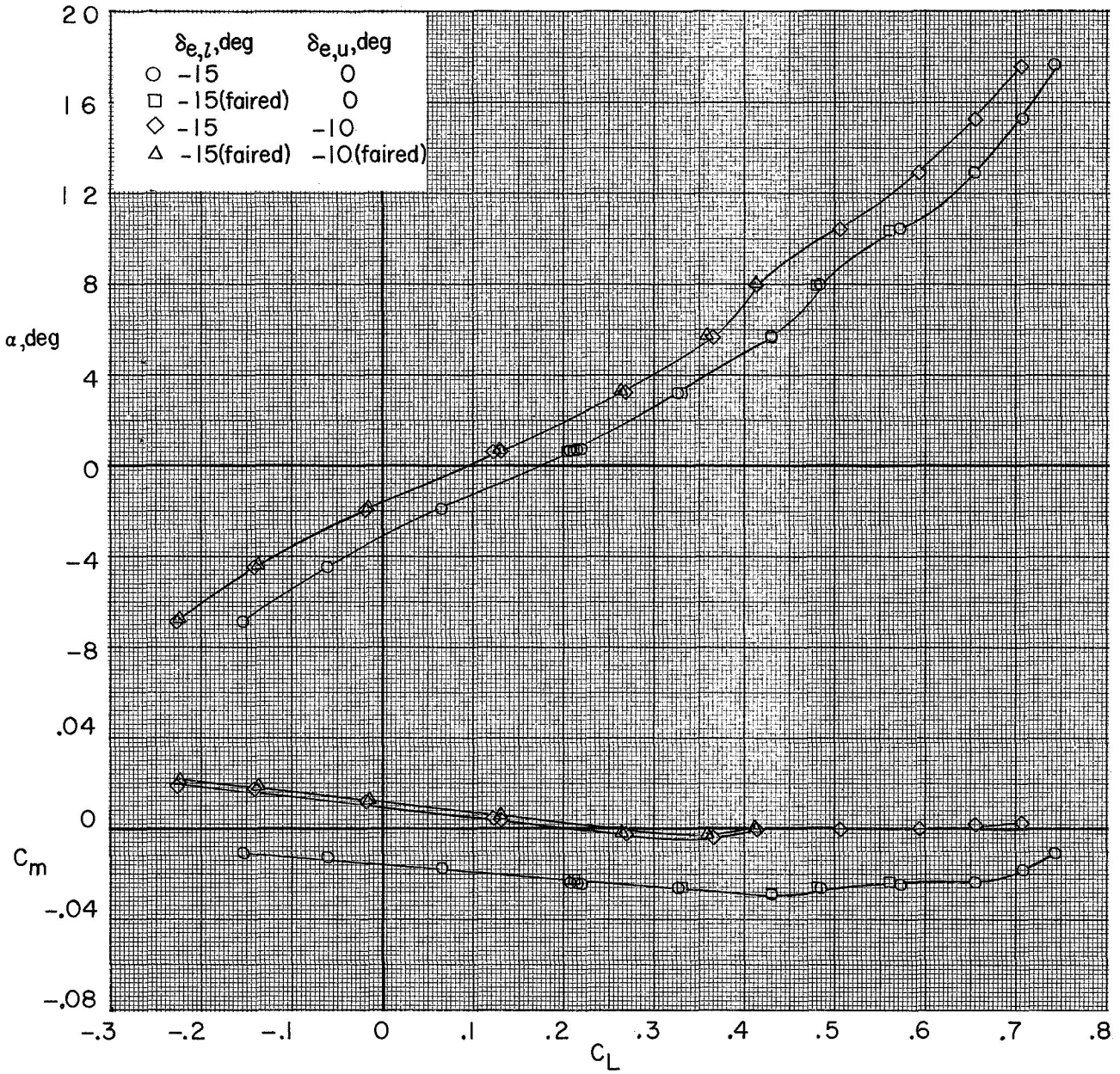

(d) M = 0.90.

Figure 5.- Continued.

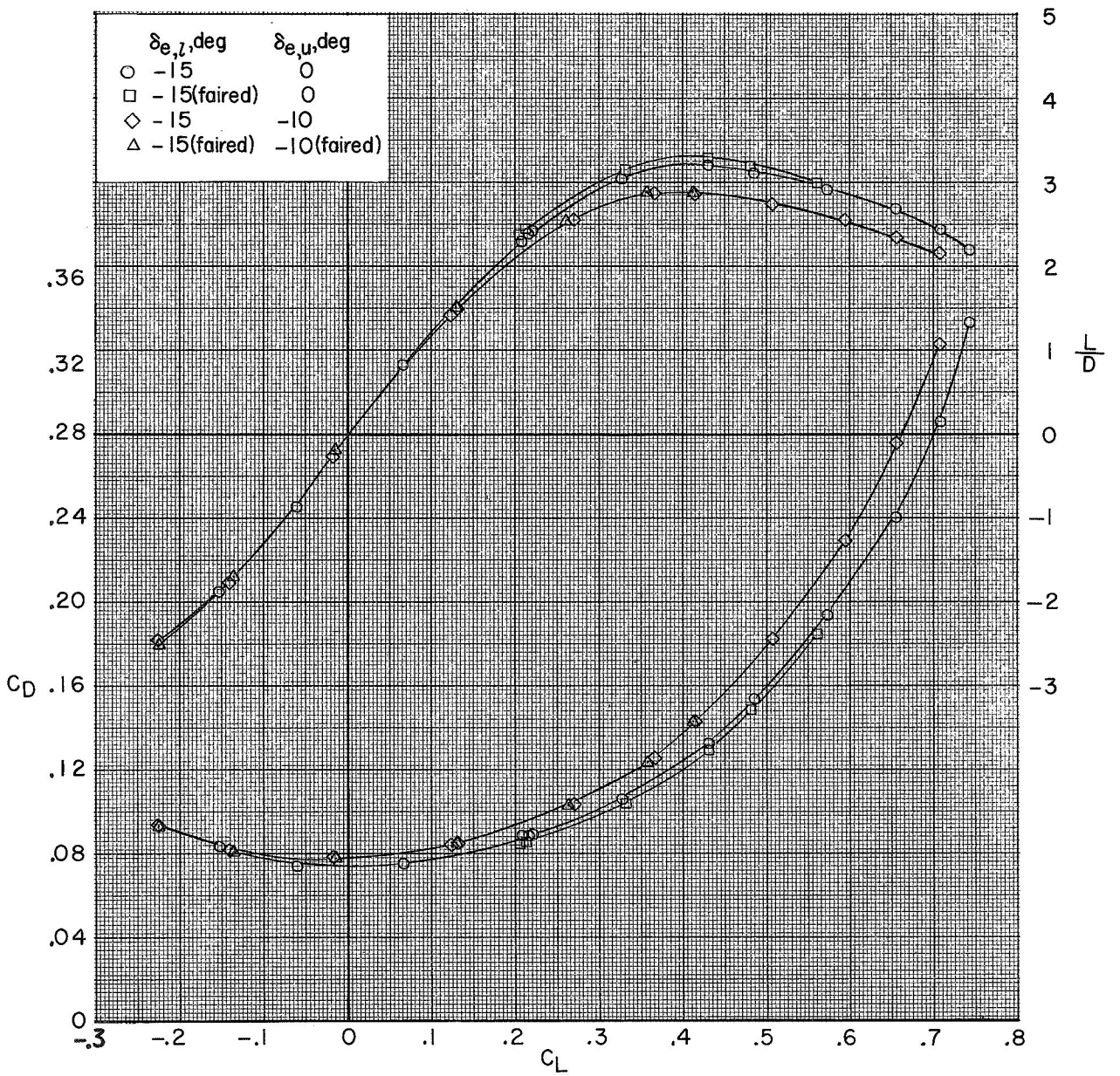

(d) Concluded.

Figure 5.- Concluded.

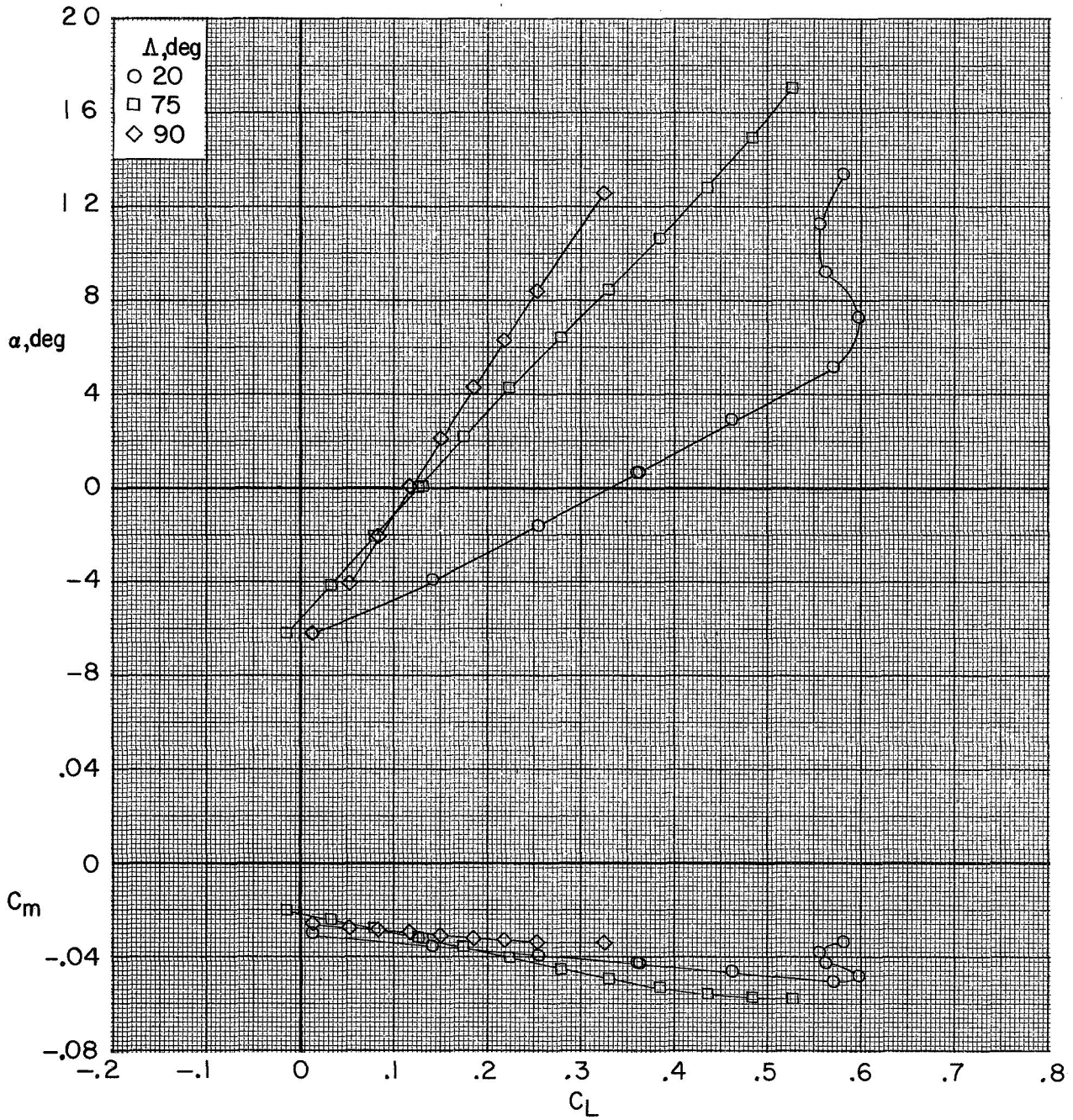

(a) M = 0.60.

Figure 6.- Effect of wing sweep on the longitudinal aerodynamic characteristics of the model. $\delta_{e,l} = 0^0$; $\delta_{e,u} = 0^0$.

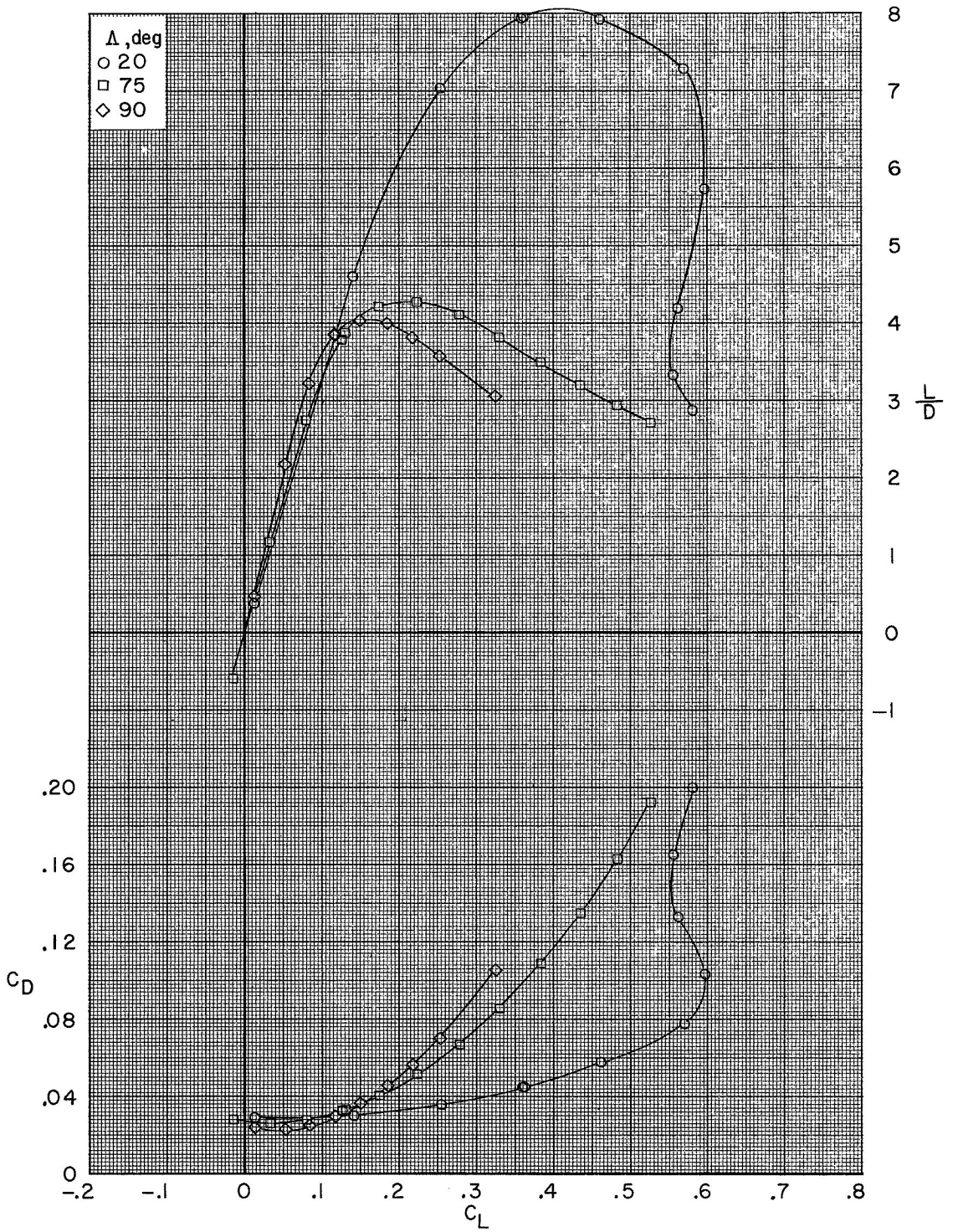

(a) Concluded.

Figure 6.- Continued.

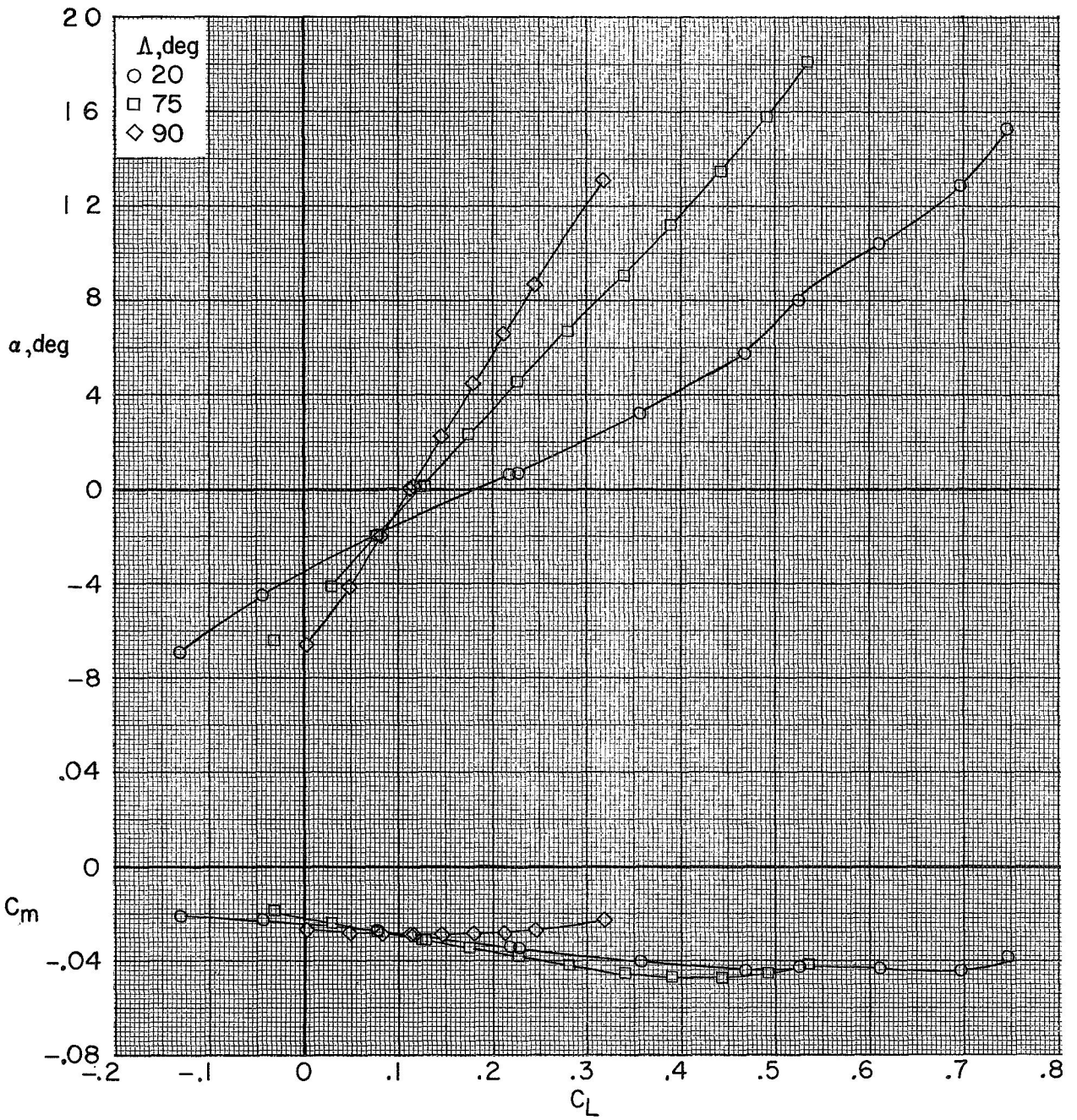

(b) M = 0.90.

Figure 6.- Continued.

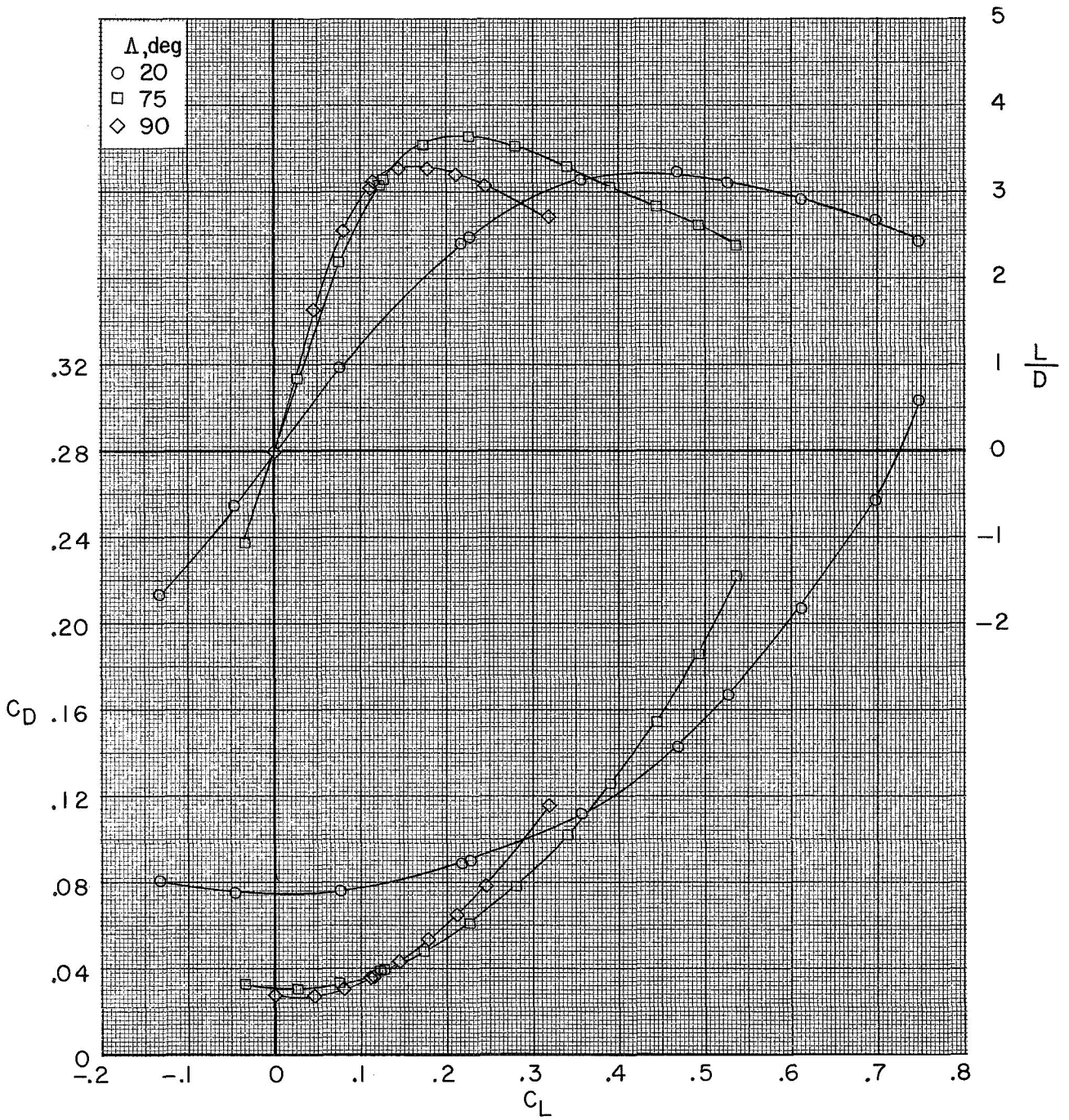

(b) Concluded.

Figure 6.- Continued.

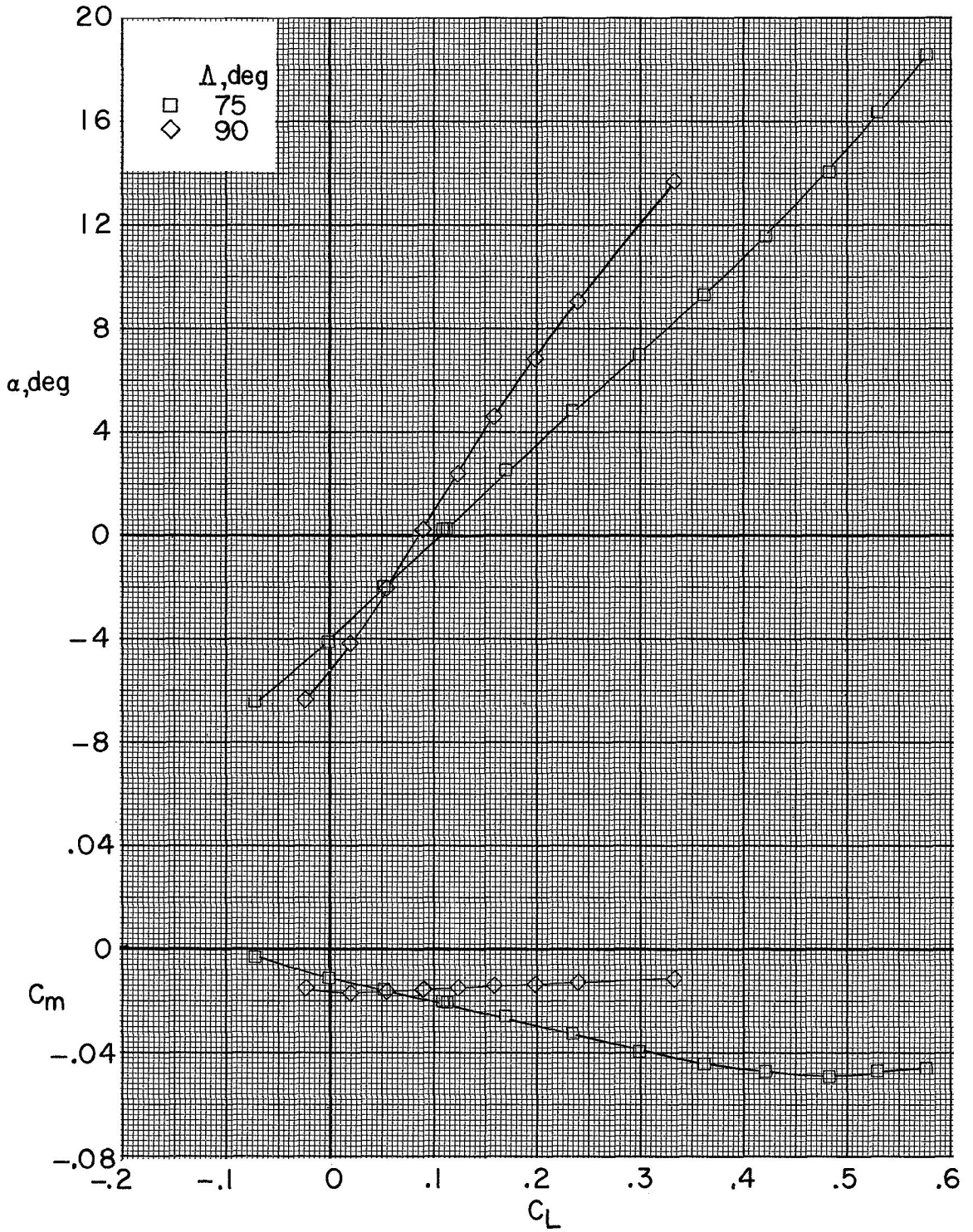

(c) M = 1.00.

Figure 6.- Continued.

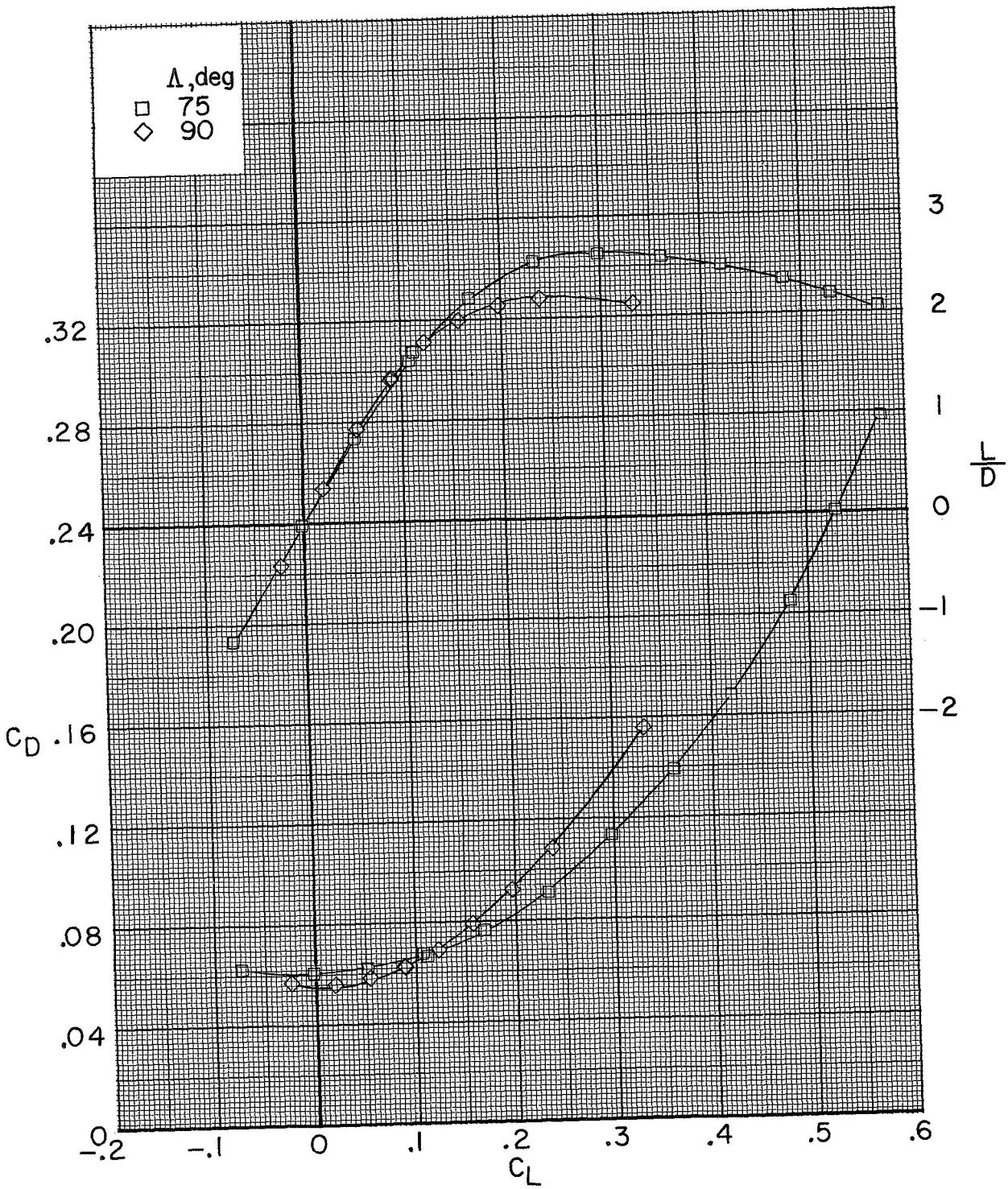

(c) Concluded.

Figure 6.- Continued.

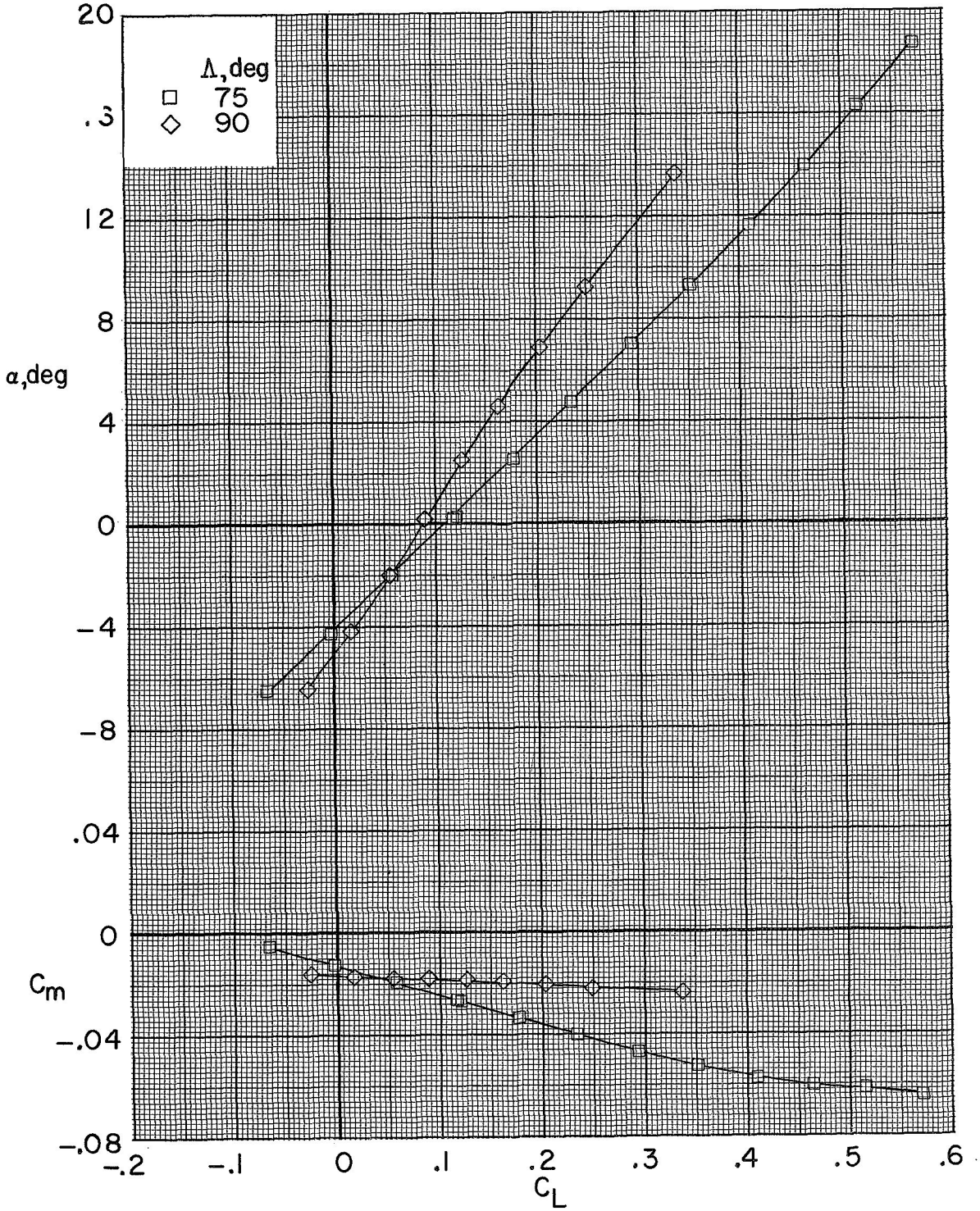

(d) M = 1.20.

Figure 6.- Continued.

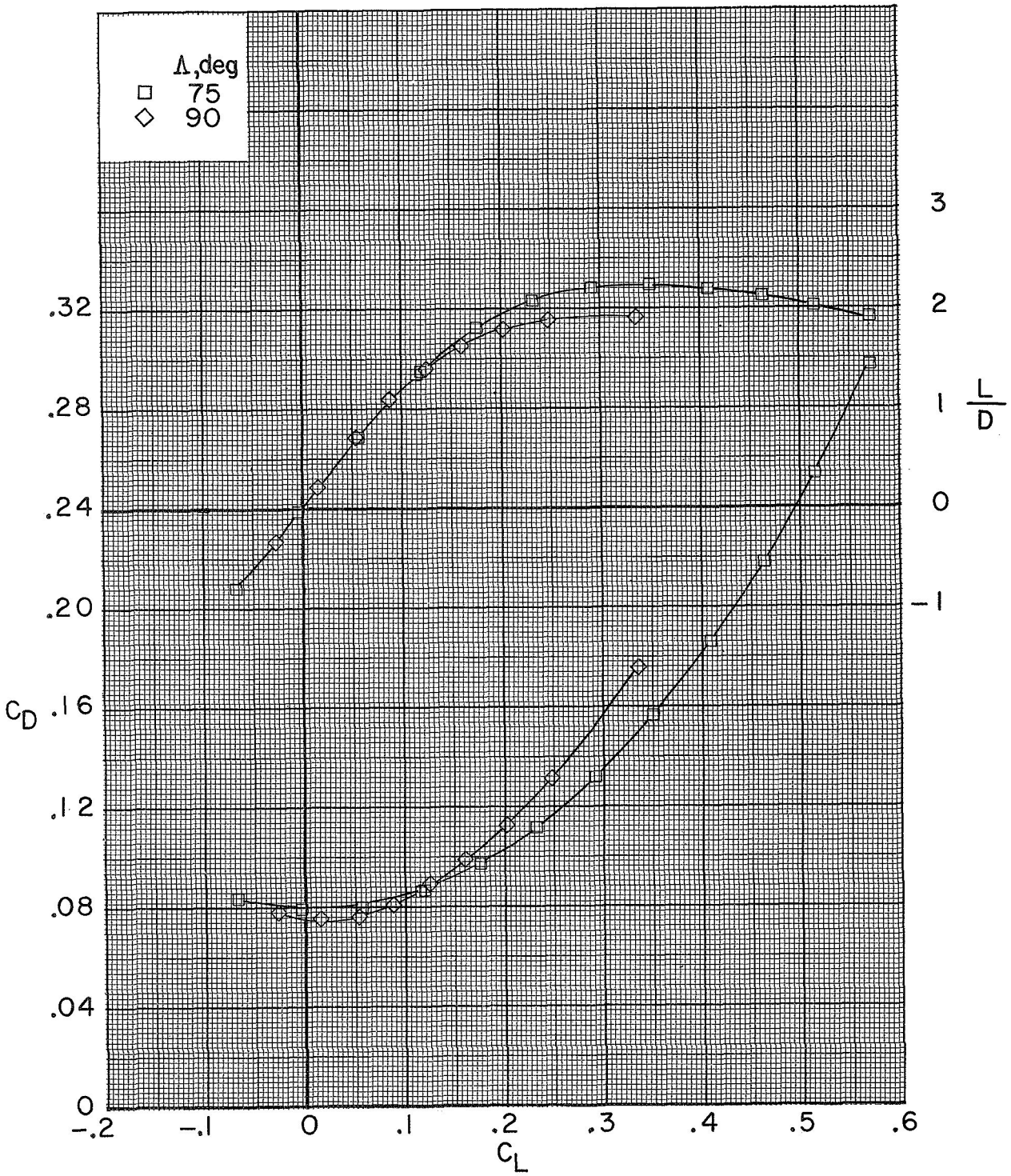

(d) Concluded.

Figure 6.- Concluded.

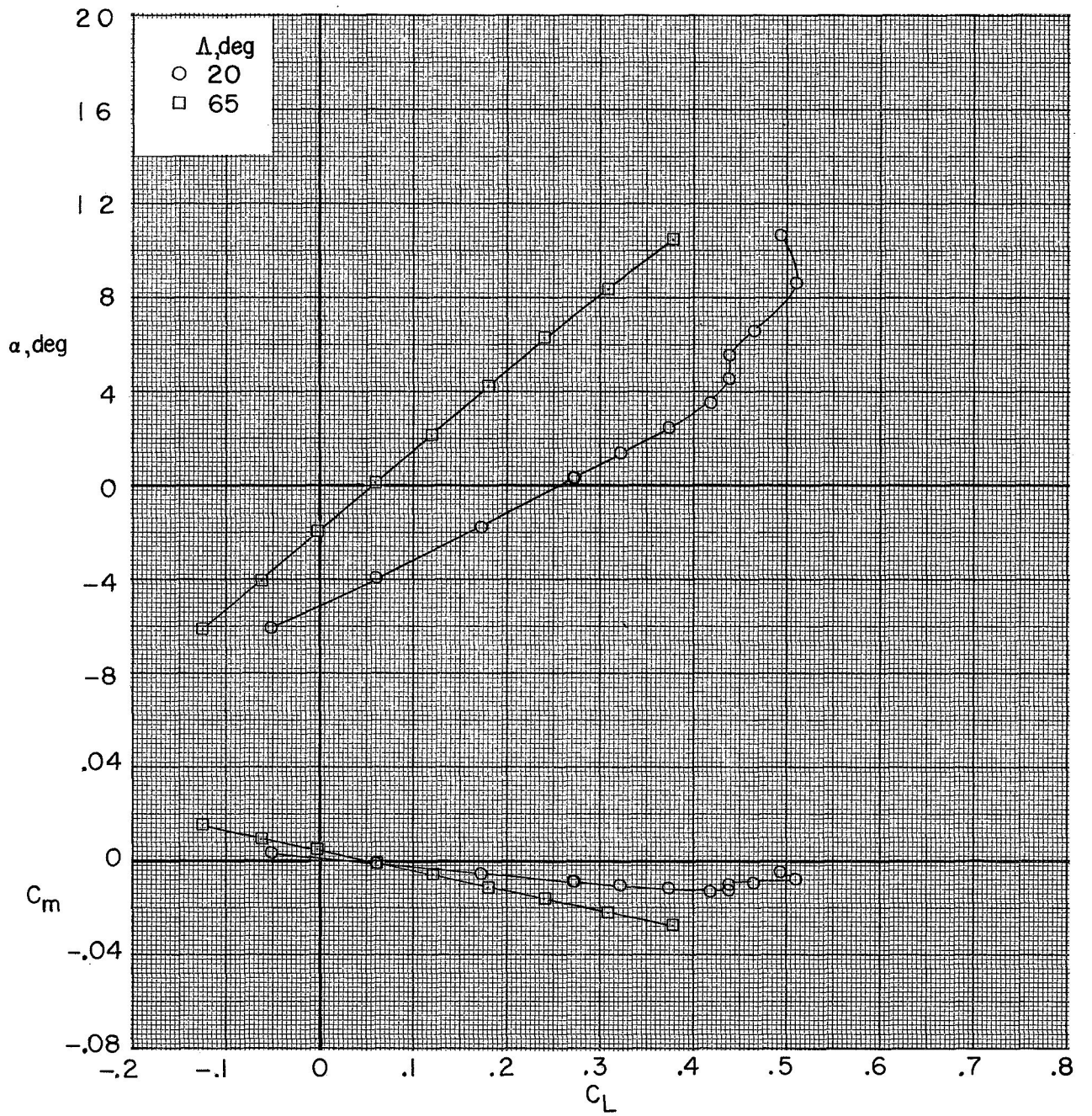

(a) M = 0.40.

Figure 7.- Effect of wing sweep on the longitudinal aerodynamic characteristics of the model. $\delta_{e,l} = -15^{0}$ (faired); $\delta_{e,u} = -10^{0}$ (faired).

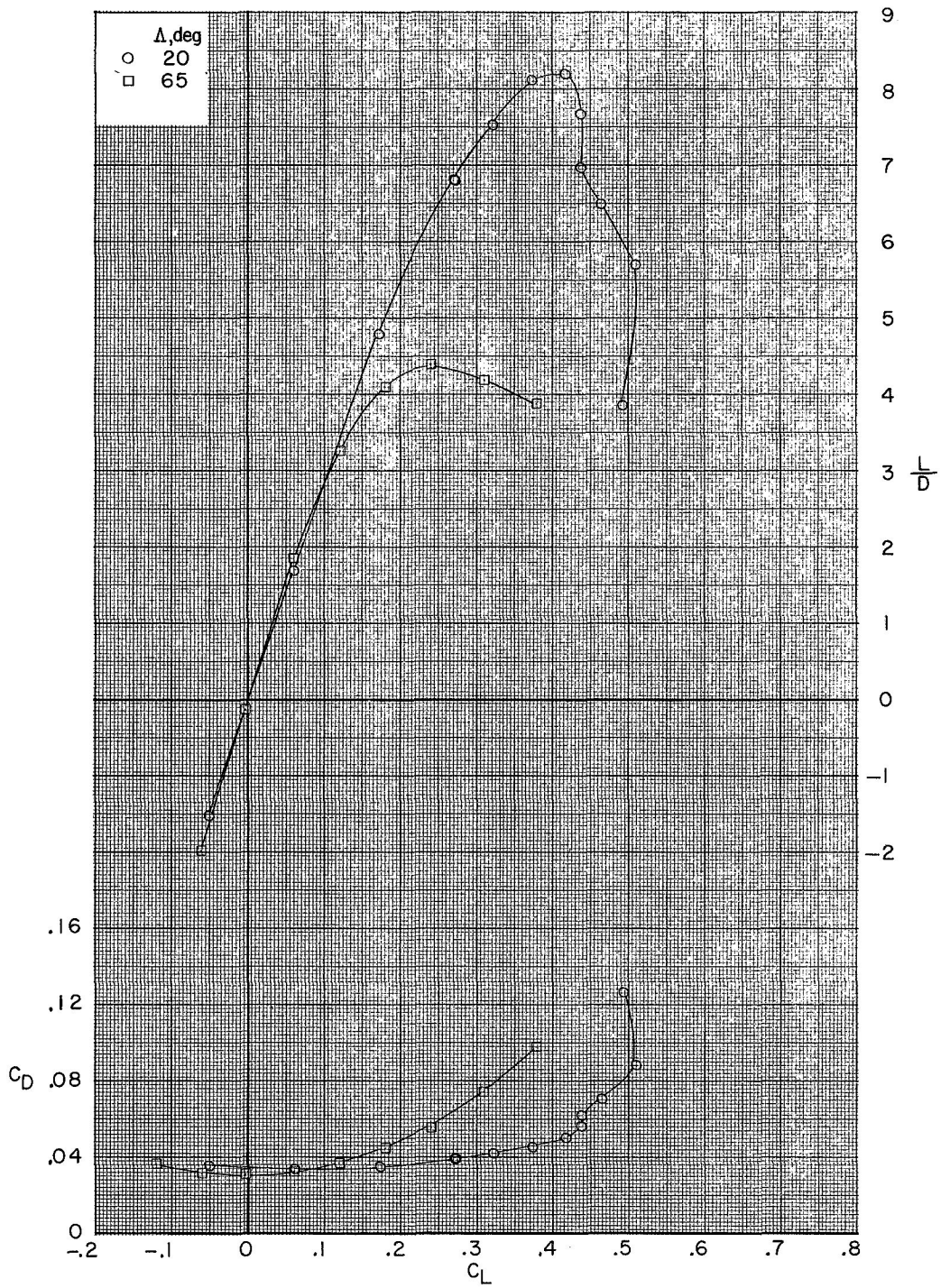

(a) Concluded.

Figure 7.- Continued.

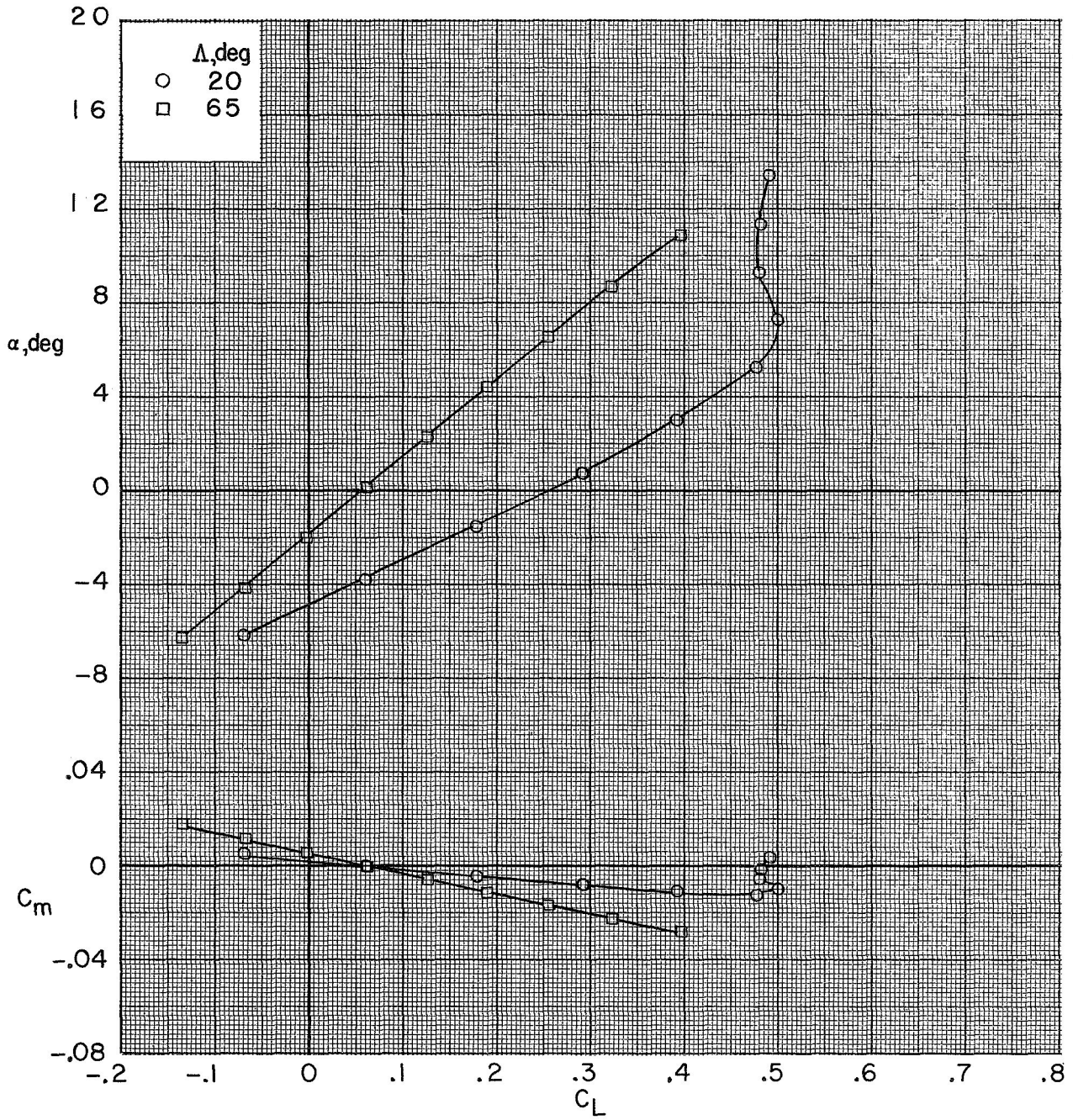

(b) M = 0.60.

Figure 7.- Continued.

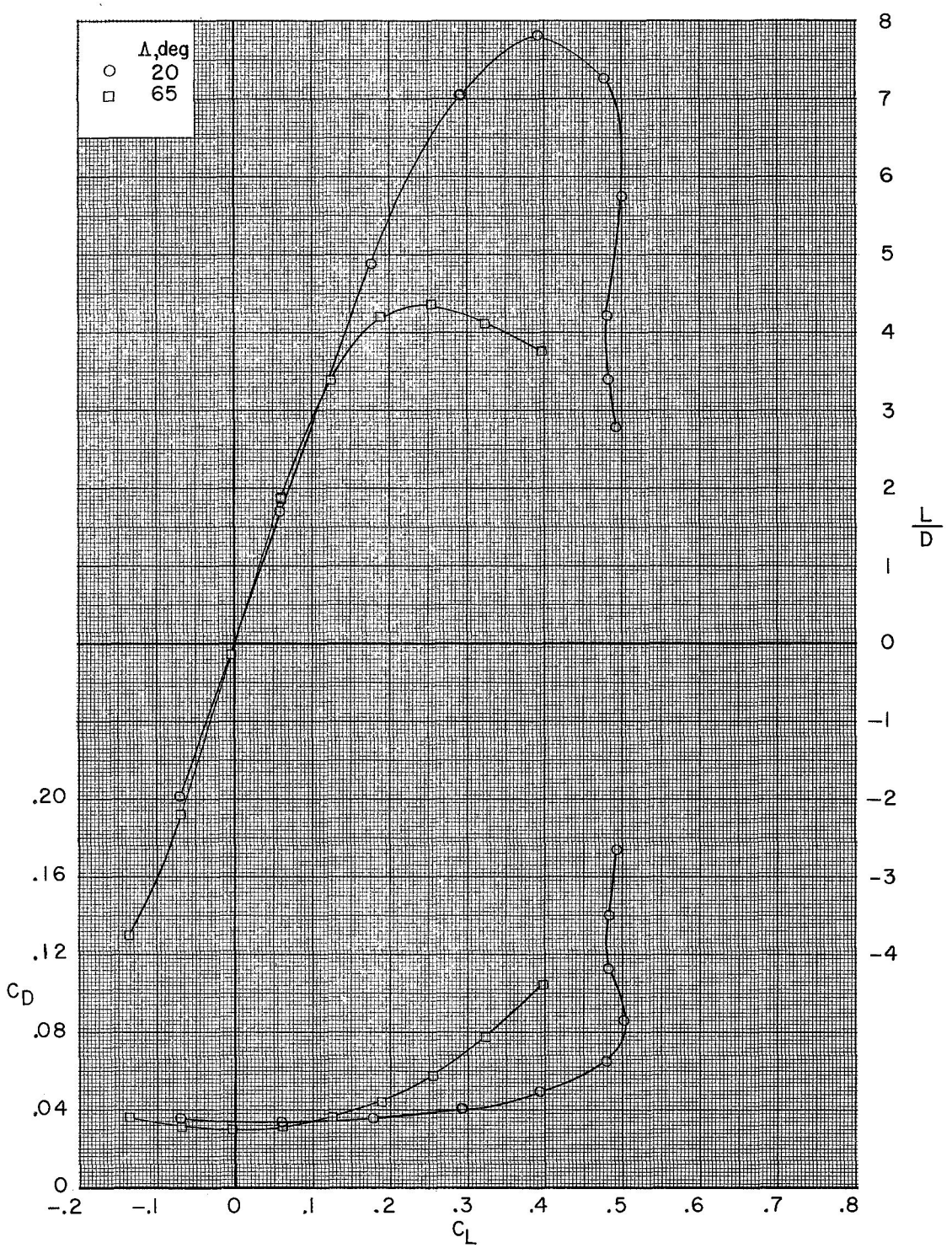

(b) Concluded.

Figure 7.- Continued.

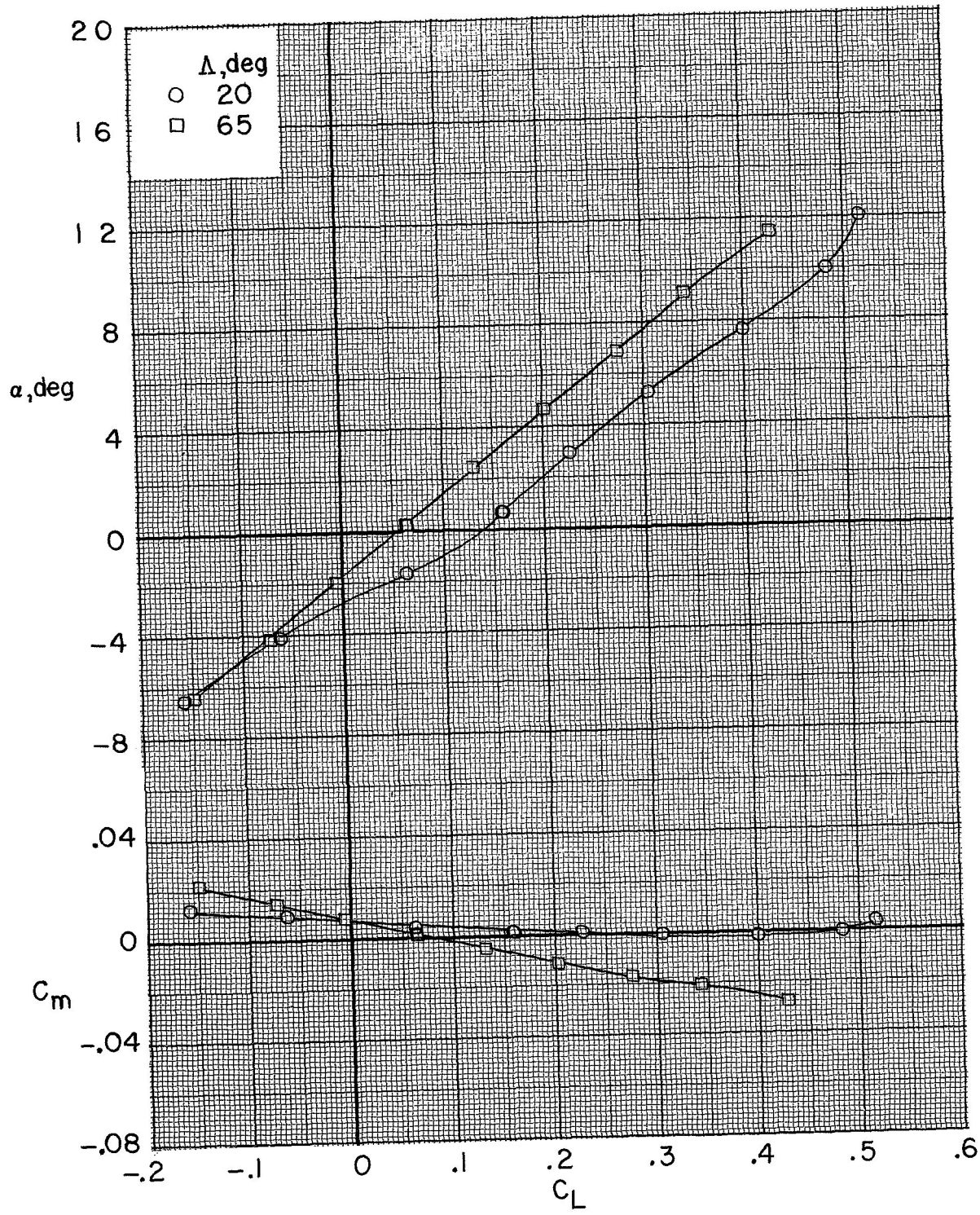

(c) M = 0.80.

Figure 7.- Continued.

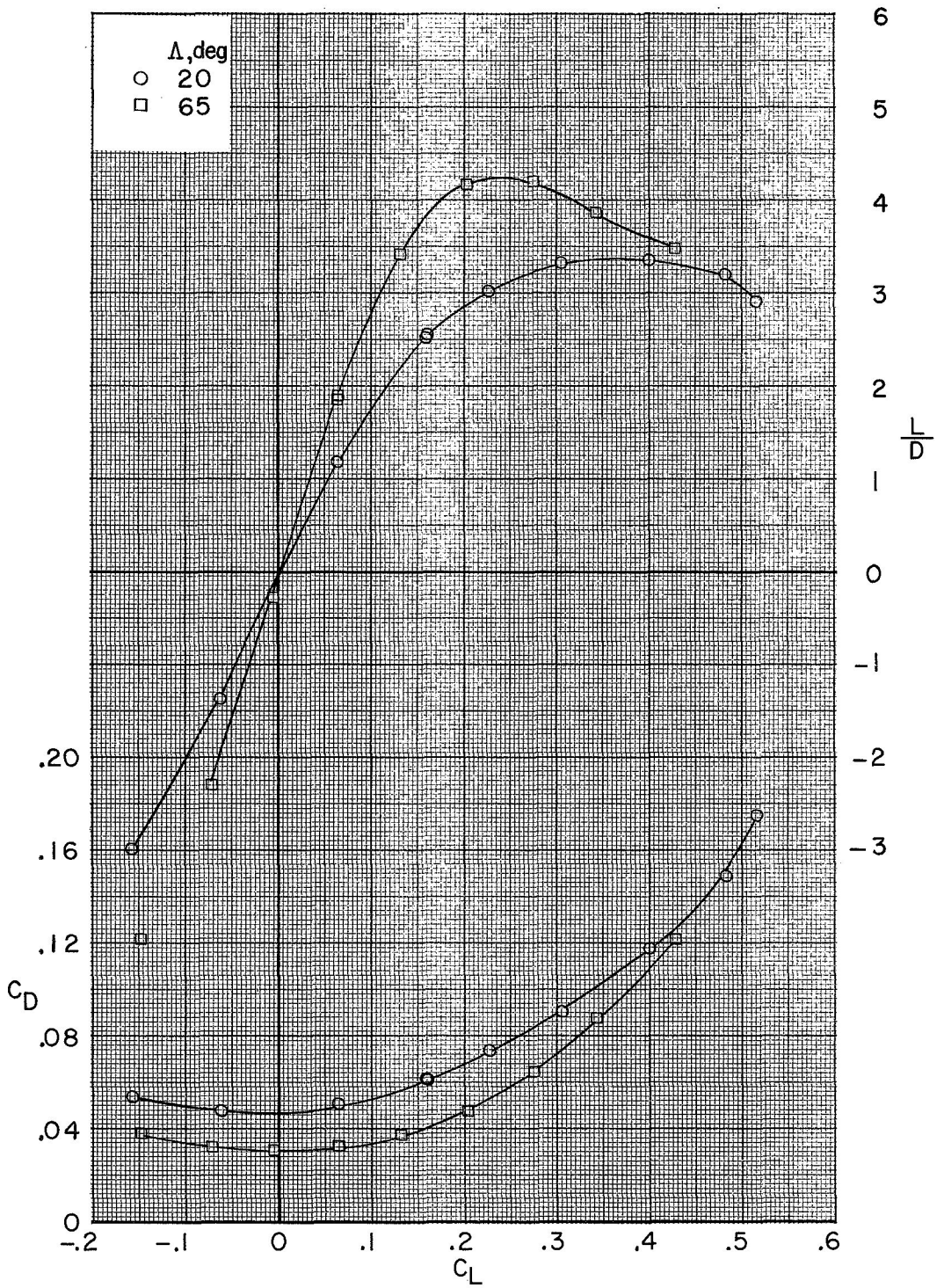

(c) Concluded.

Figure 7.- Continued.

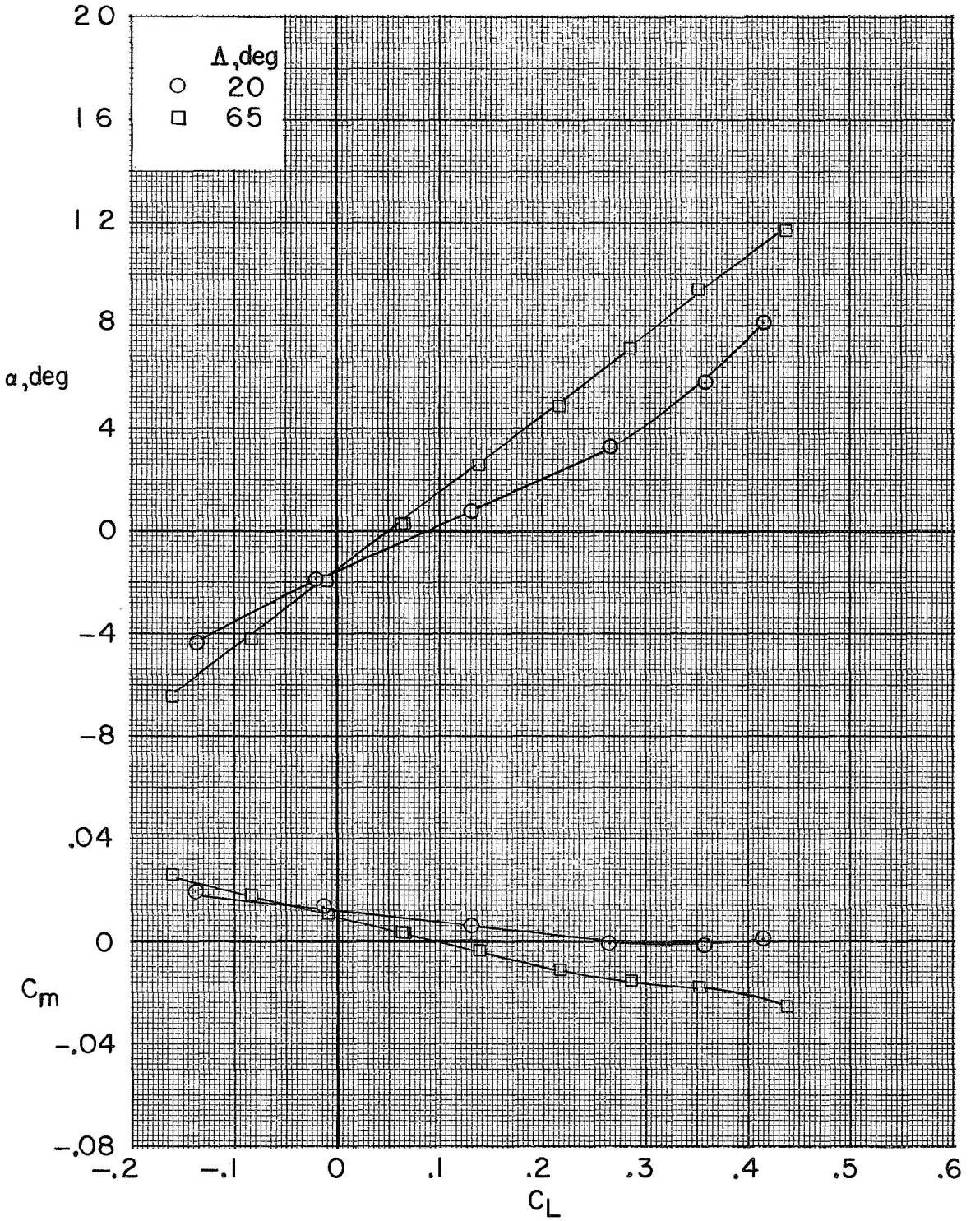

(d) M = 0.90.

Figure 7.- Continued.

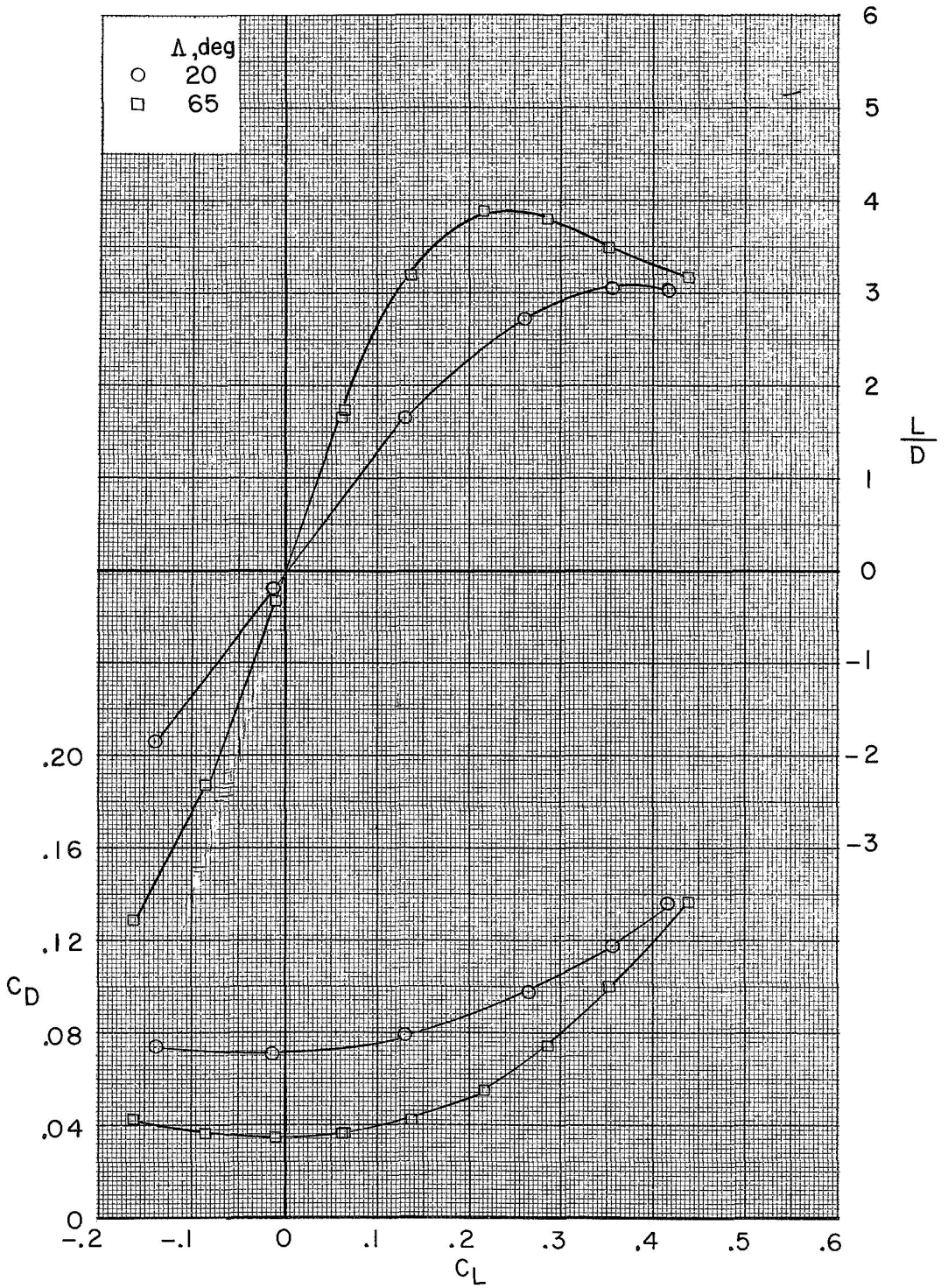

(d) Concluded.

Figure 7.- Concluded.

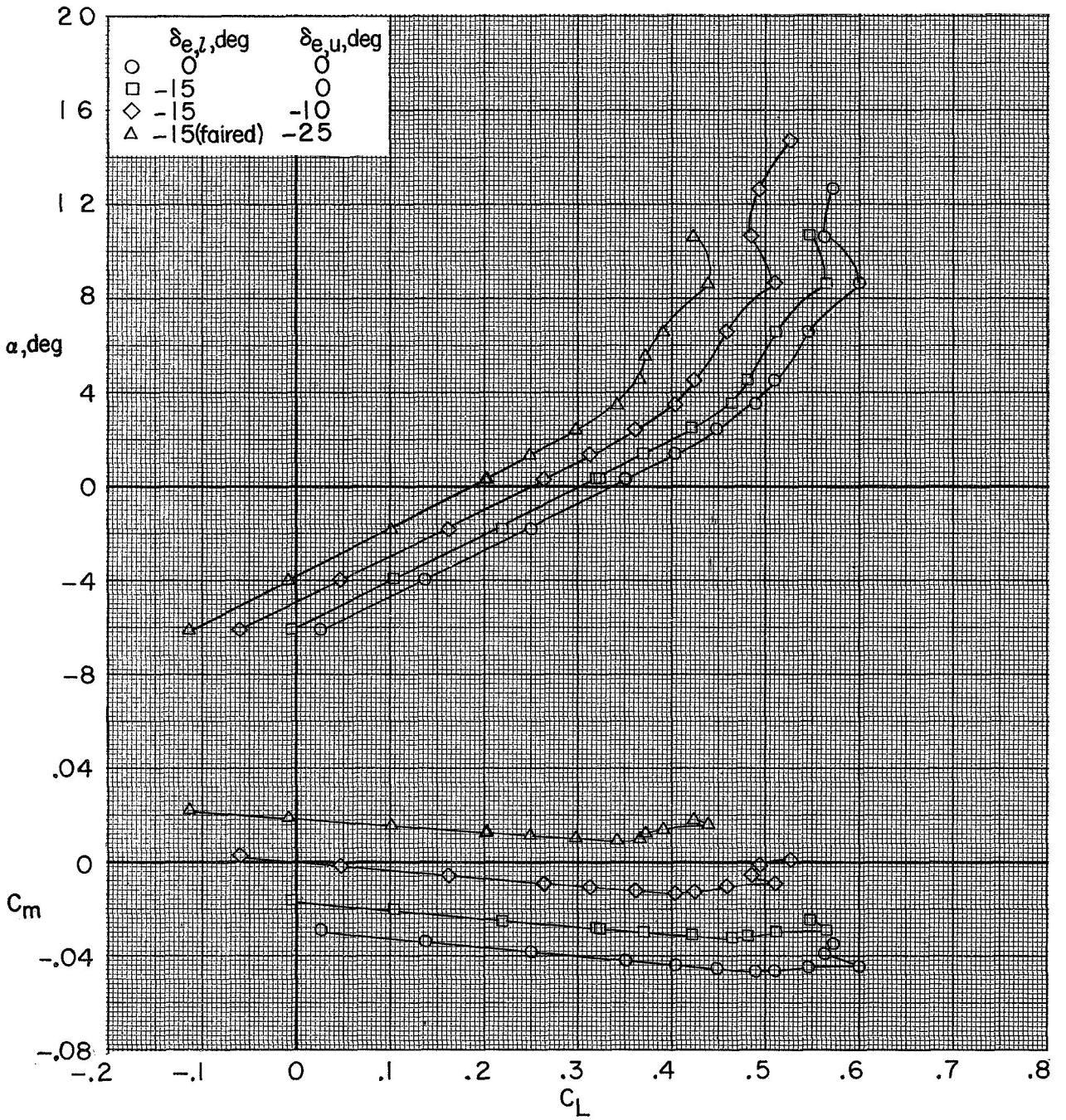

(a) M = 0.40.

Figure 8.- Effect of elevon deflections on the longitudinal aerodynamic characteristics of the model with wings deployed to $\Lambda = 20^{o}$.

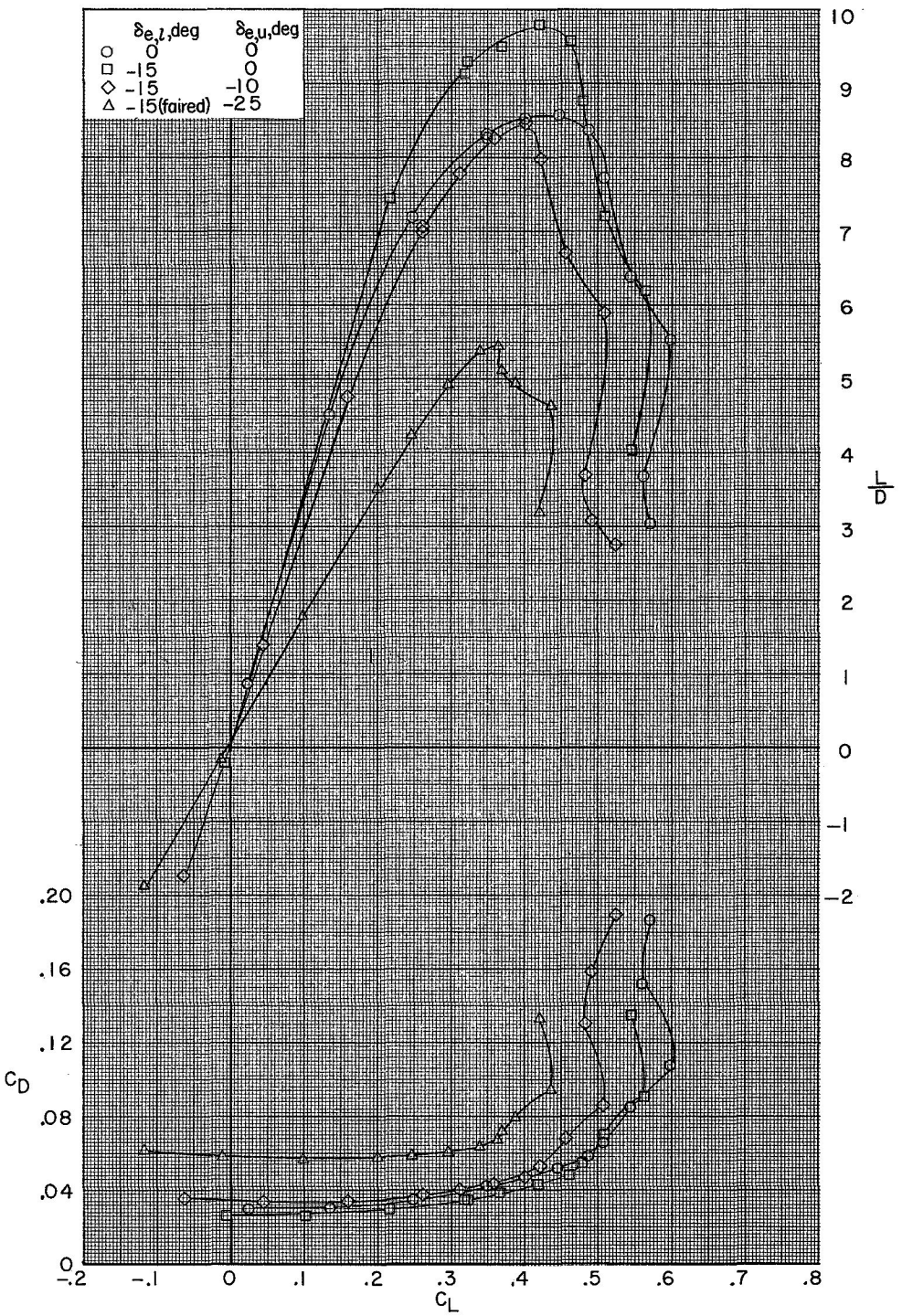

(a) Concluded.

Figure 8.- Continued.

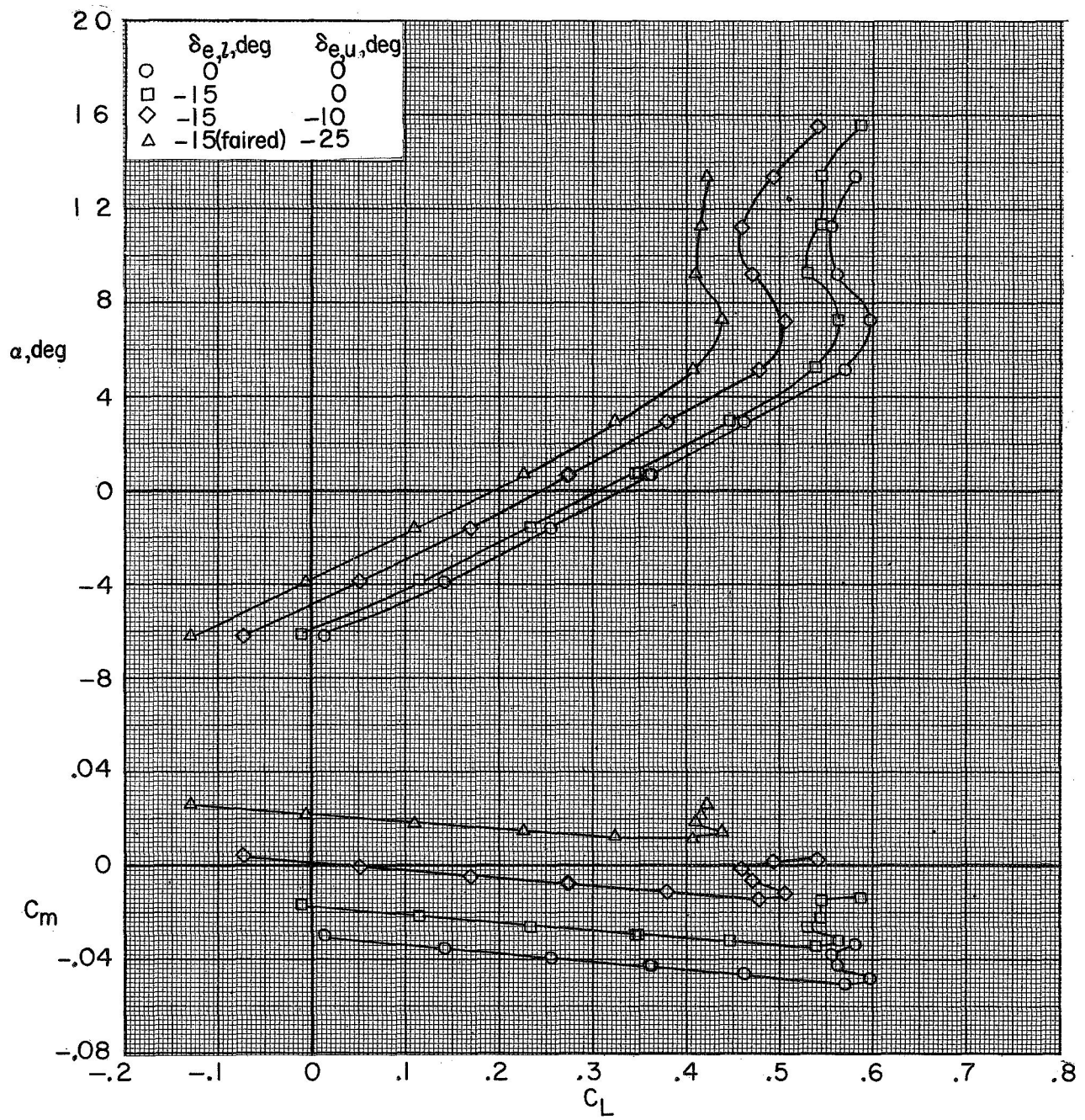

(b) M = 0.60.

Figure 8.- Continued.

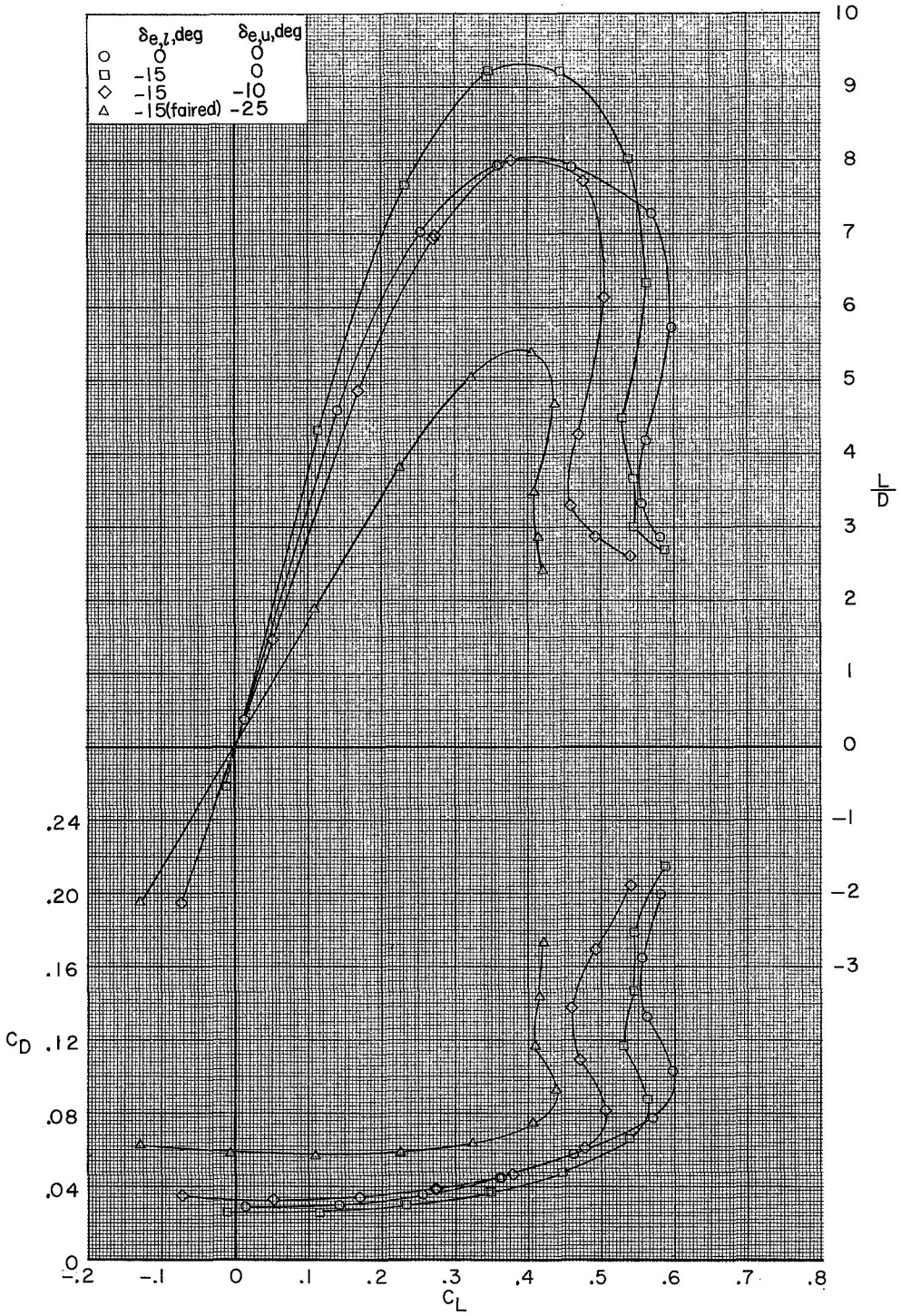

(b) Concluded.

Figure 8.- Continued.

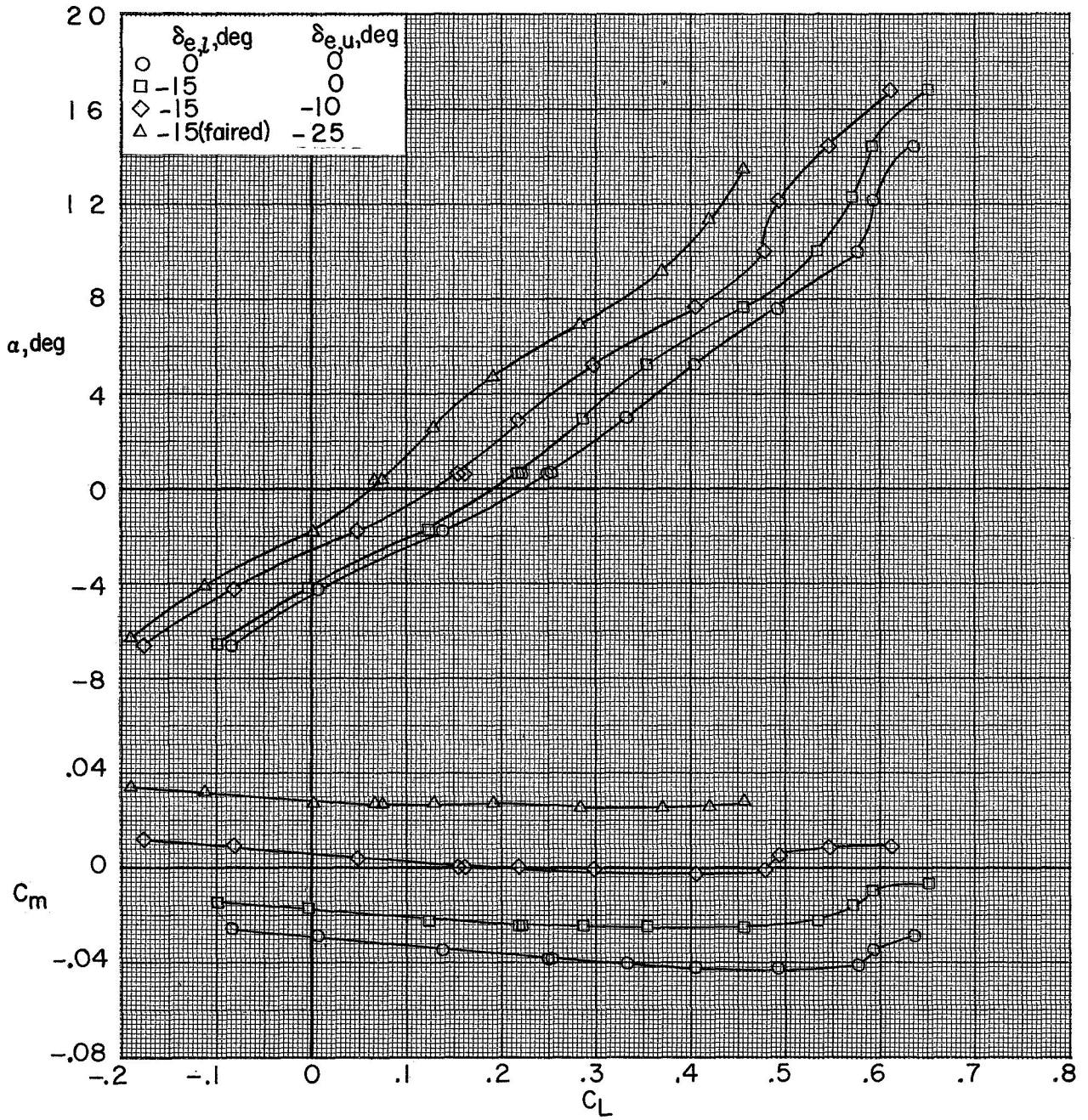

(c) M = 0.80.

Figure 8.- Continued.

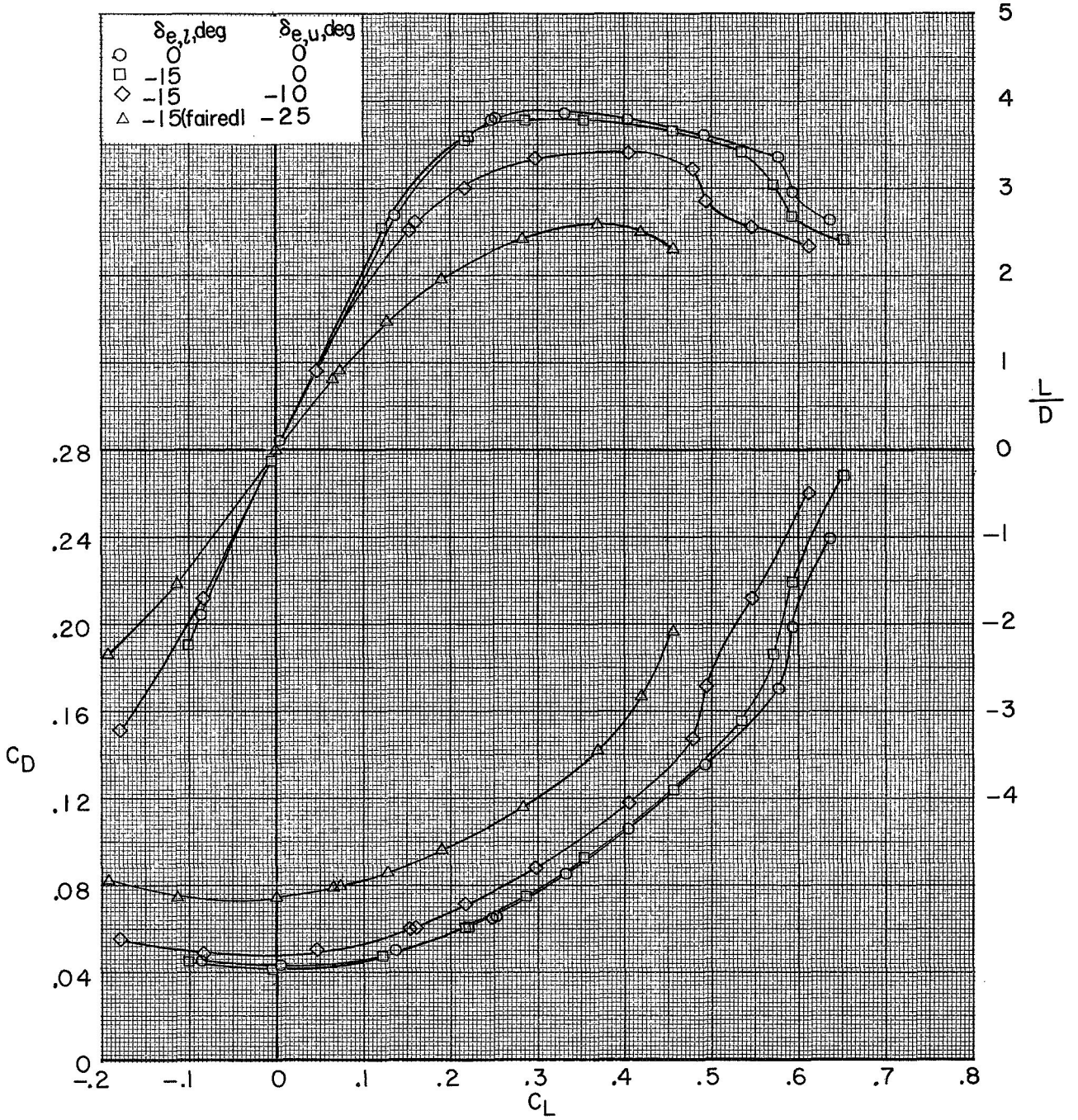

(c) Concluded.

Figure 8.- Continued.

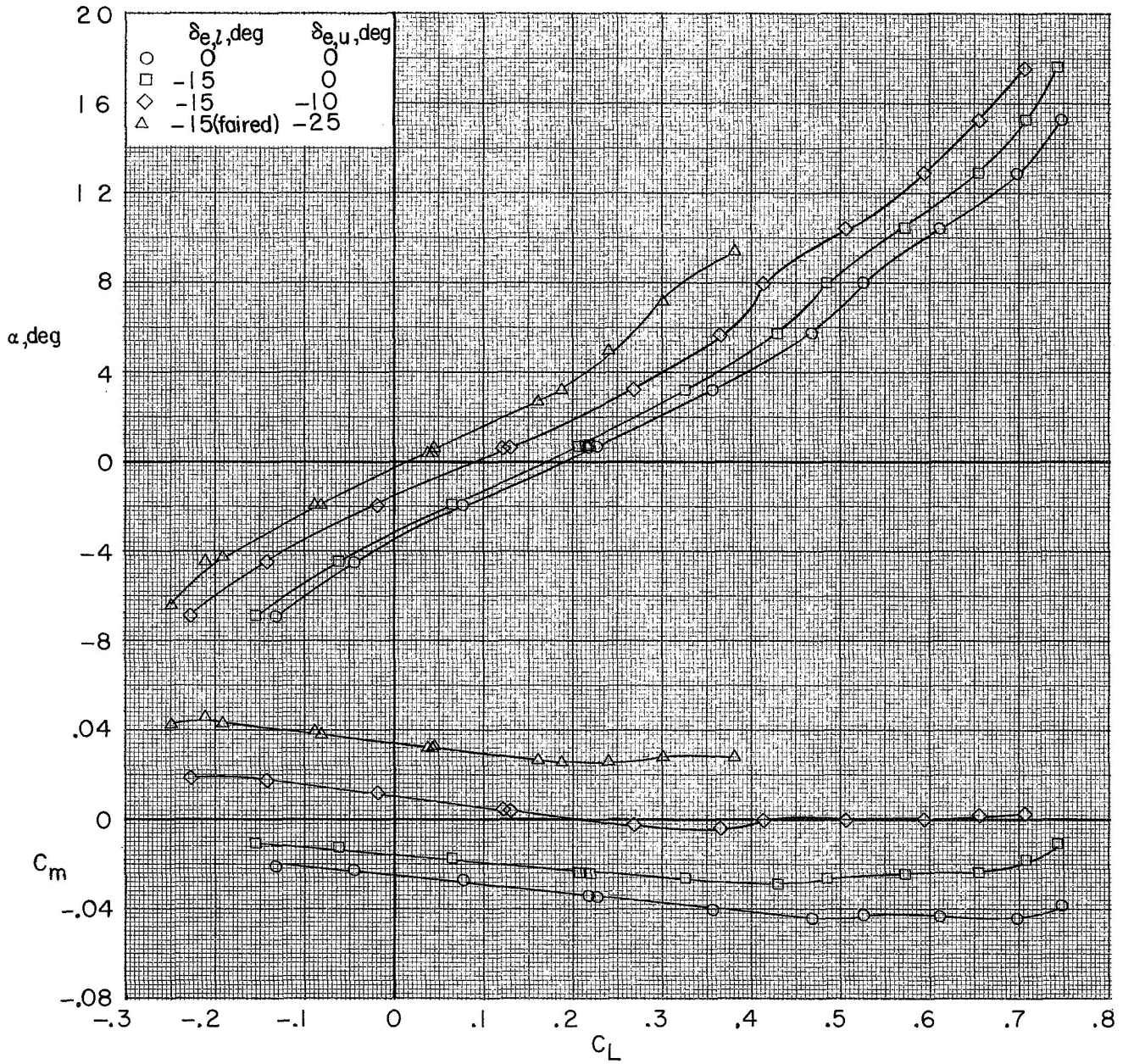

(d) M = 0.90.

Figure 8.- Continued.

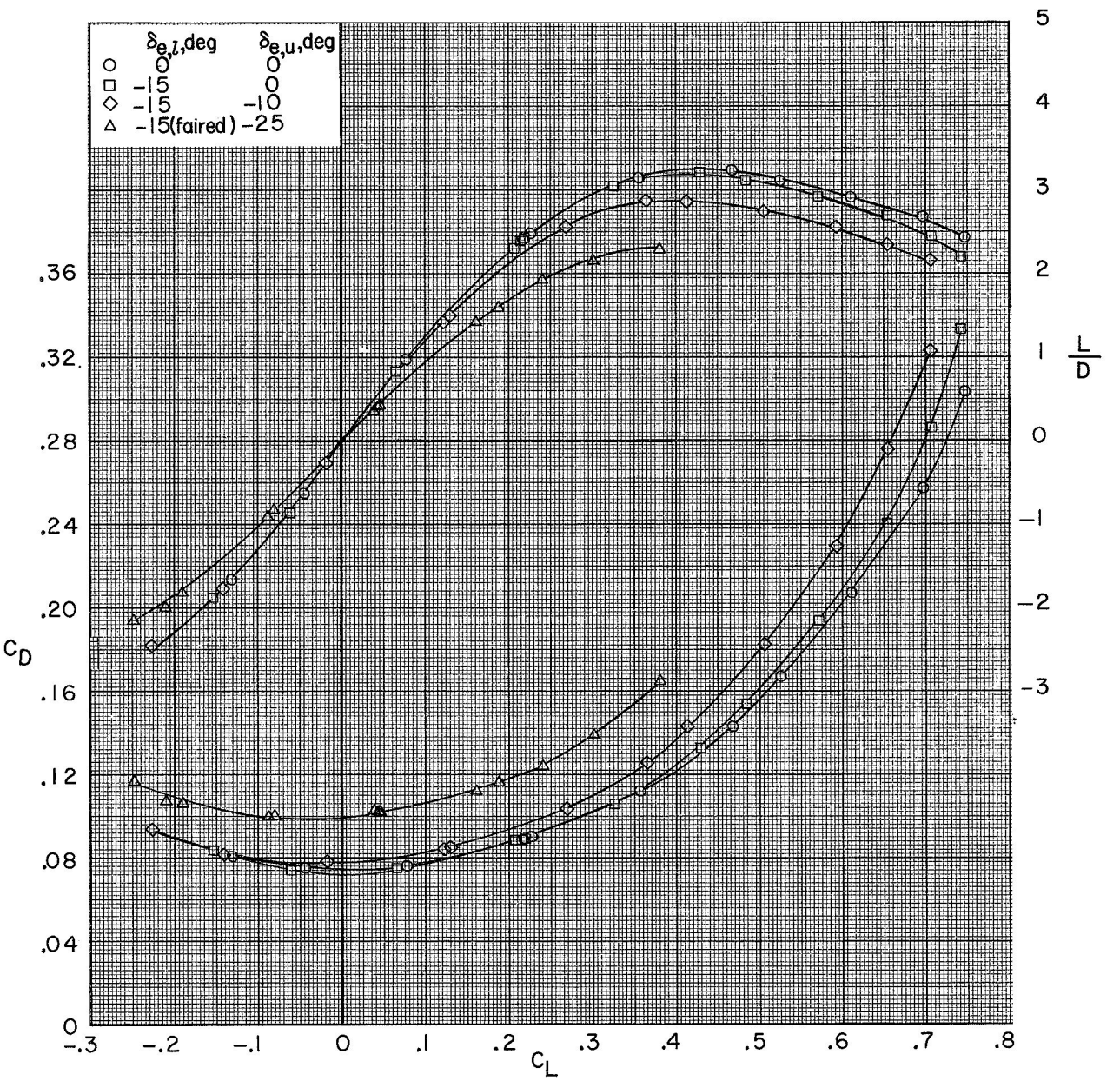

(d) Concluded.

Figure 8.- Concluded.

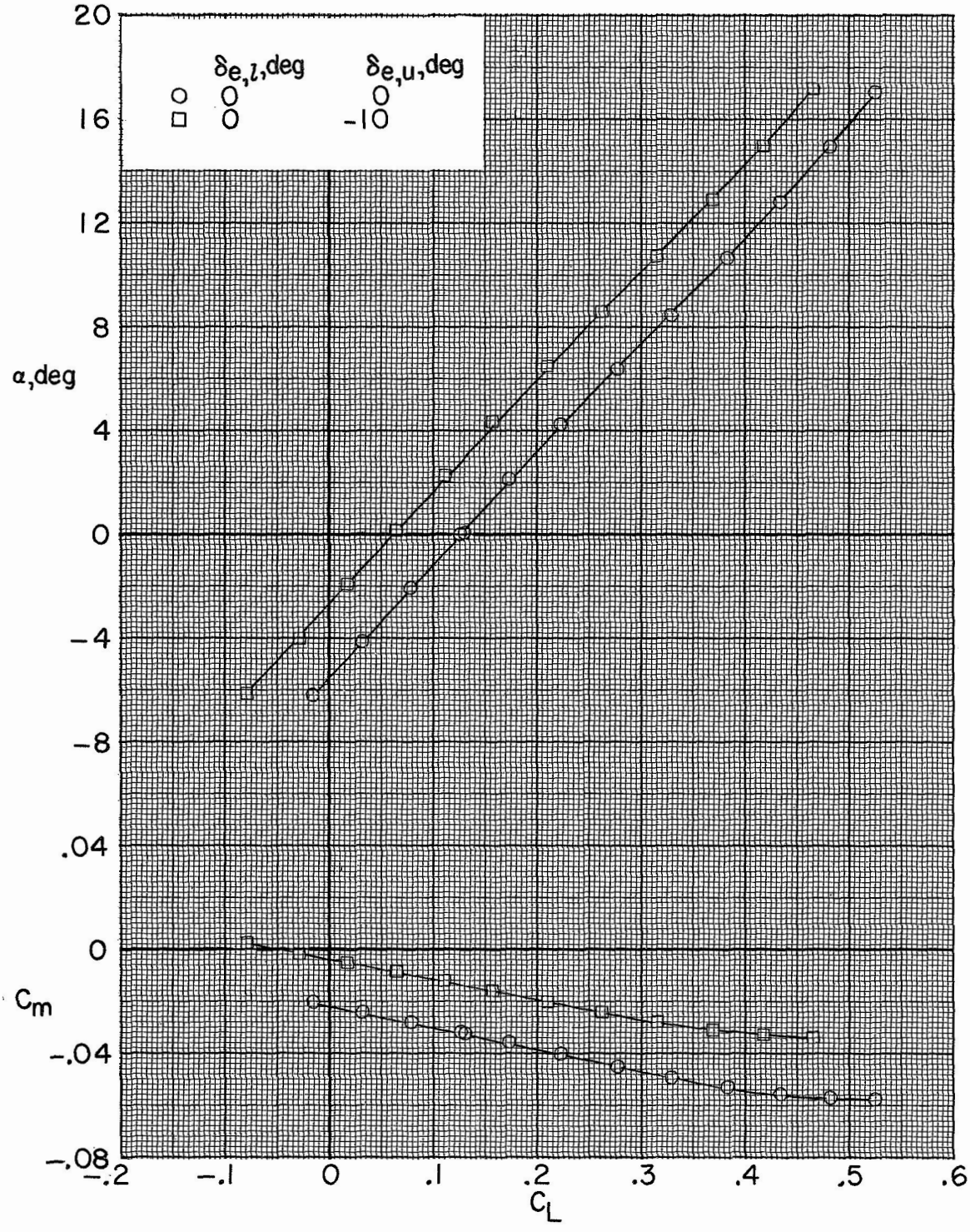

(a) M = 0.60.

Figure 9.- Effect of elevon deflections on the longitudinal aerodynamic characteristics of the model with wings deployed to $\Lambda = 75^0$.

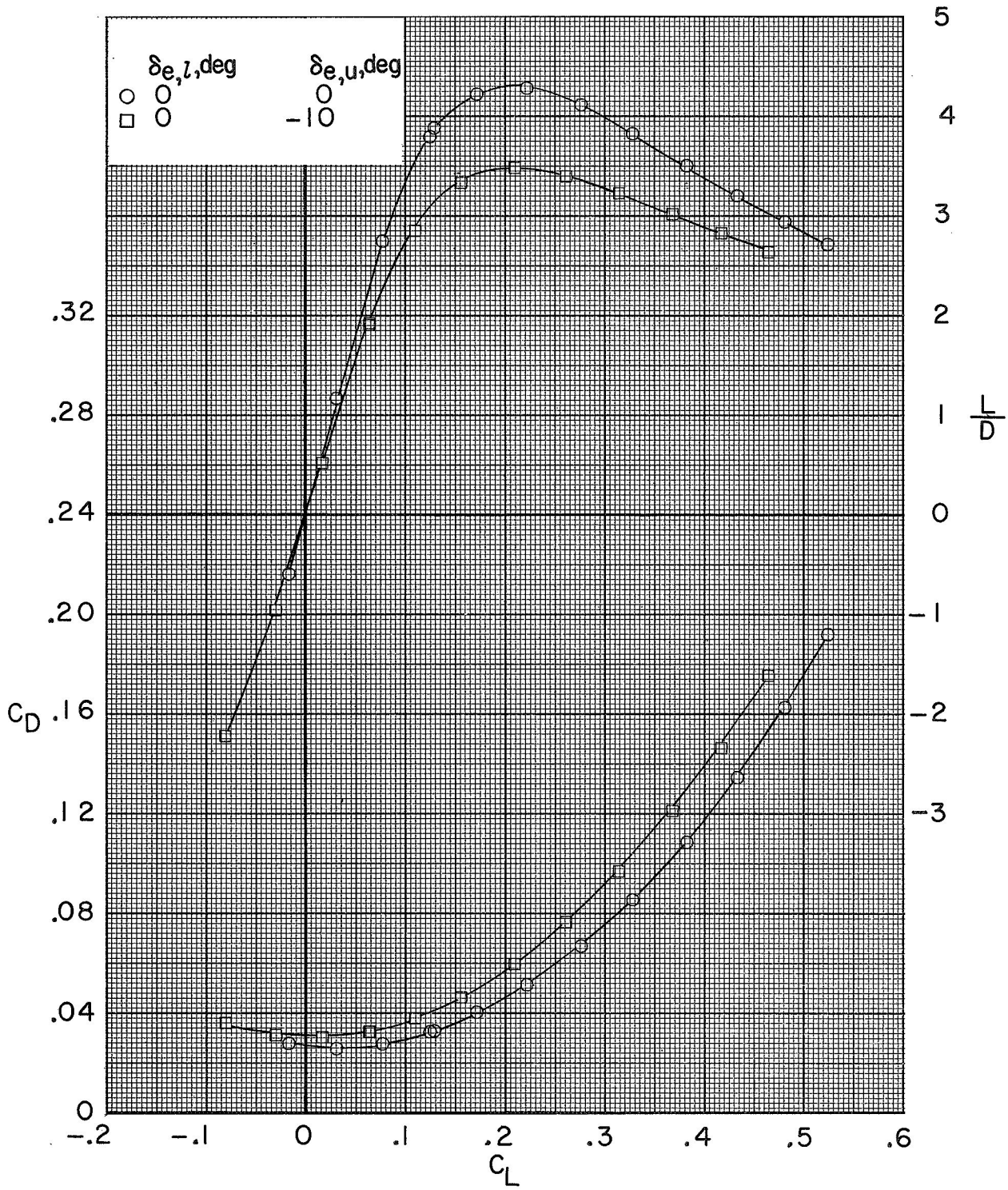

(a) Concluded.

Figure 9.- Continued.

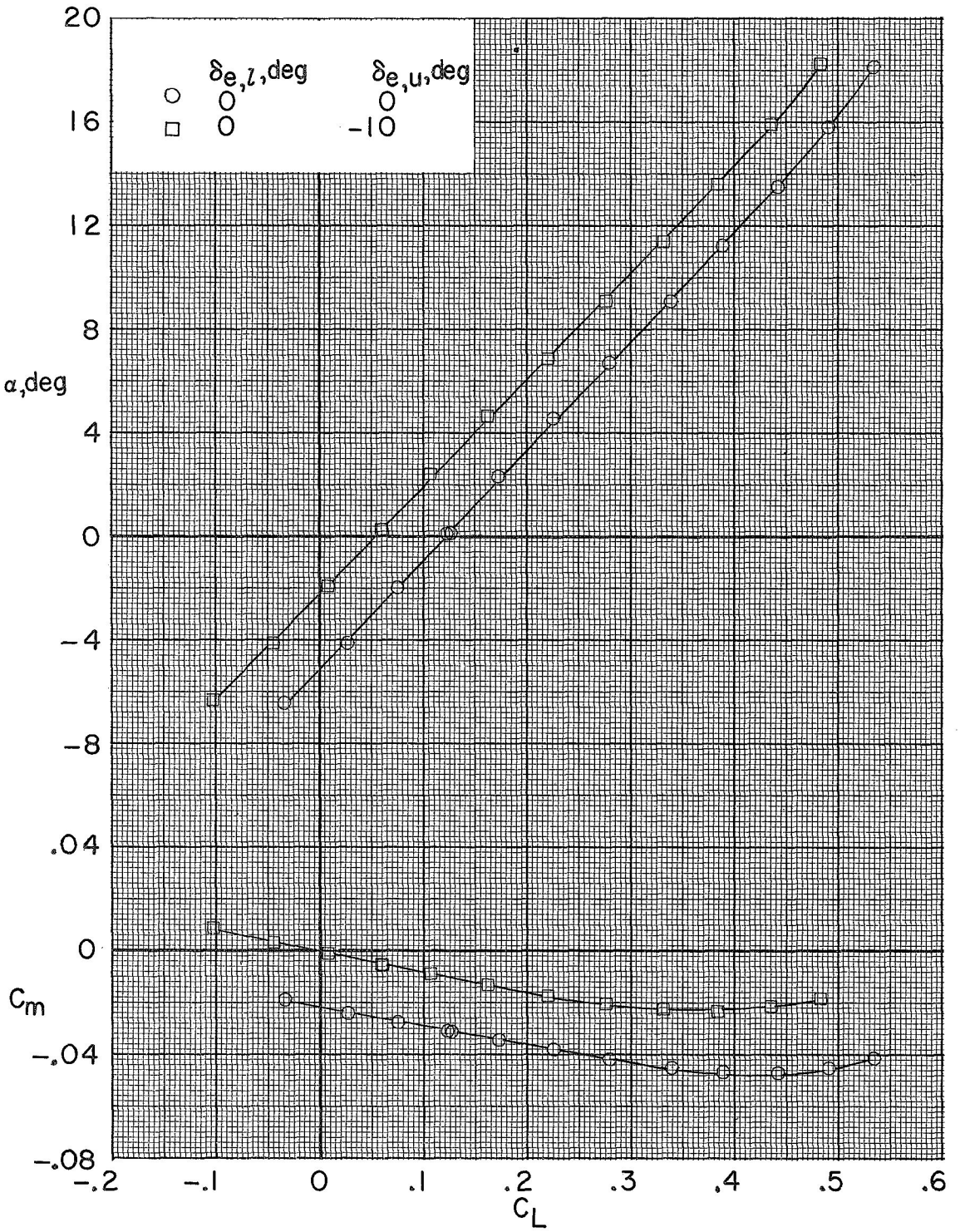

(b) M = 0.90.

Figure 9.- Continued.

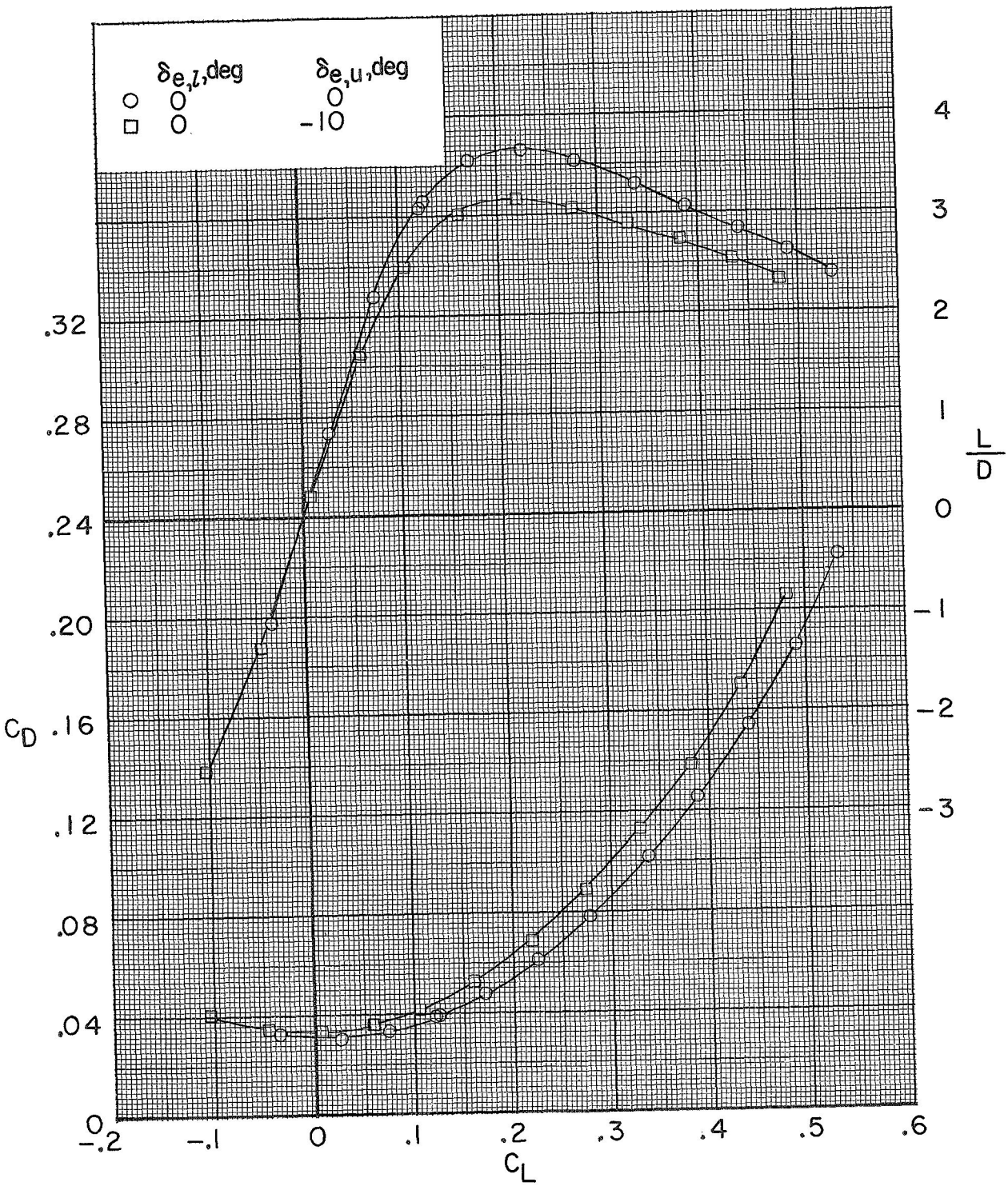

(b) Concluded.

Figure 9.- Continued.

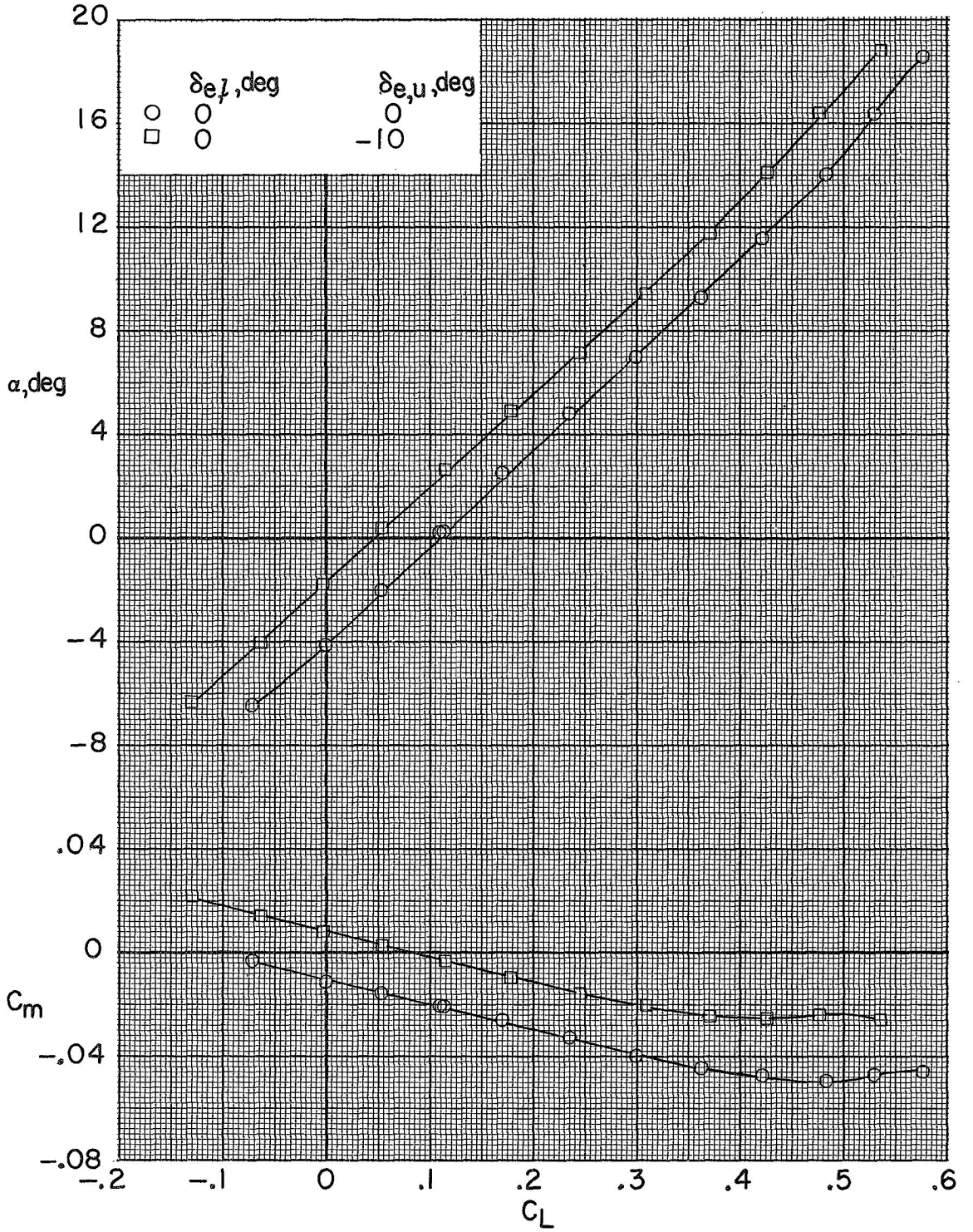

(c) M = 1.00.

Figure 9.- Continued.

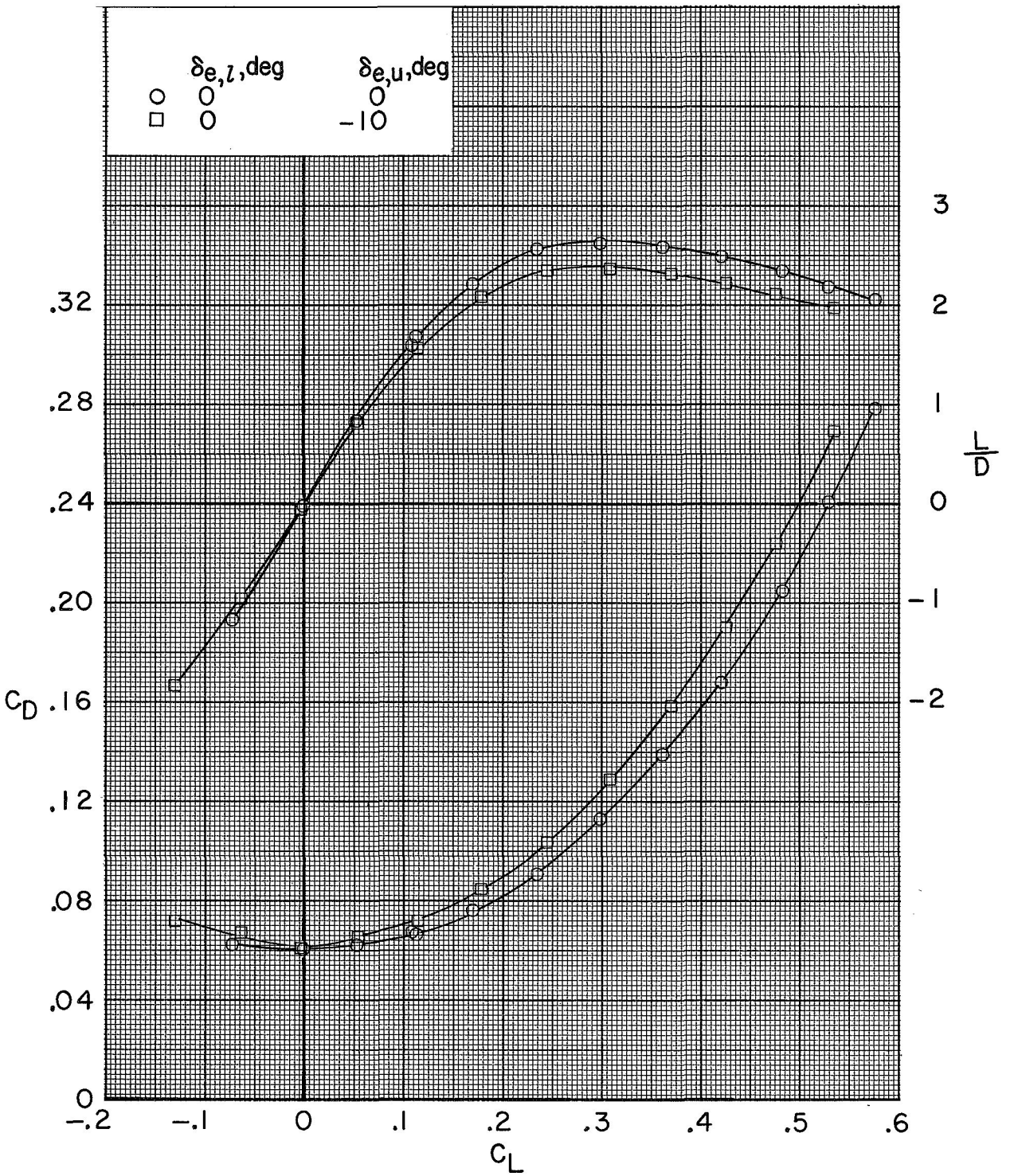

(c) Concluded.

Figure 9.- Continued.

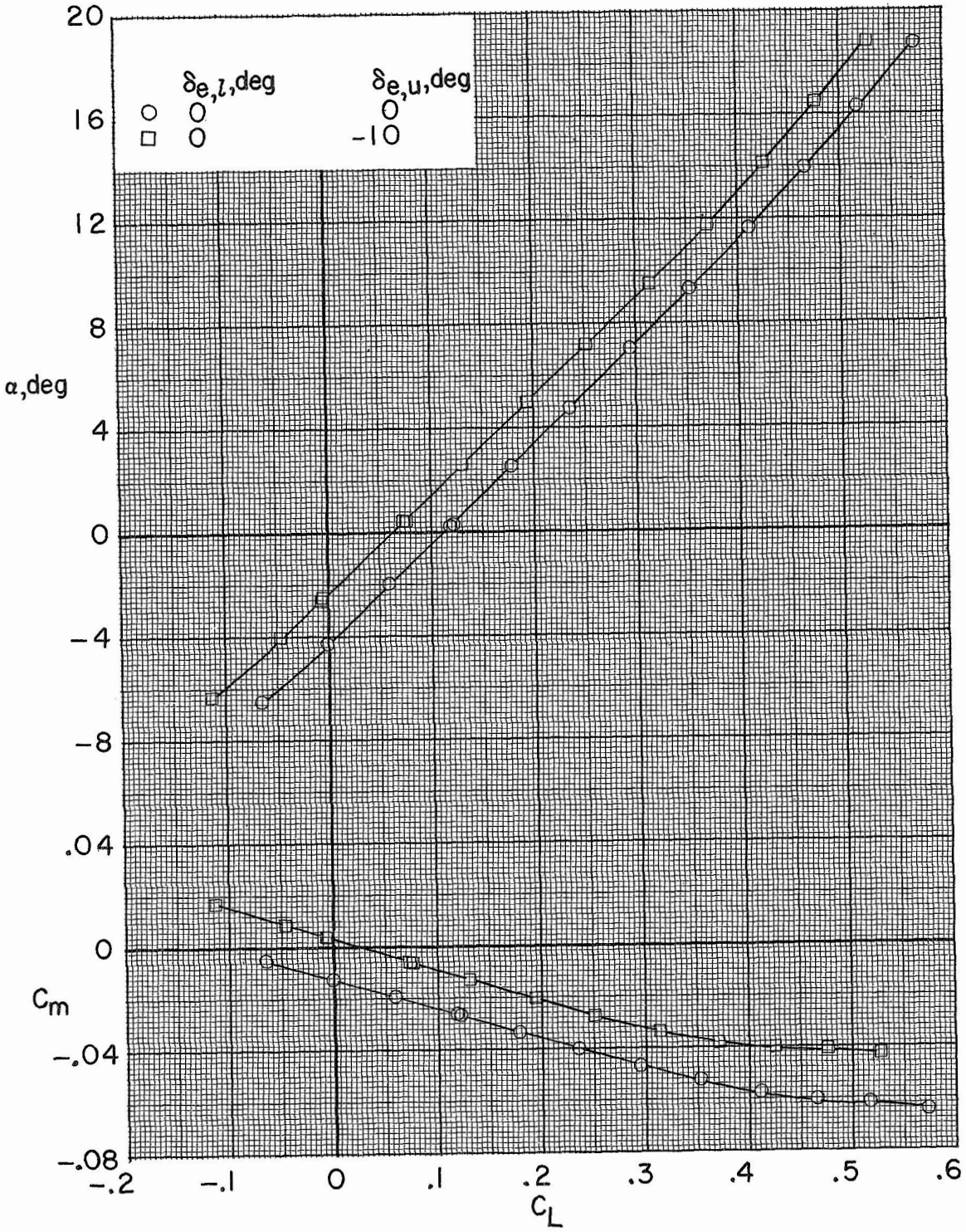

(d) M = 1.20.

Figure 9.- Continued.

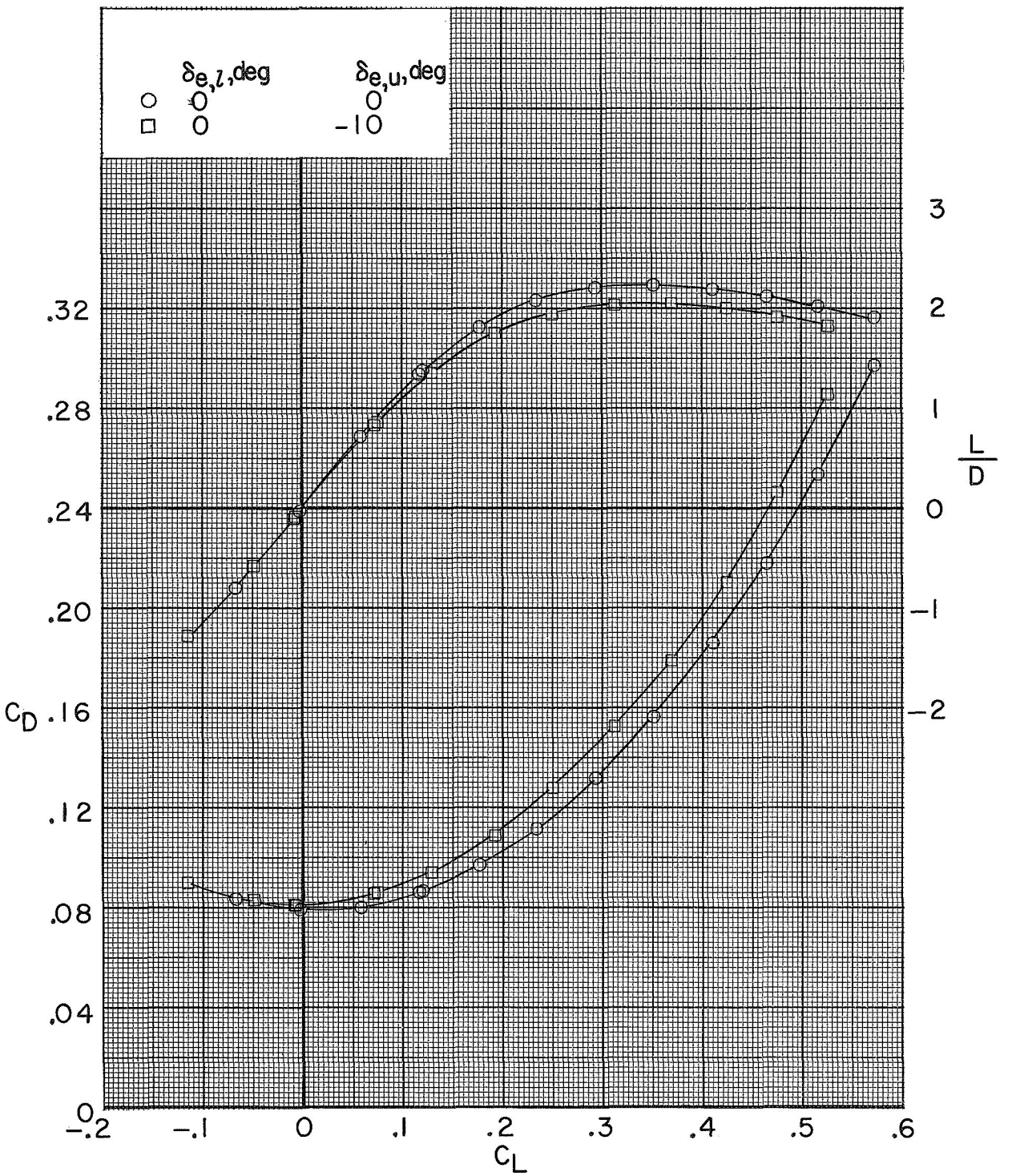

(d) Concluded.

Figure 9.- Concluded.

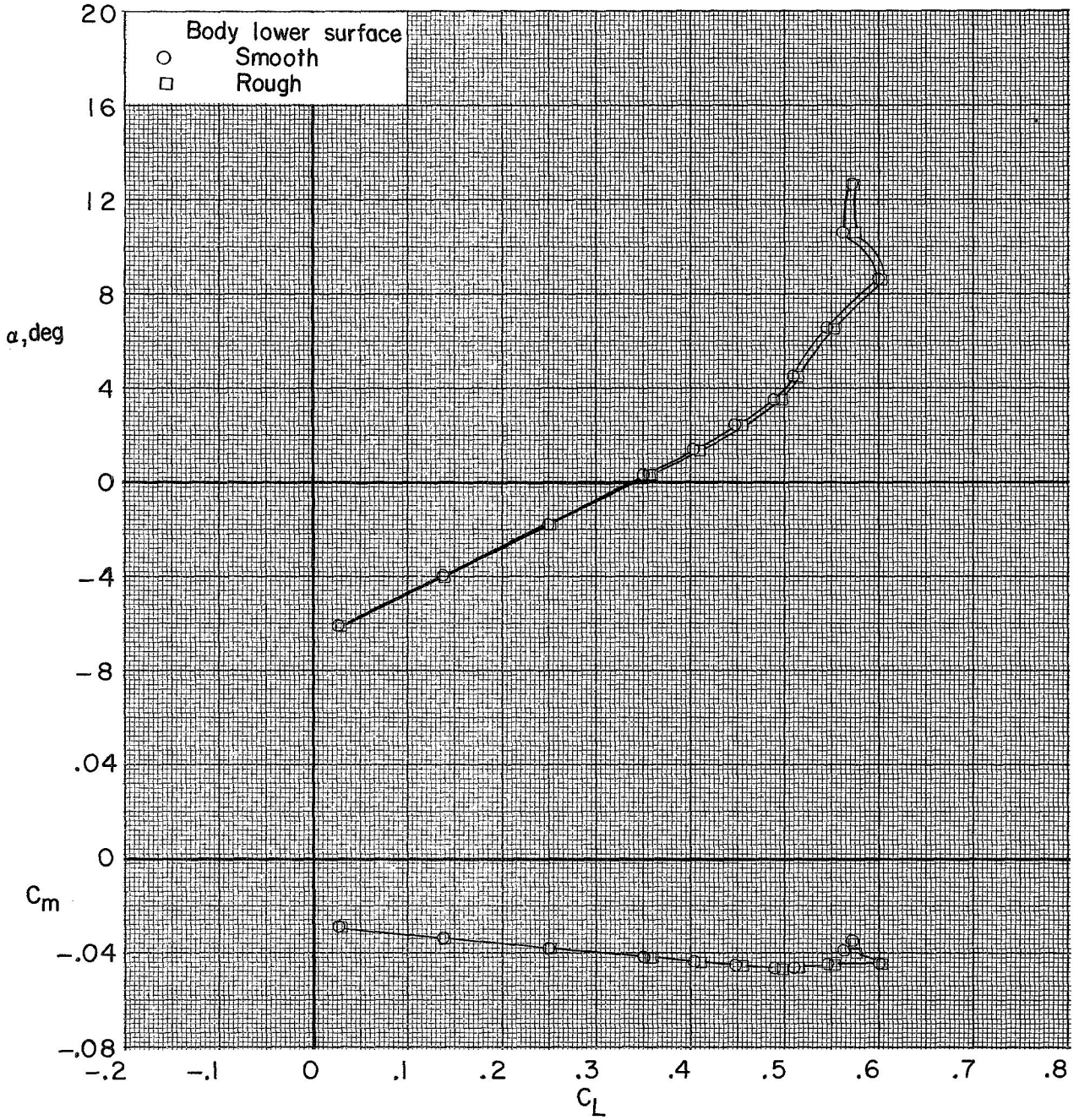

(a) M = 0.40.

Figure 10.- Effect of thermal-protection-system roughness on the longitudinal aerodynamic characteristics of the model with wings deployed to $\Lambda = 20^0$. $\delta_{e,l} = 0^0$; $\delta_{e,u} = 0^0$.

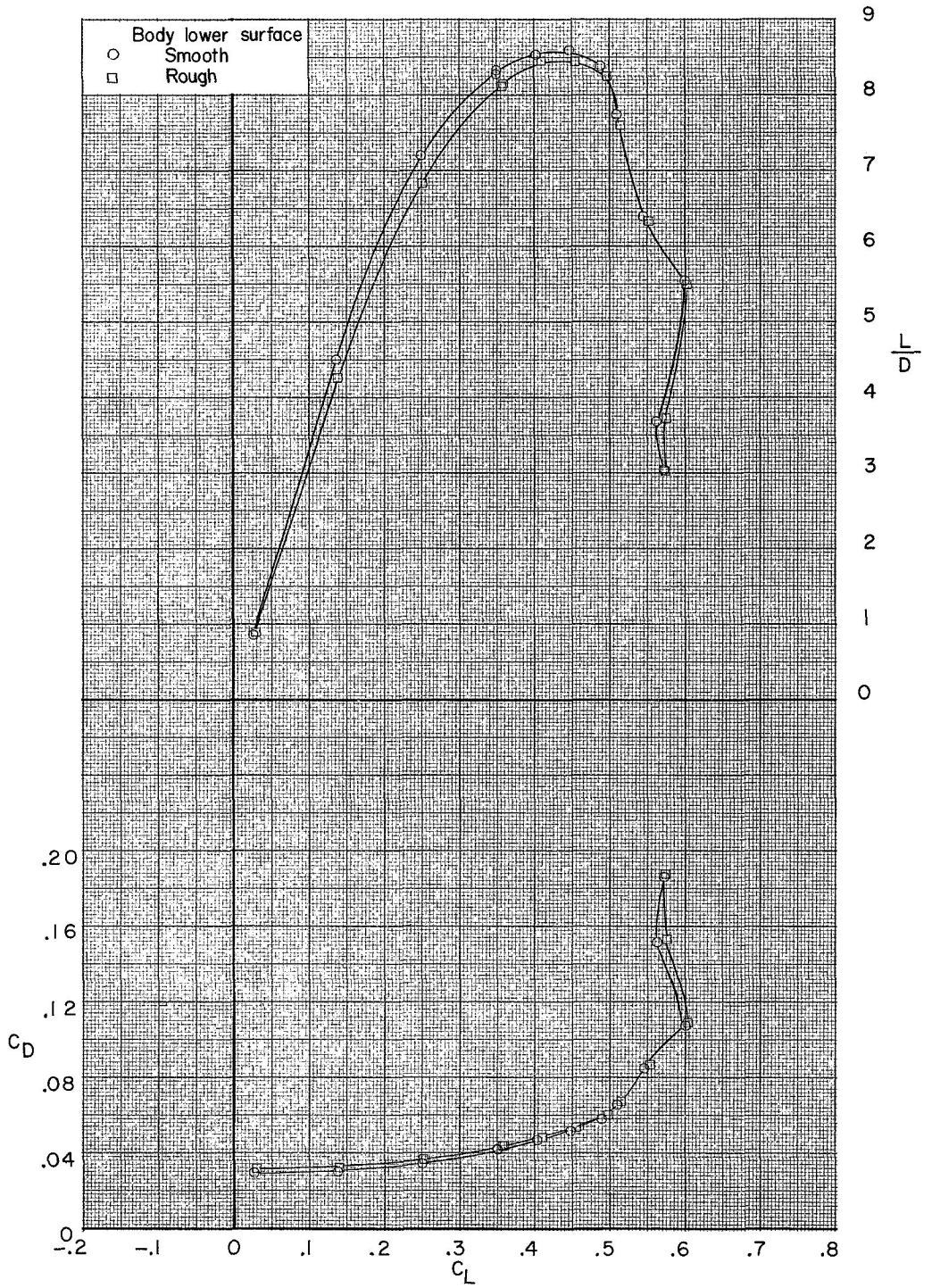

(a) Concluded.

Figure 10.- Continued.

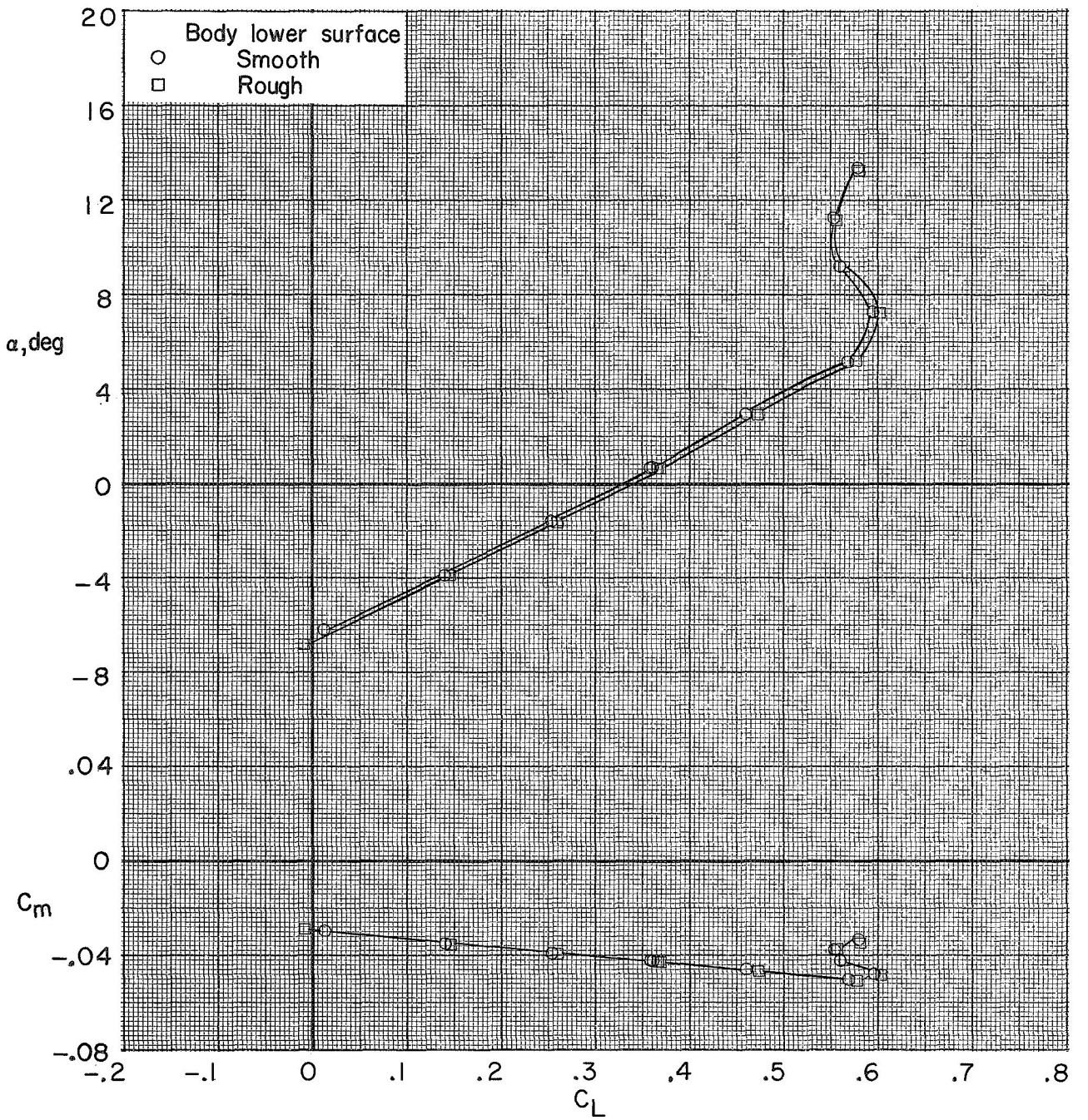

(b) M = 0.60.

Figure 10.- Continued.

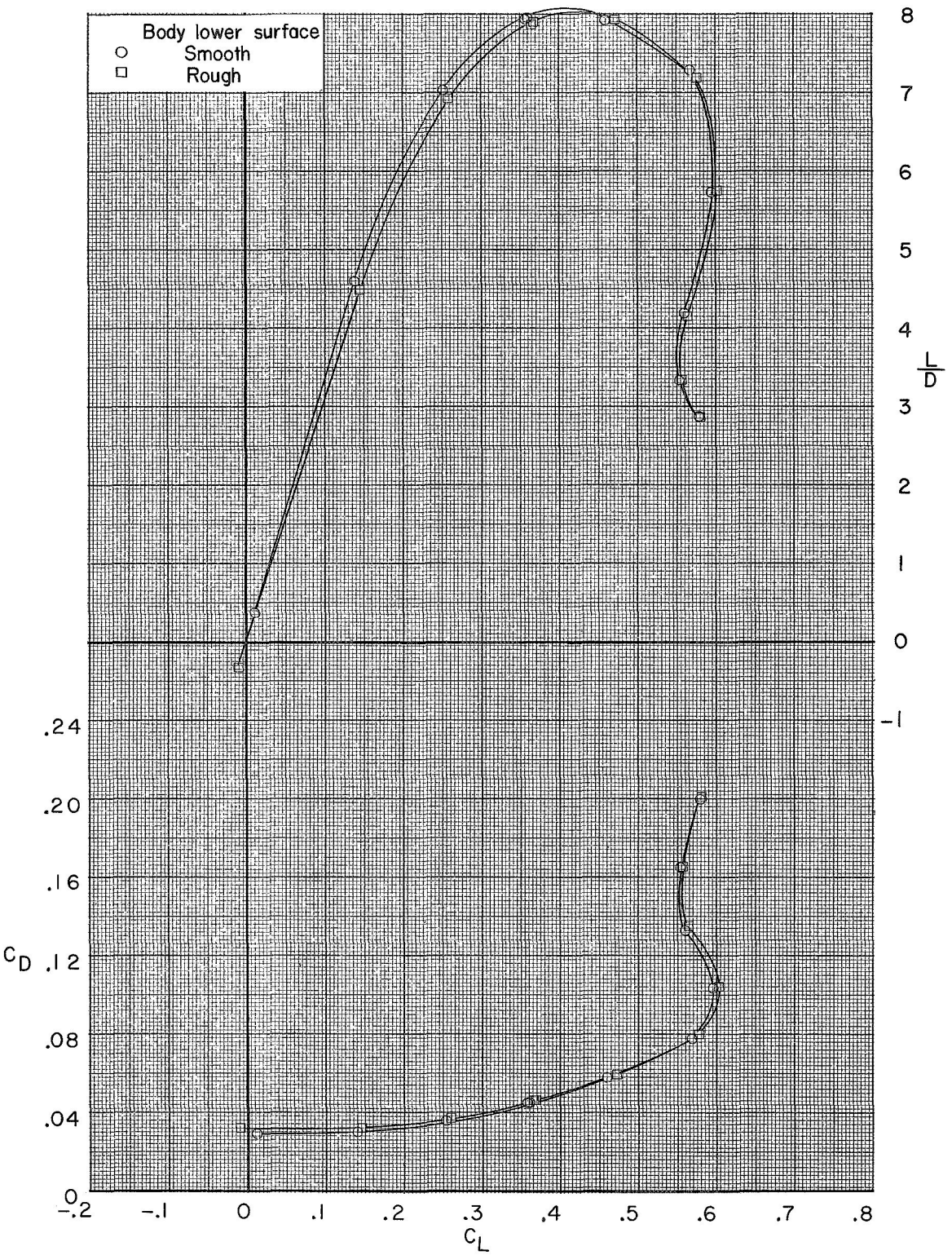

(b) Concluded.

Figure 10.- Continued.

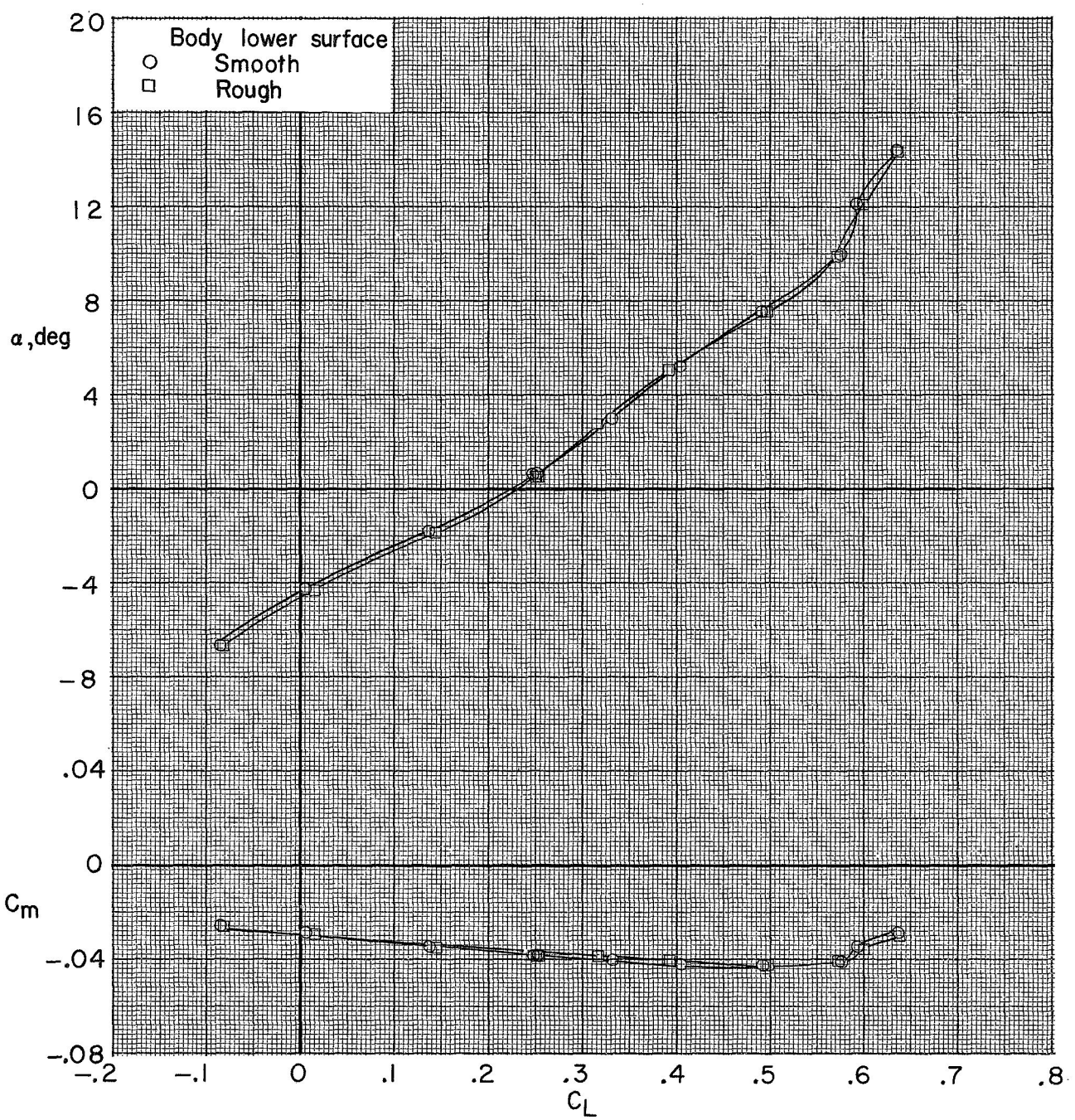

(c) M = 0.80.

Figure 10.- Continued.

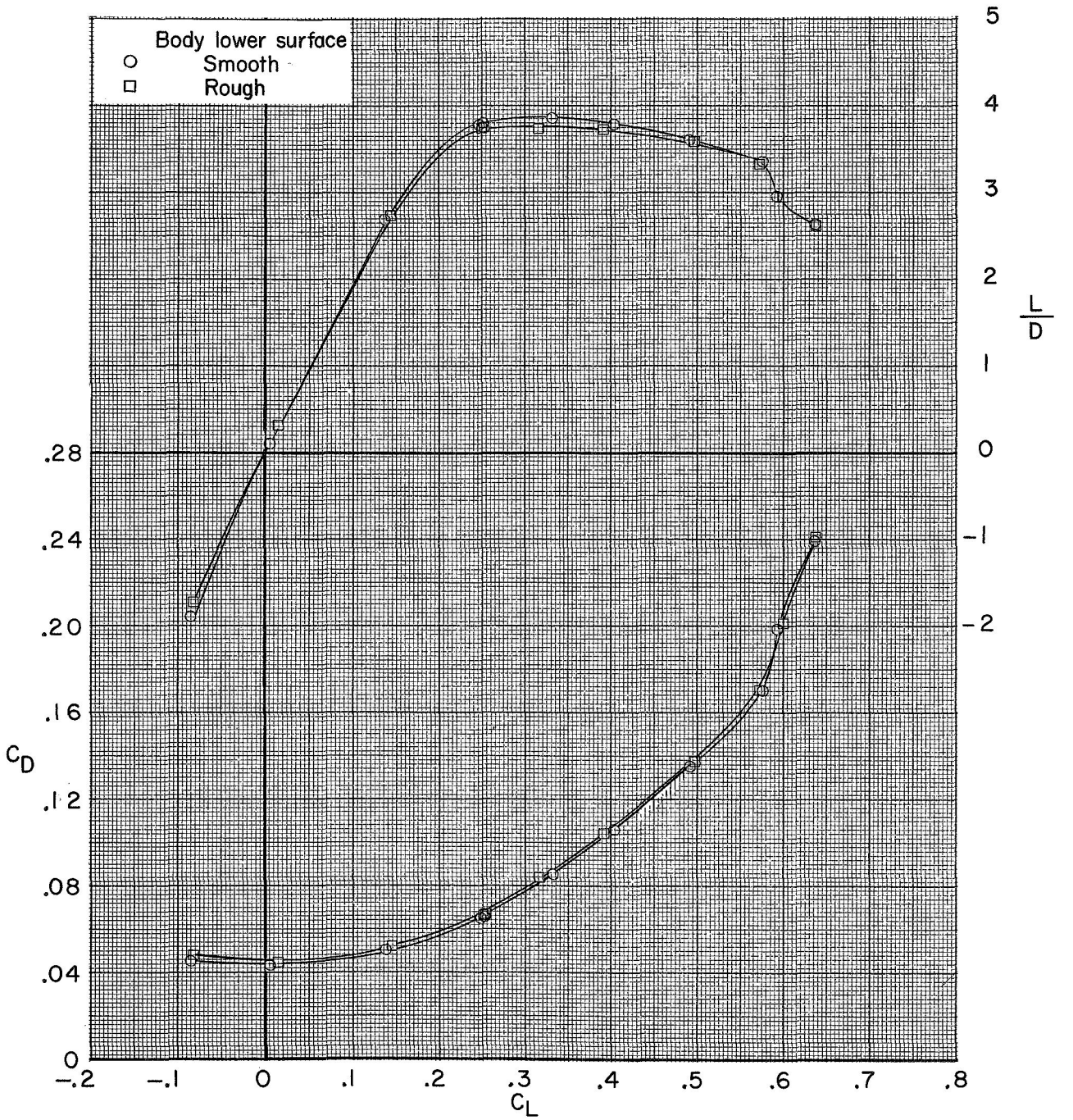

(c) Concluded.

Figure 10.- Continued.

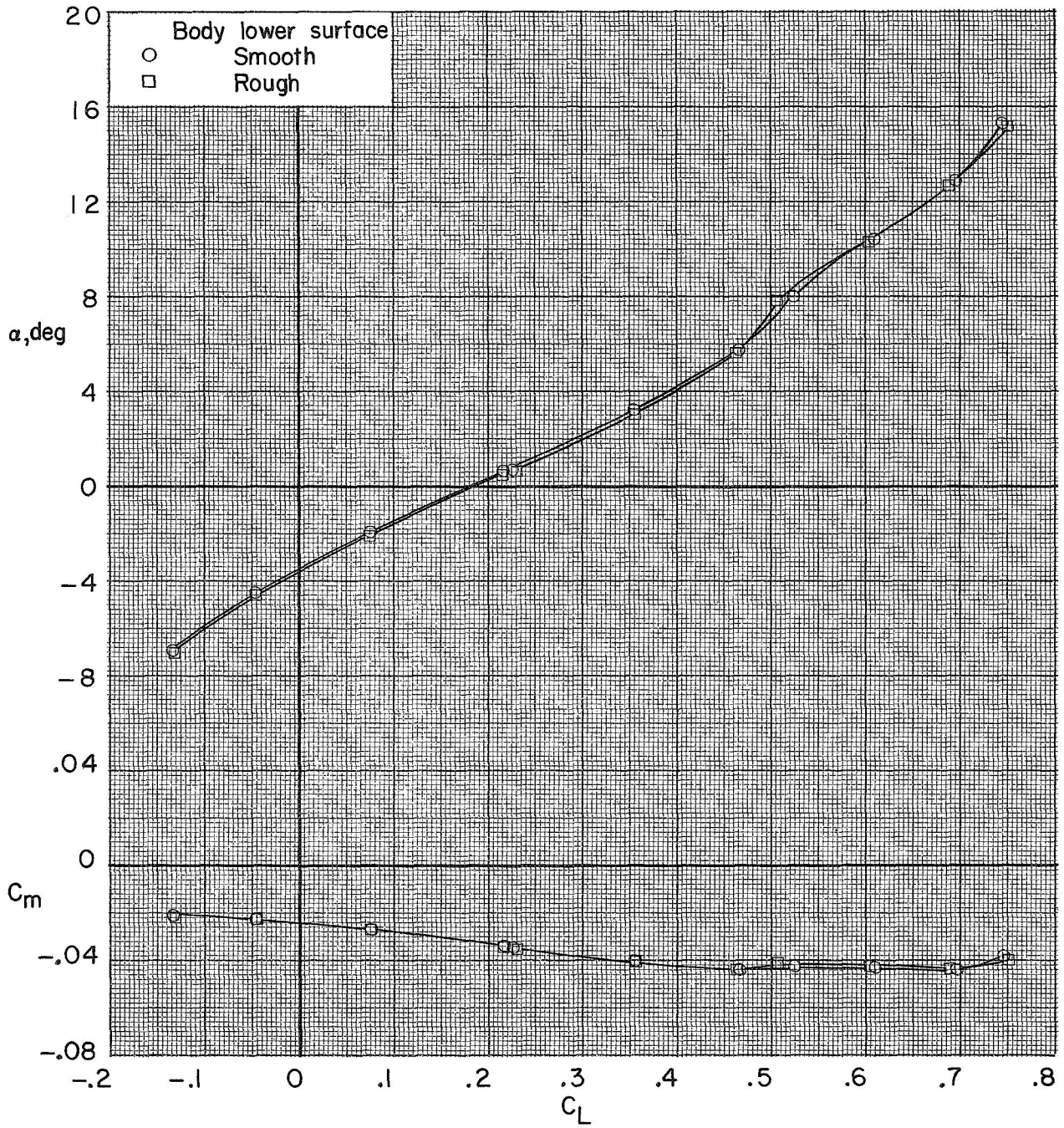

(d) M = 0.90.

Figure 10.- Continued.

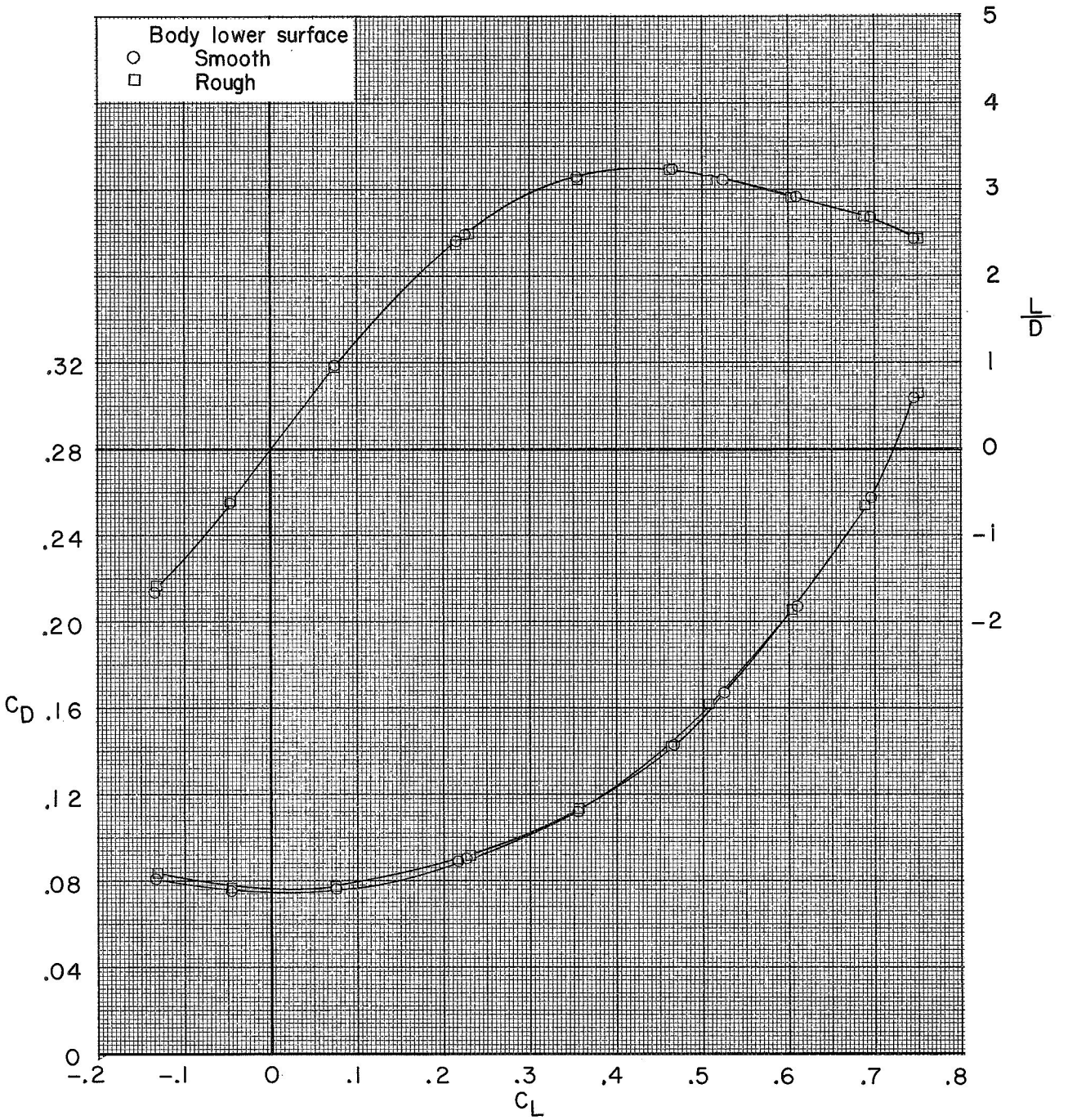

(d) Concluded.

Figure 10.- Concluded.

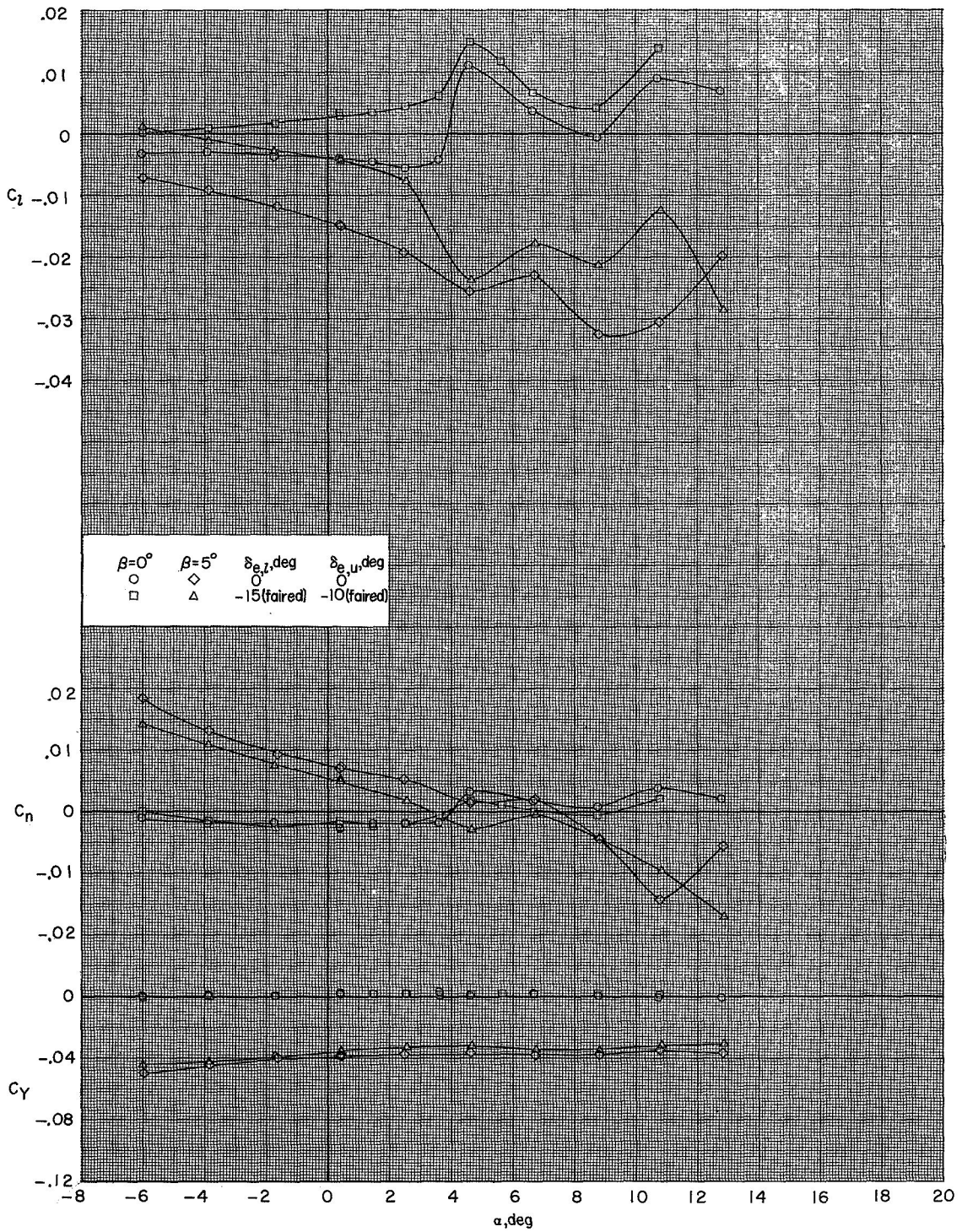

(a) M = 0.40.

Figure 11.- Lateral-directional aerodynamic characteristics of the model with wings deployed to $\Lambda = 20^0$.

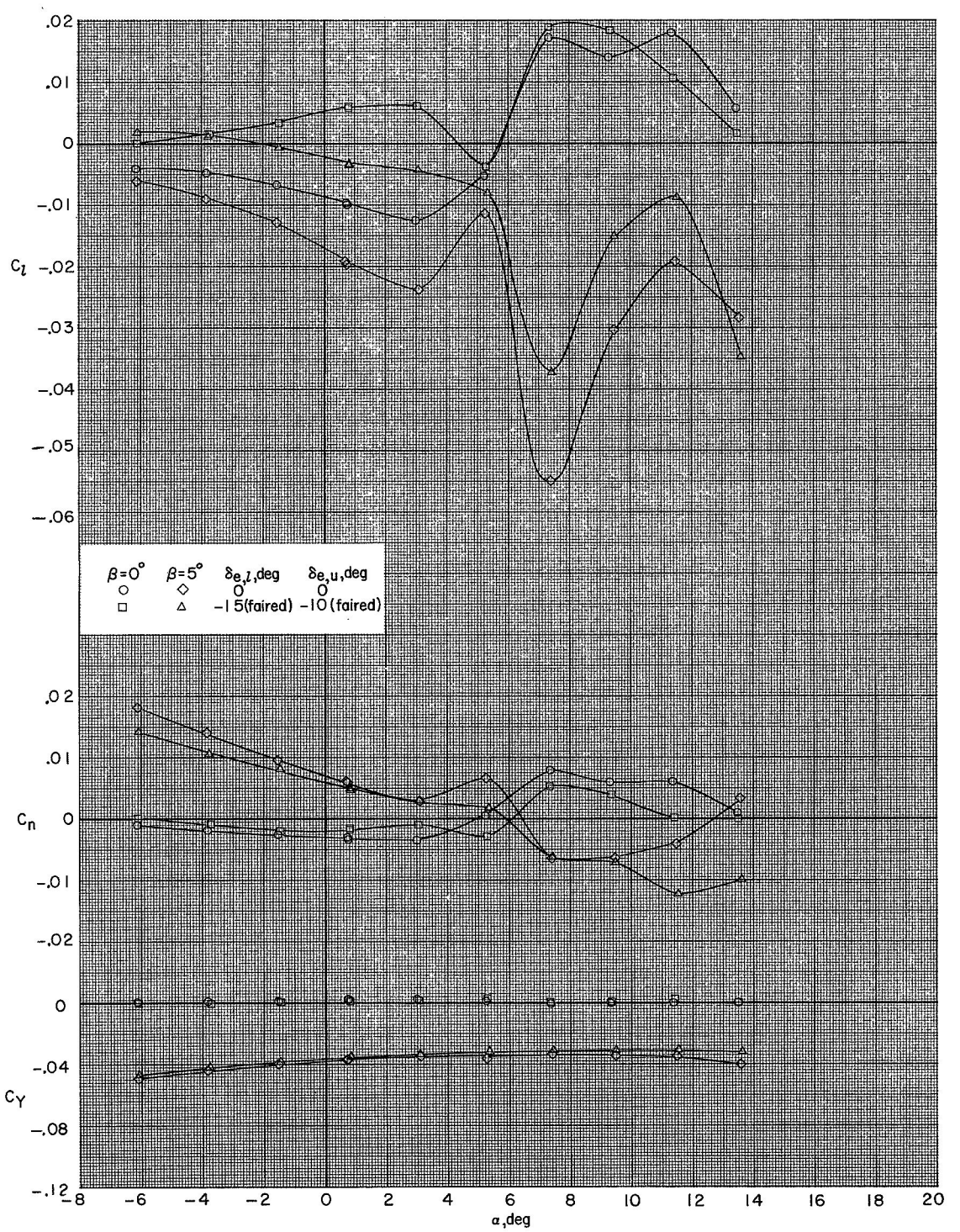

(b) M = 0.60.

Figure 11.- Continued.

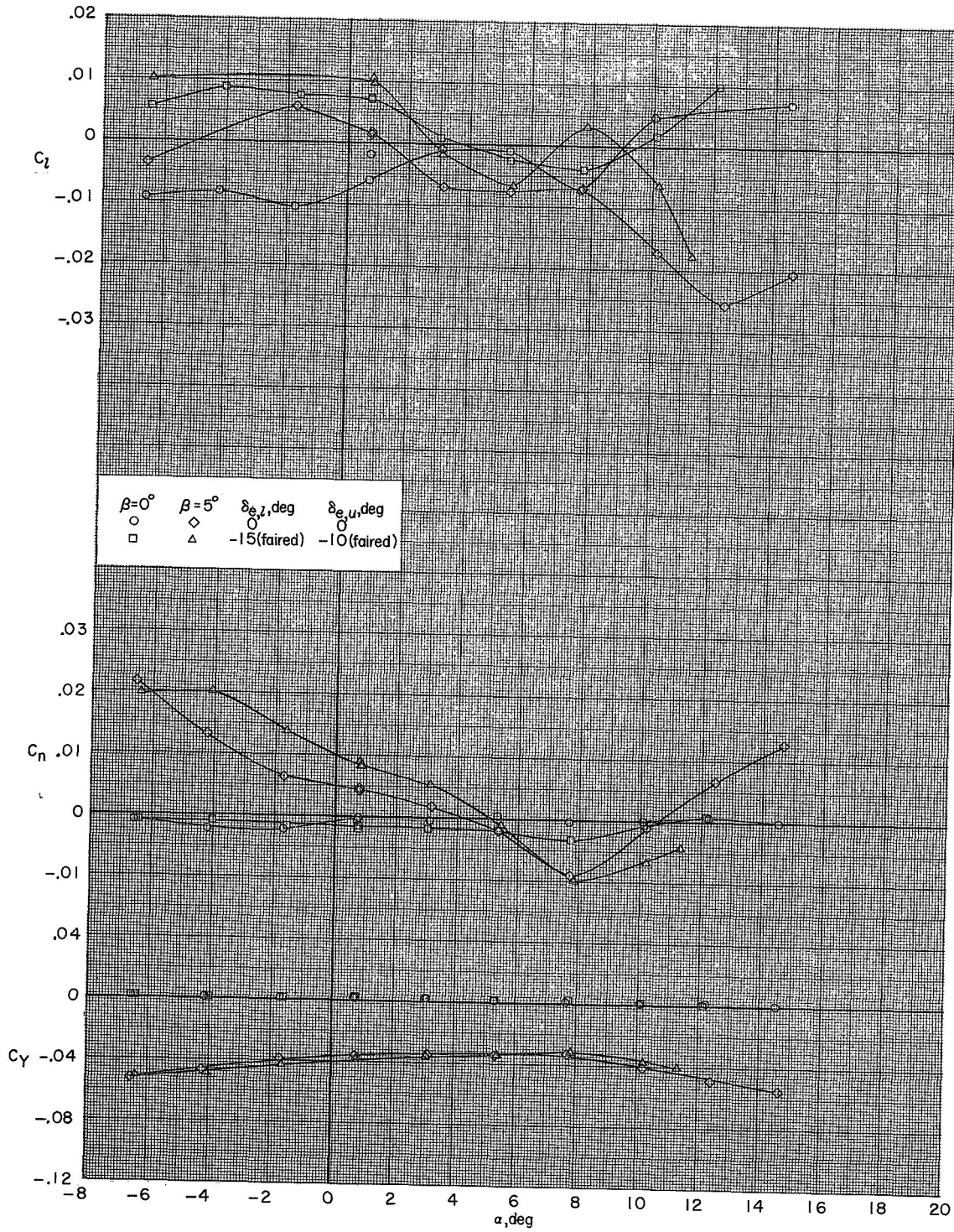

(c) M = 0.80.

Figure 11.- Continued.

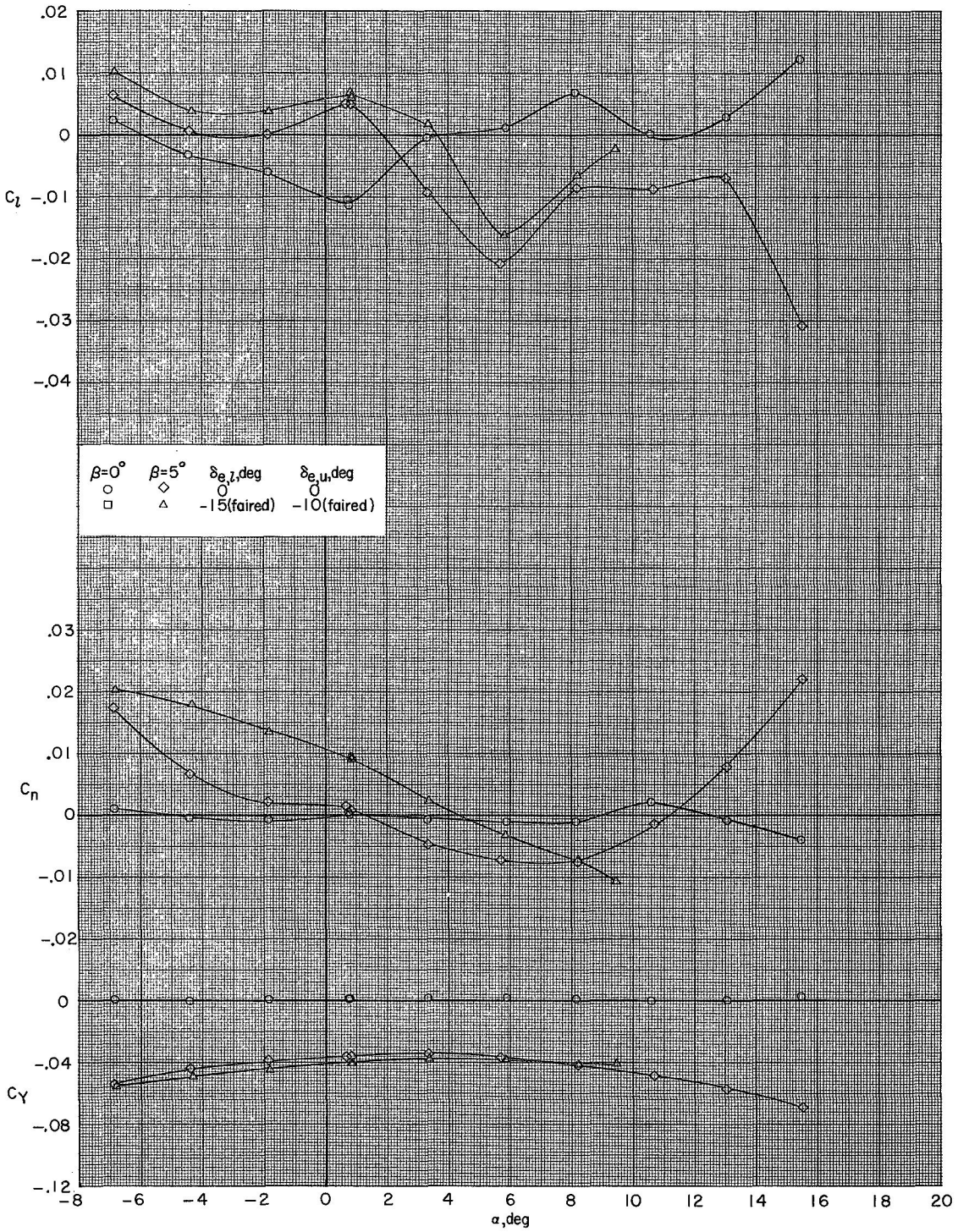

(d) M = 0.90.

Figure 11.- Concluded.

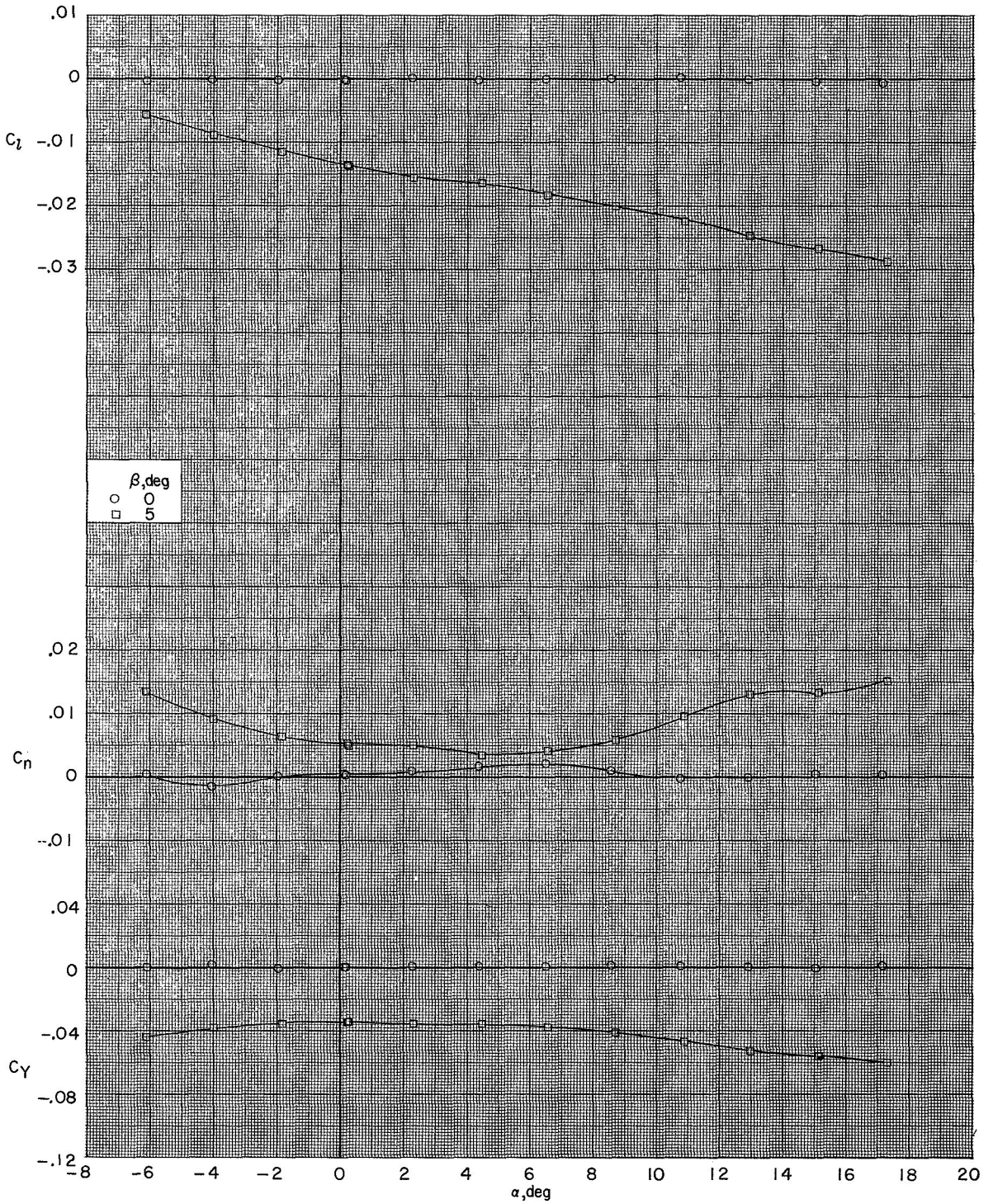

(a) M = 0.60.

Figure 12.- Lateral-directional aerodynamic characteristics of the model with wings deployed to $\Lambda = 75^0$. $\delta_{e,l} = 0^0$; $\delta_{e,u} = 0^0$.

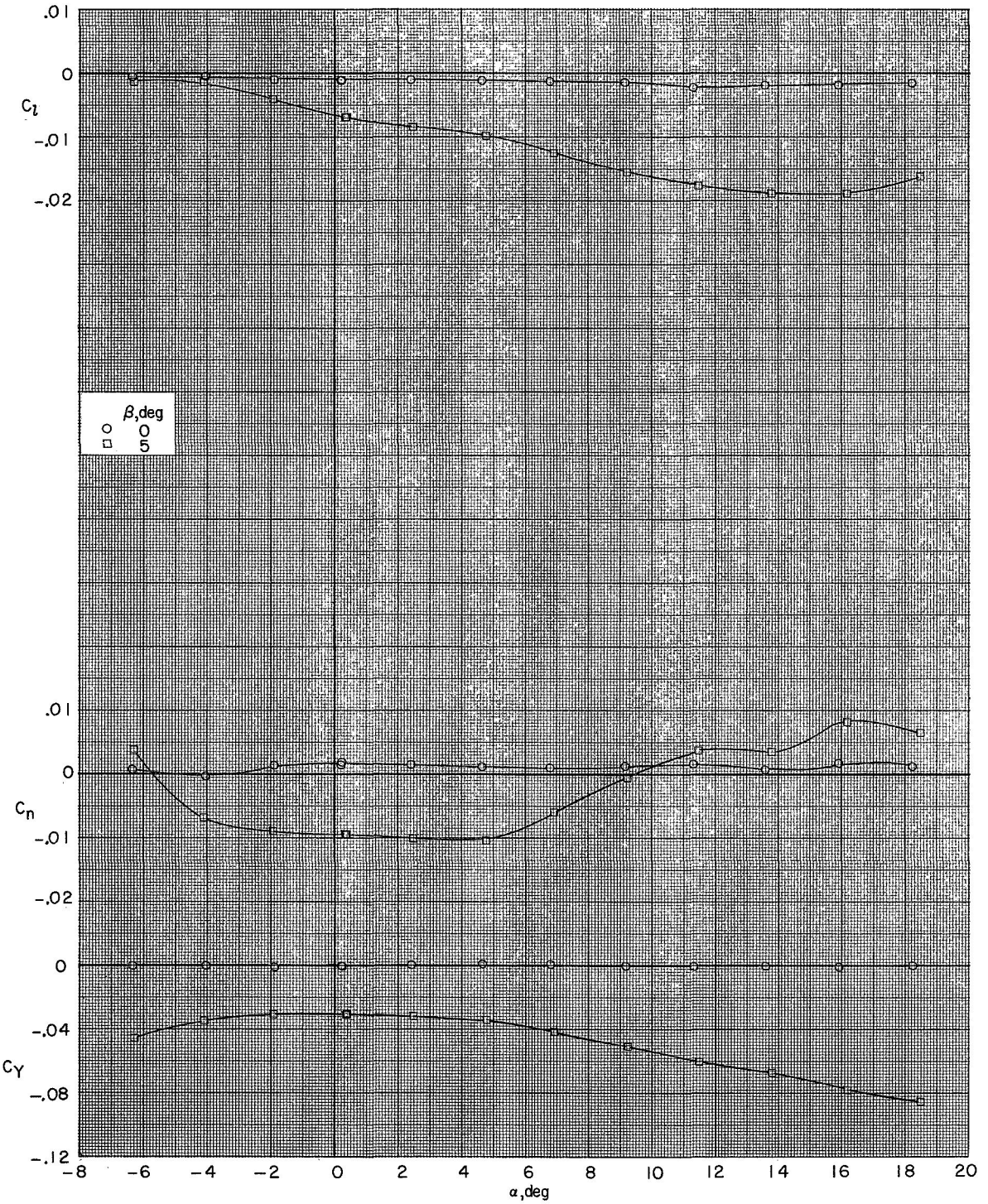

(b) M = 0.90.

Figure 12.- Continued.

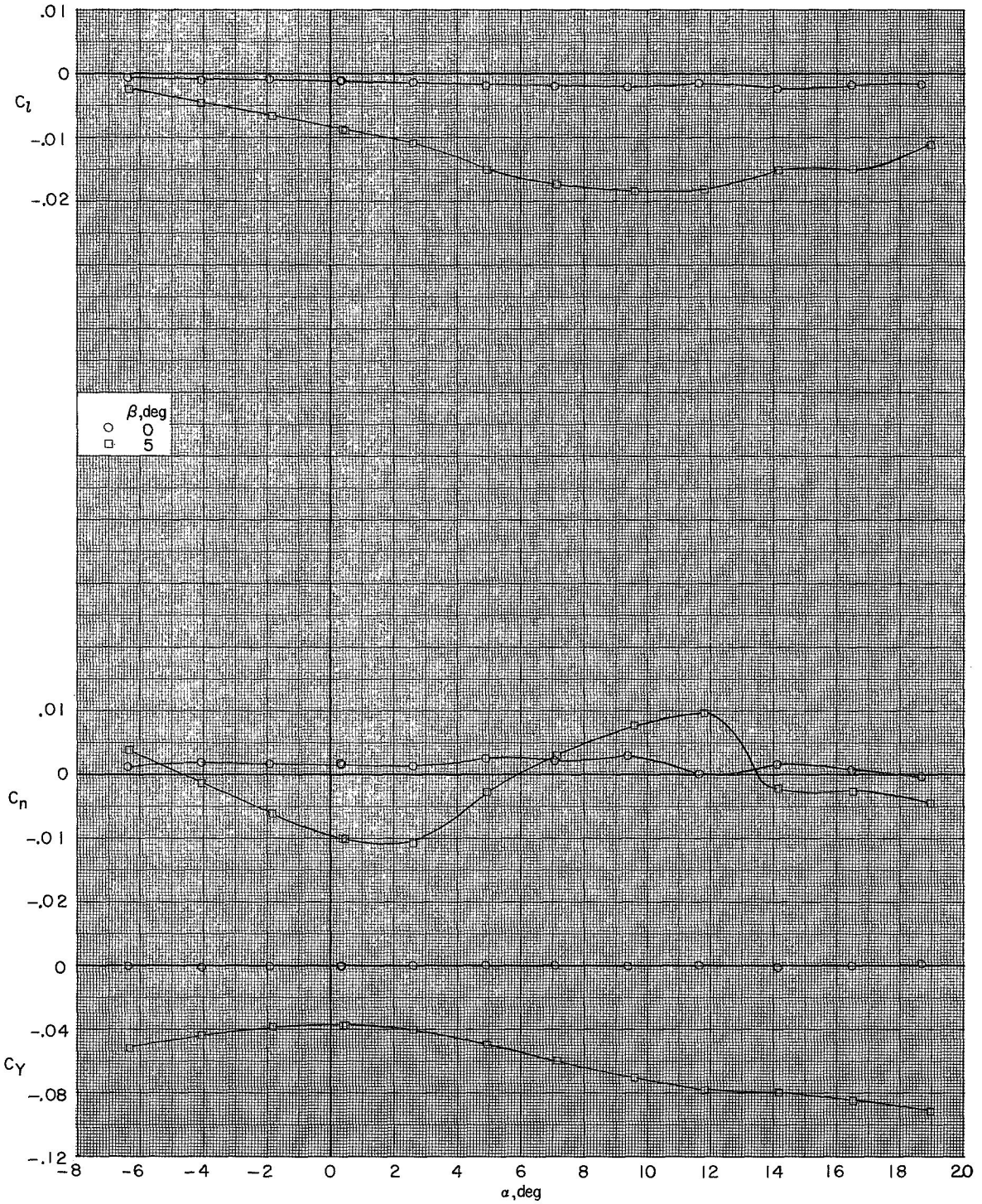

(c) M = 1.00.

Figure 12.- Continued.

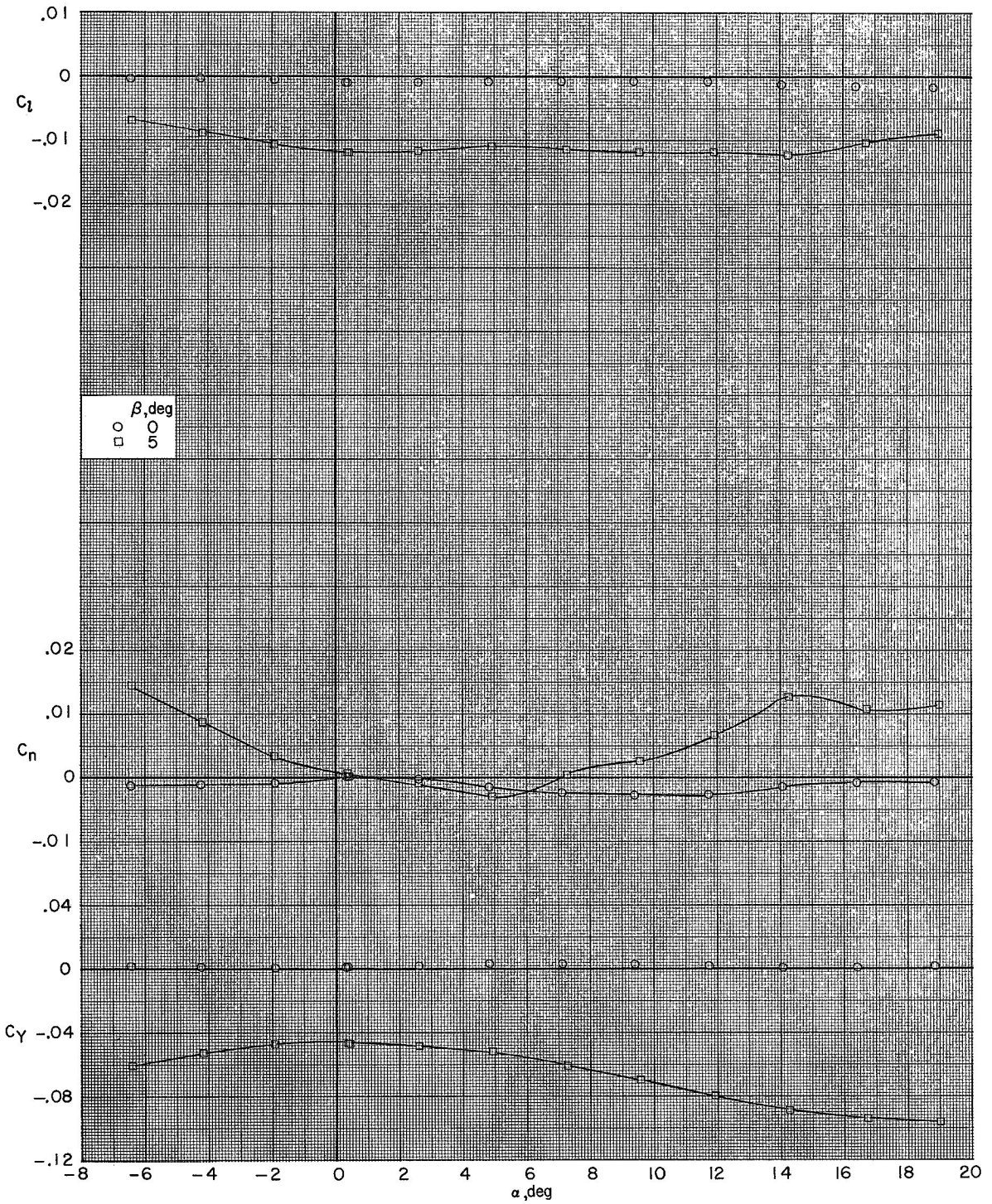

(d) M = 1.20.

Figure 12.- Concluded.

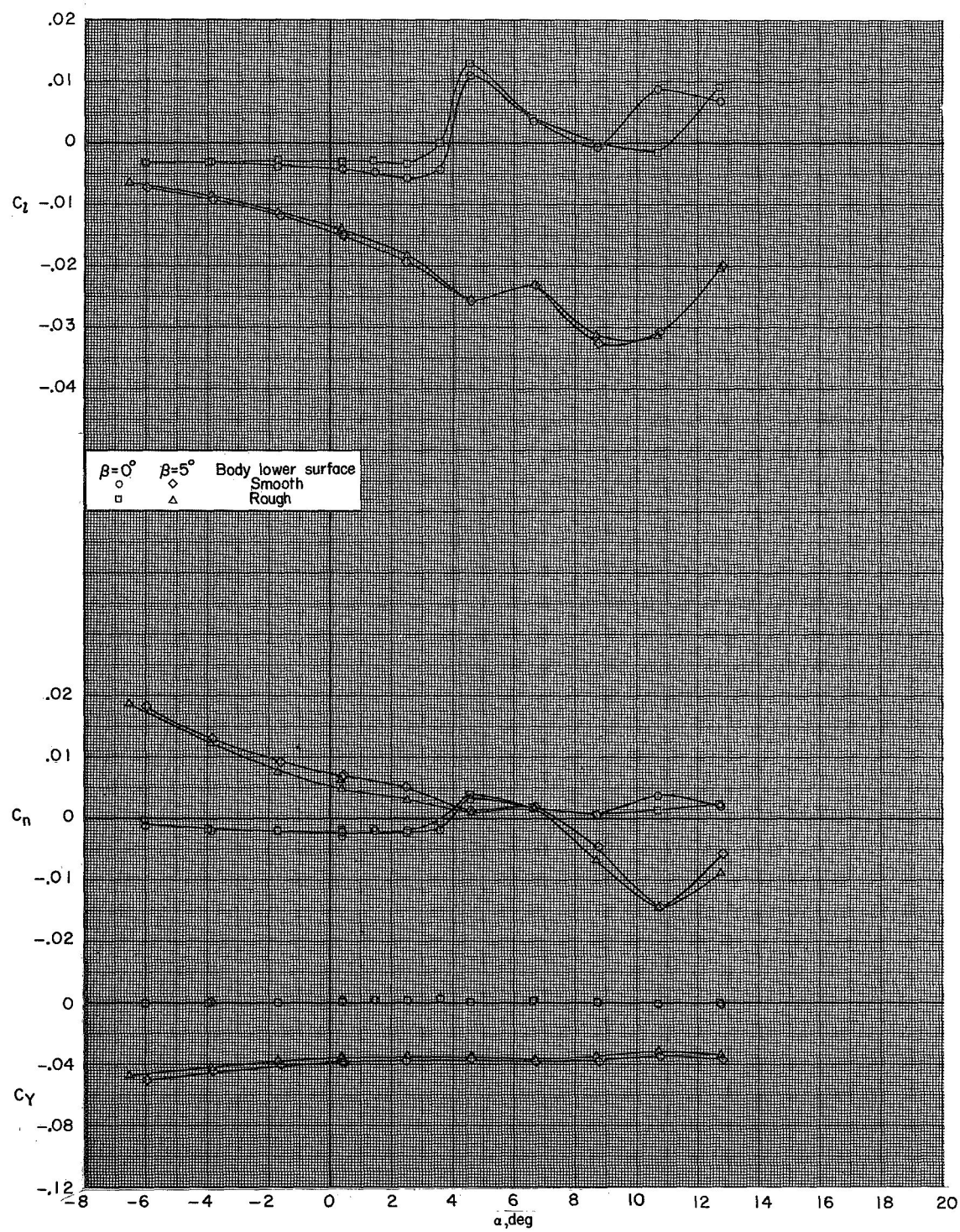

(a) M = 0.40.

Figure 13.- Effect of thermal-protection-system roughness on the lateral-directional aerodynamic characteristics of the model with wings deployed to $\Lambda = 20^0$. $\delta_{e,l} = 0^0$; $\delta_{e,u} = 0^0$.

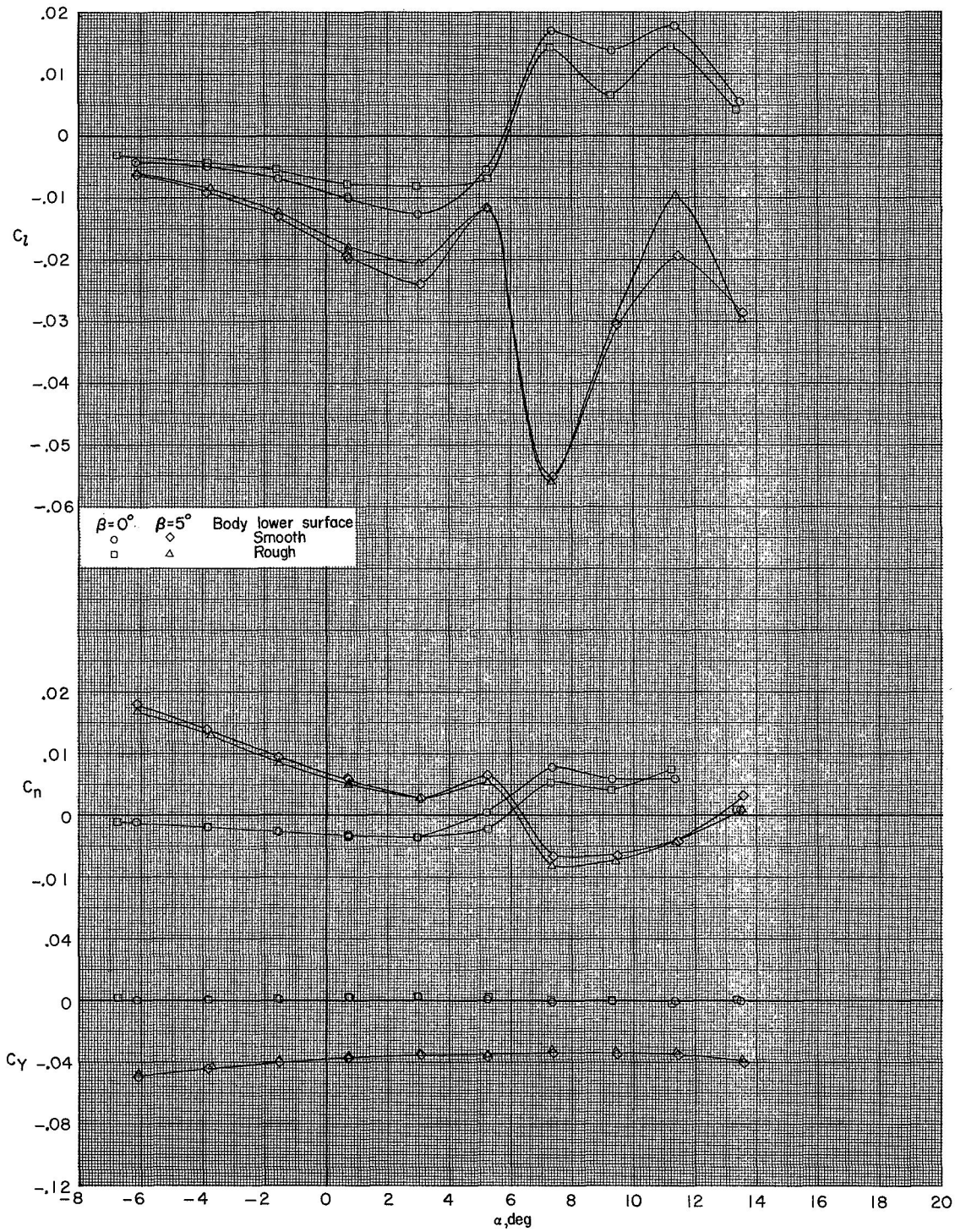

(b) M = 0.60.

Figure 13.- Continued.

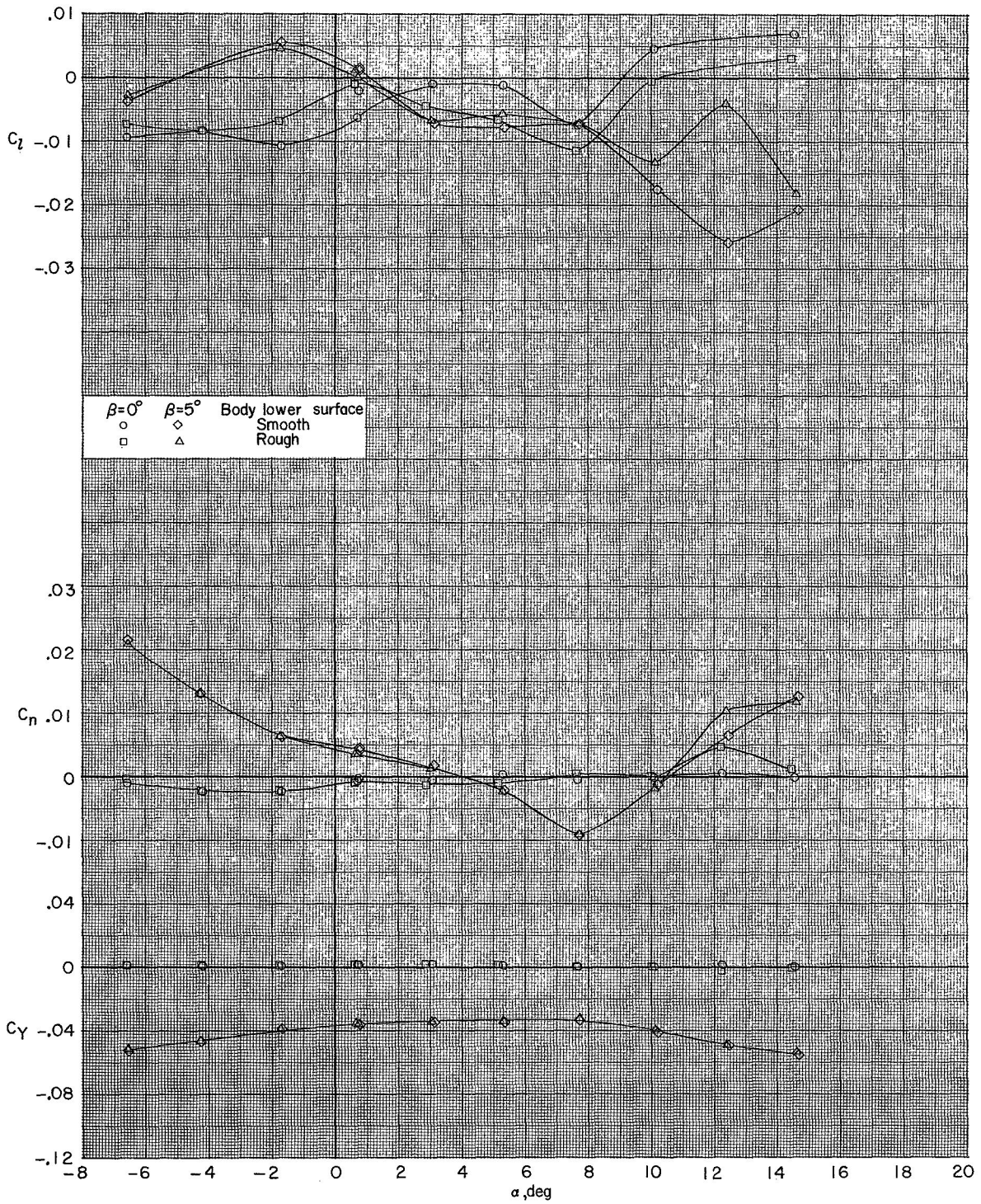

(c) M = 0.80.

Figure 13.- Continued.

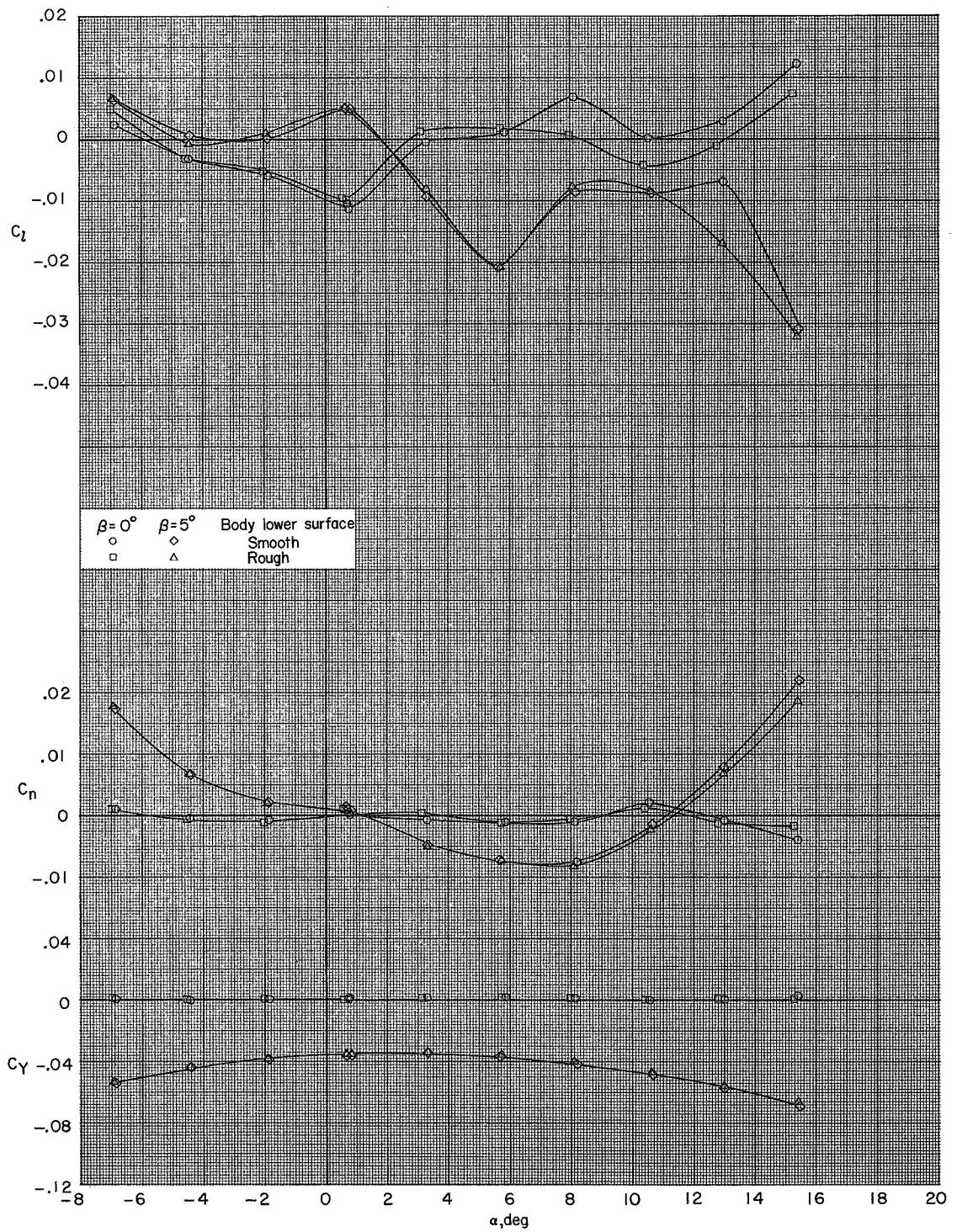

(d) M = 0.90.

Figure 13.- Concluded.

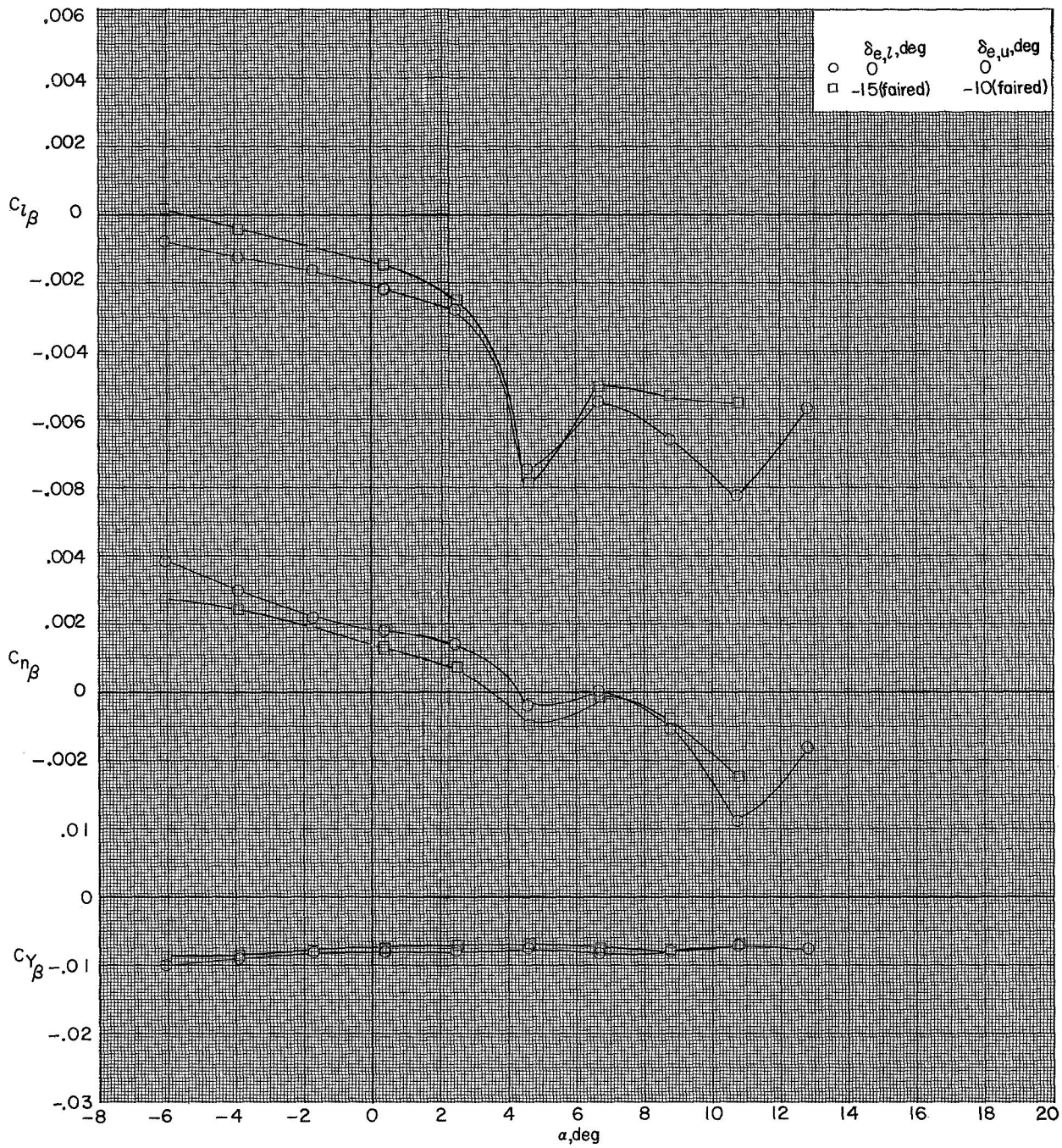

(a) M = 0.40.

Figure 14.- Lateral-directional stability parameters of the model with wings deployed to $\Lambda = 20^0$.

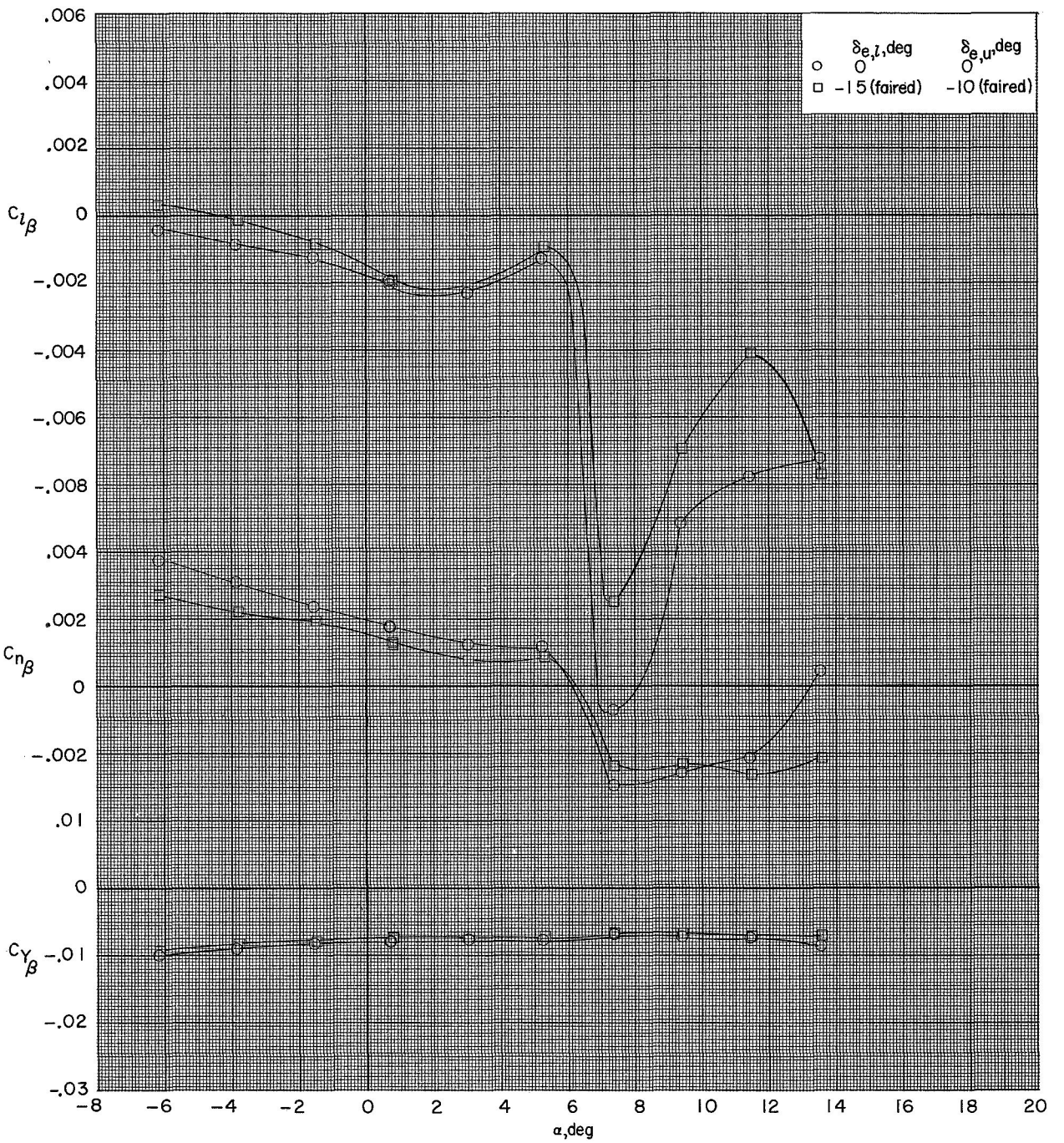

(b) M = 0.60.

Figure 14.- Continued.

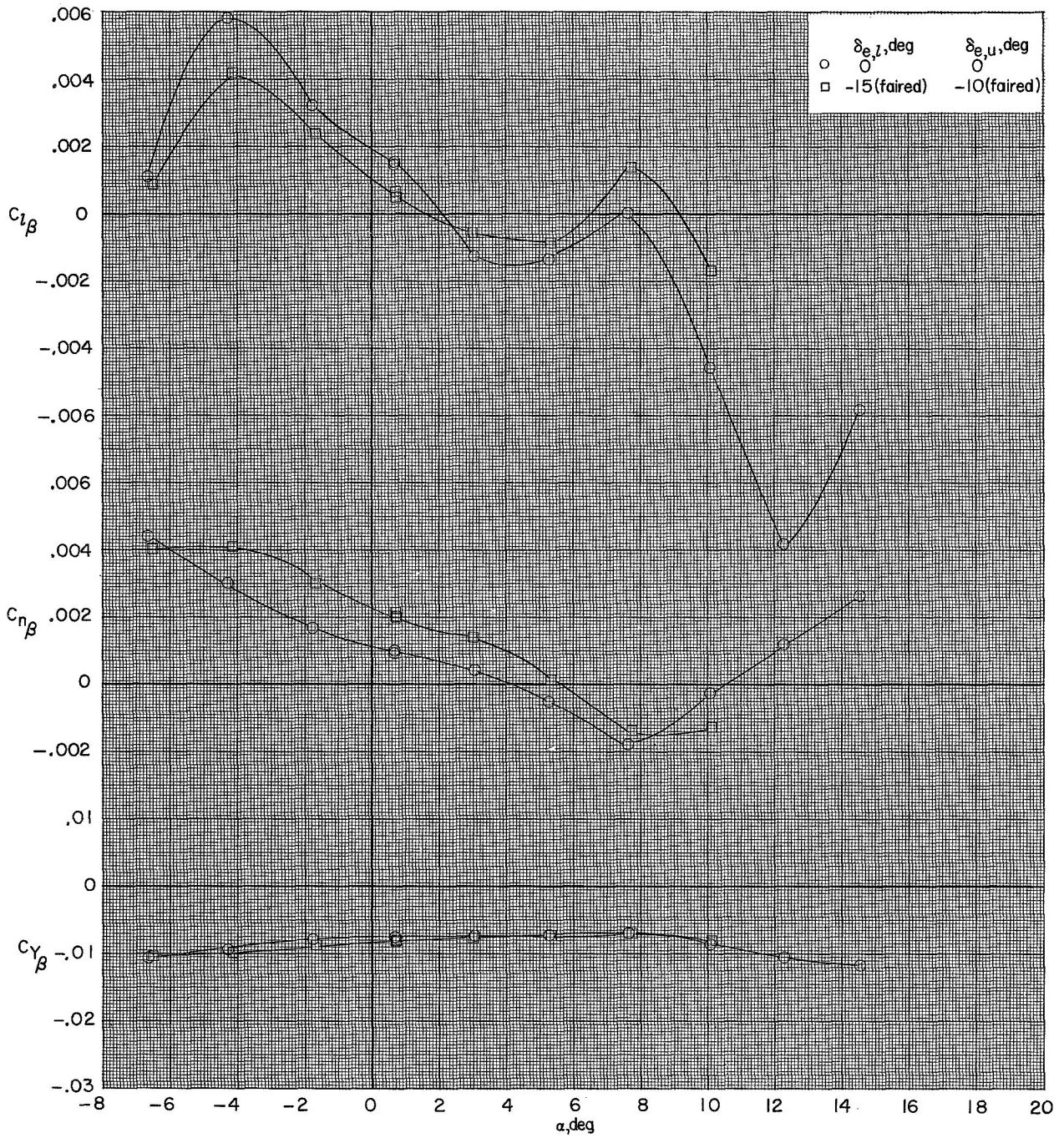

(c) M = 0.80.

Figure 14.- Continued.

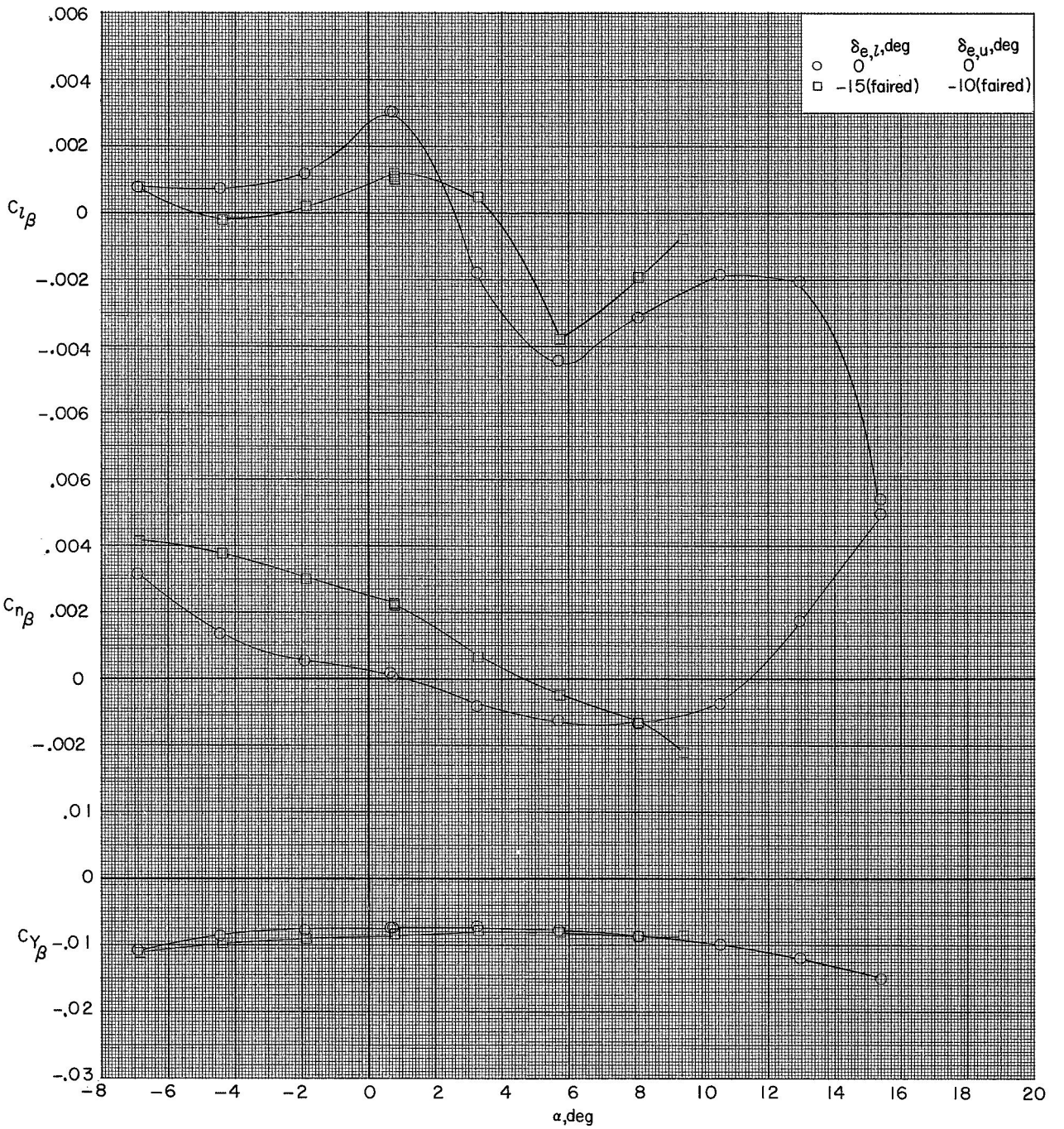

(d) M = 0.90.

Figure 14.- Concluded.

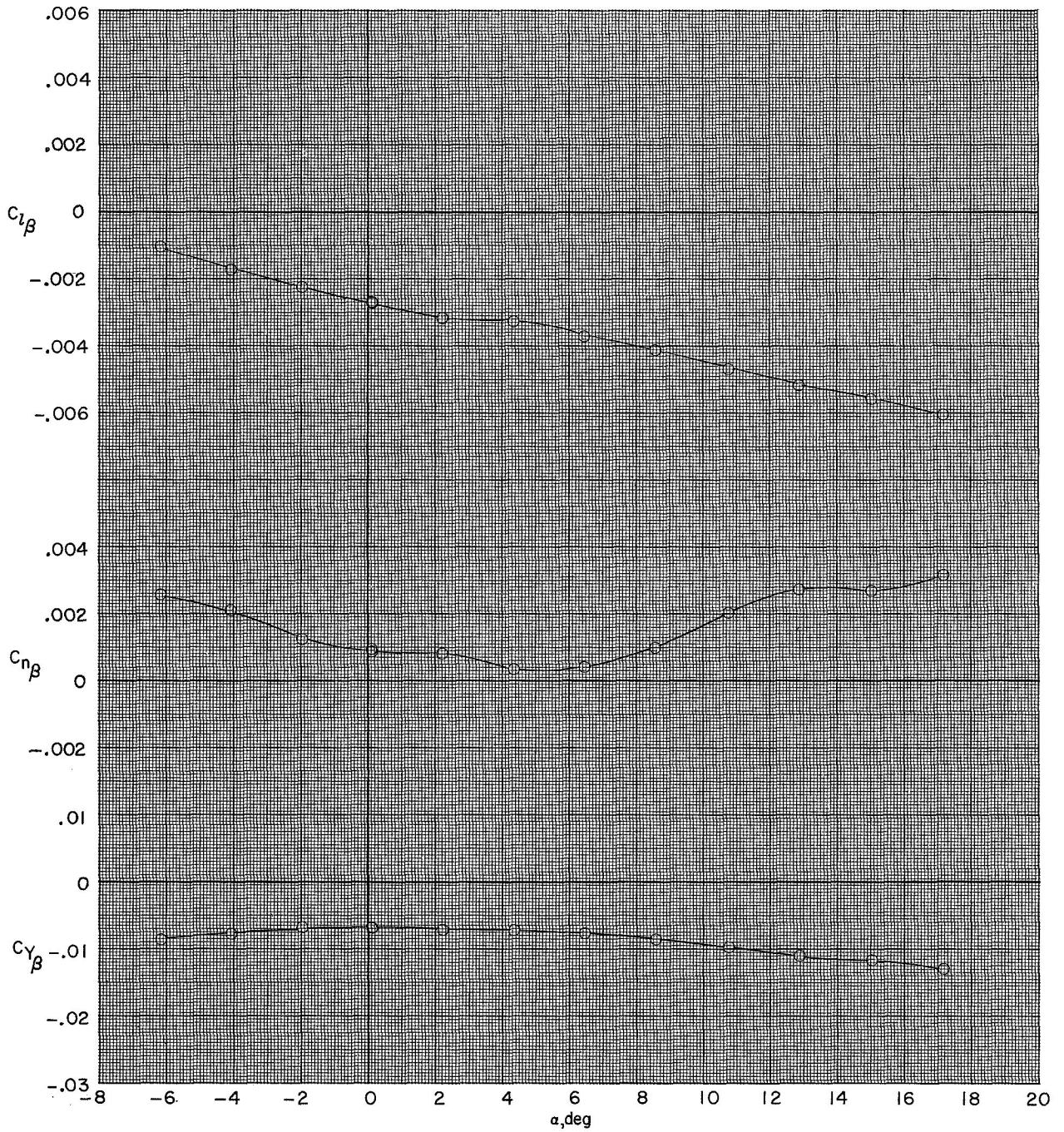

(a) M = 0.60.

Figure 15.- Lateral-directional stability parameters of the model with wings deployed to $\Lambda = 75^{o}$. $\delta_{e,l} = 0^{o}$; $\delta_{e,u} = 0^{o}$.

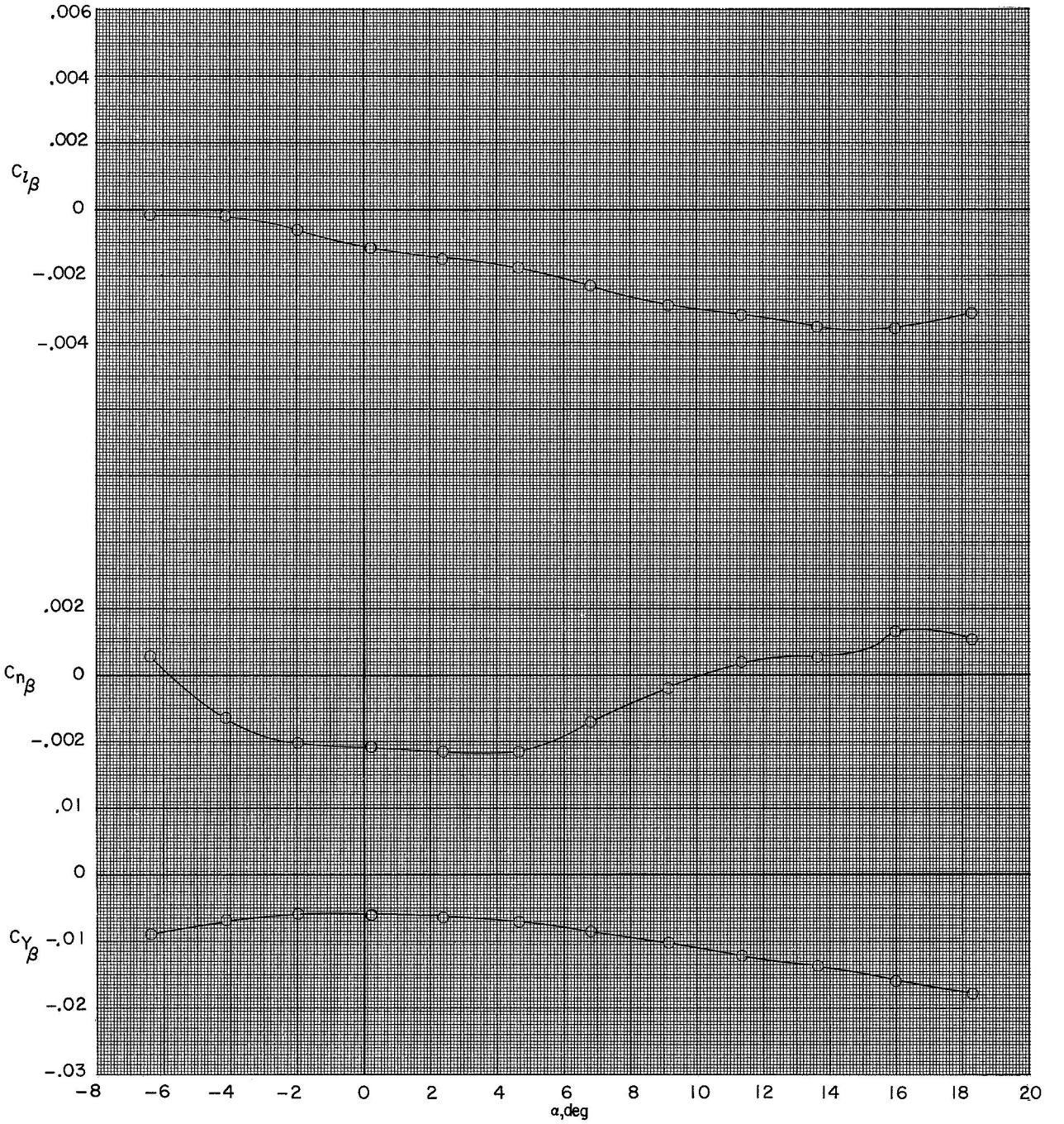

(b) M = 0.90.

Figure 15.- Continued.

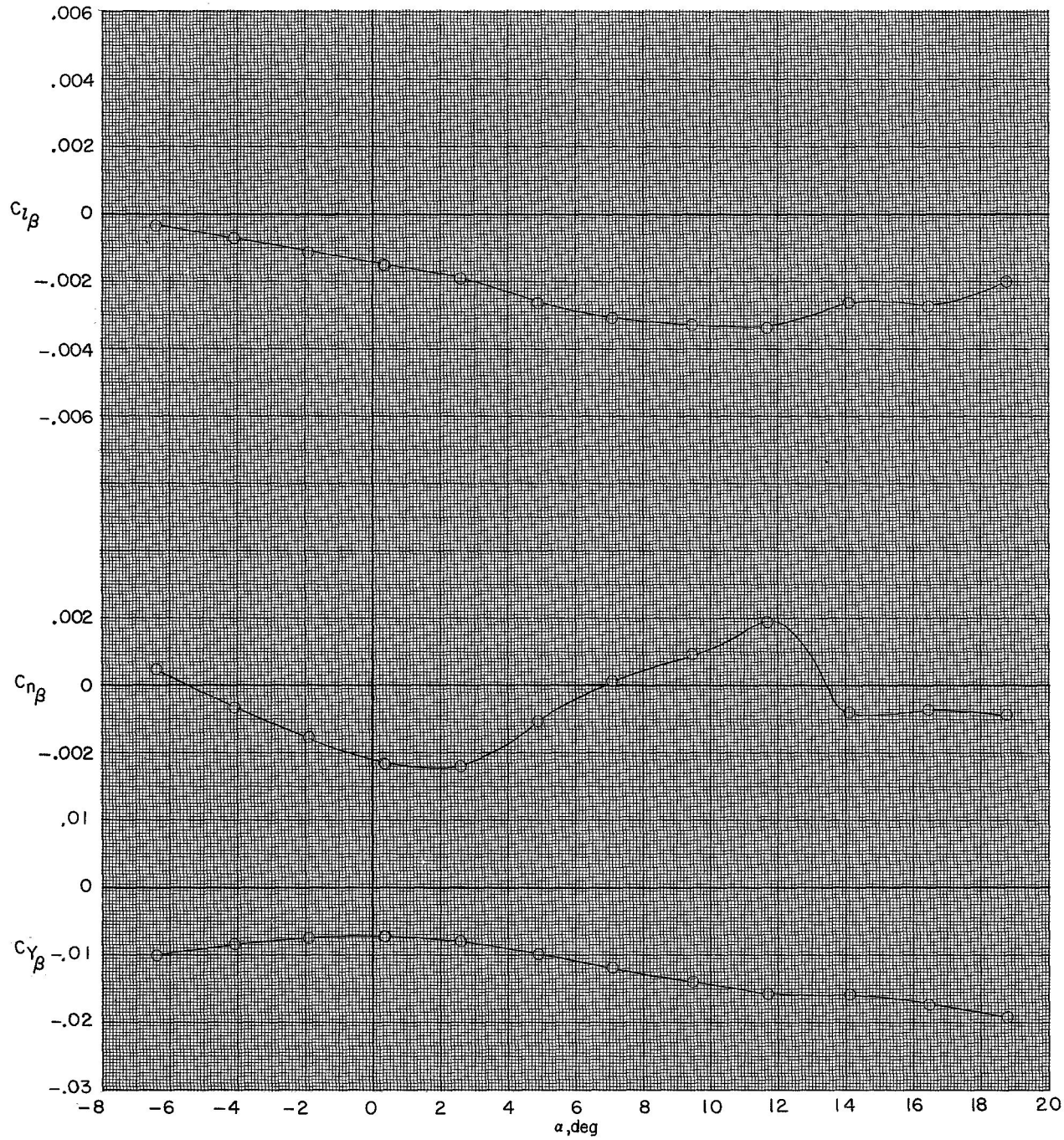

(c) M = 1.00.

Figure 15.- Continued.

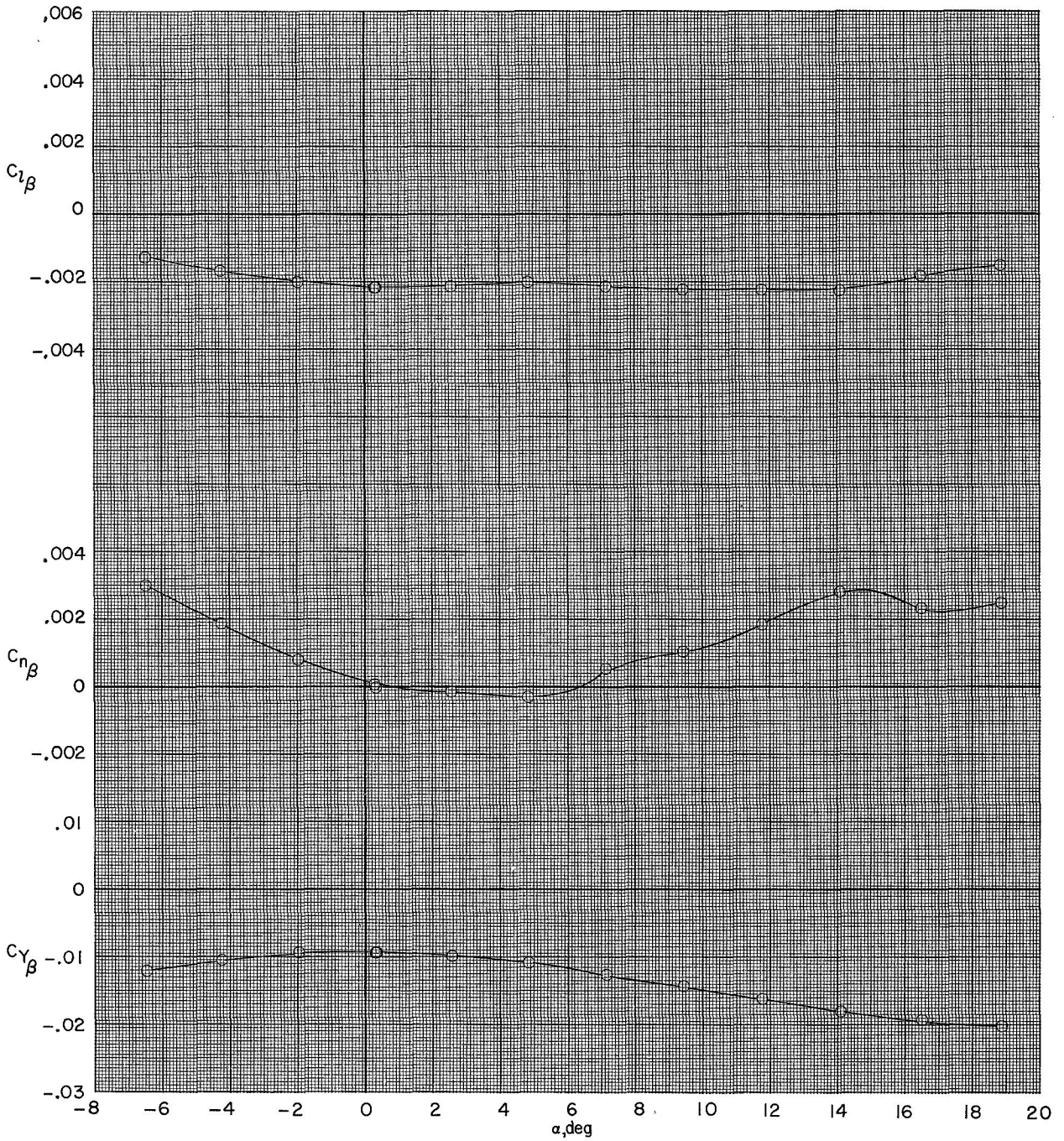

(d) M = 1.20.

Figure 15.- Concluded.

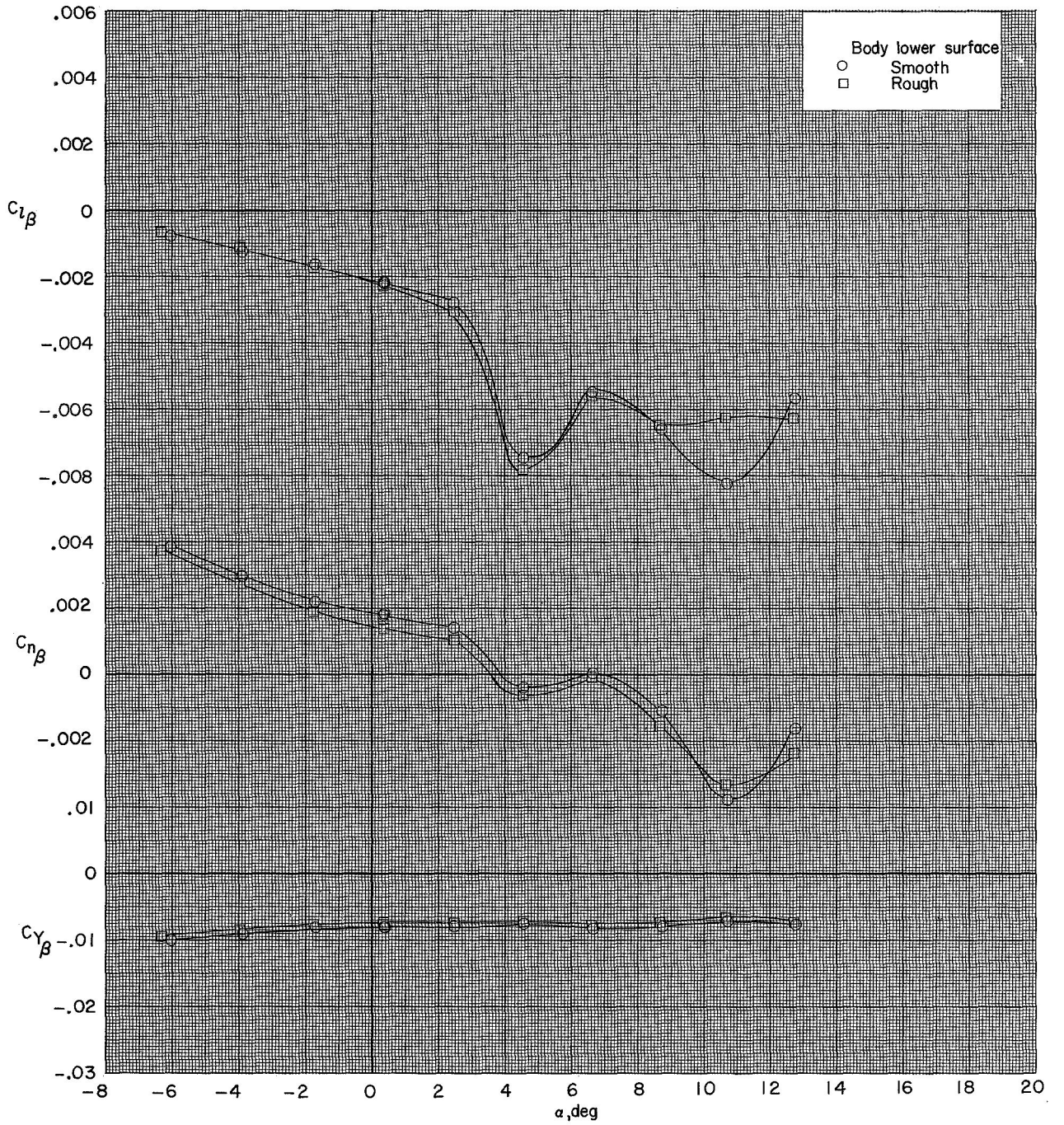

(a) M = 0.40.

Figure 16.- Effect of thermal-protection-system roughness on the lateral stability parameters of the model with wings deployed to $\Lambda = 20^0$. $\delta_{e,l} = 0^0$; $\delta_{e,u} = 0^0$.

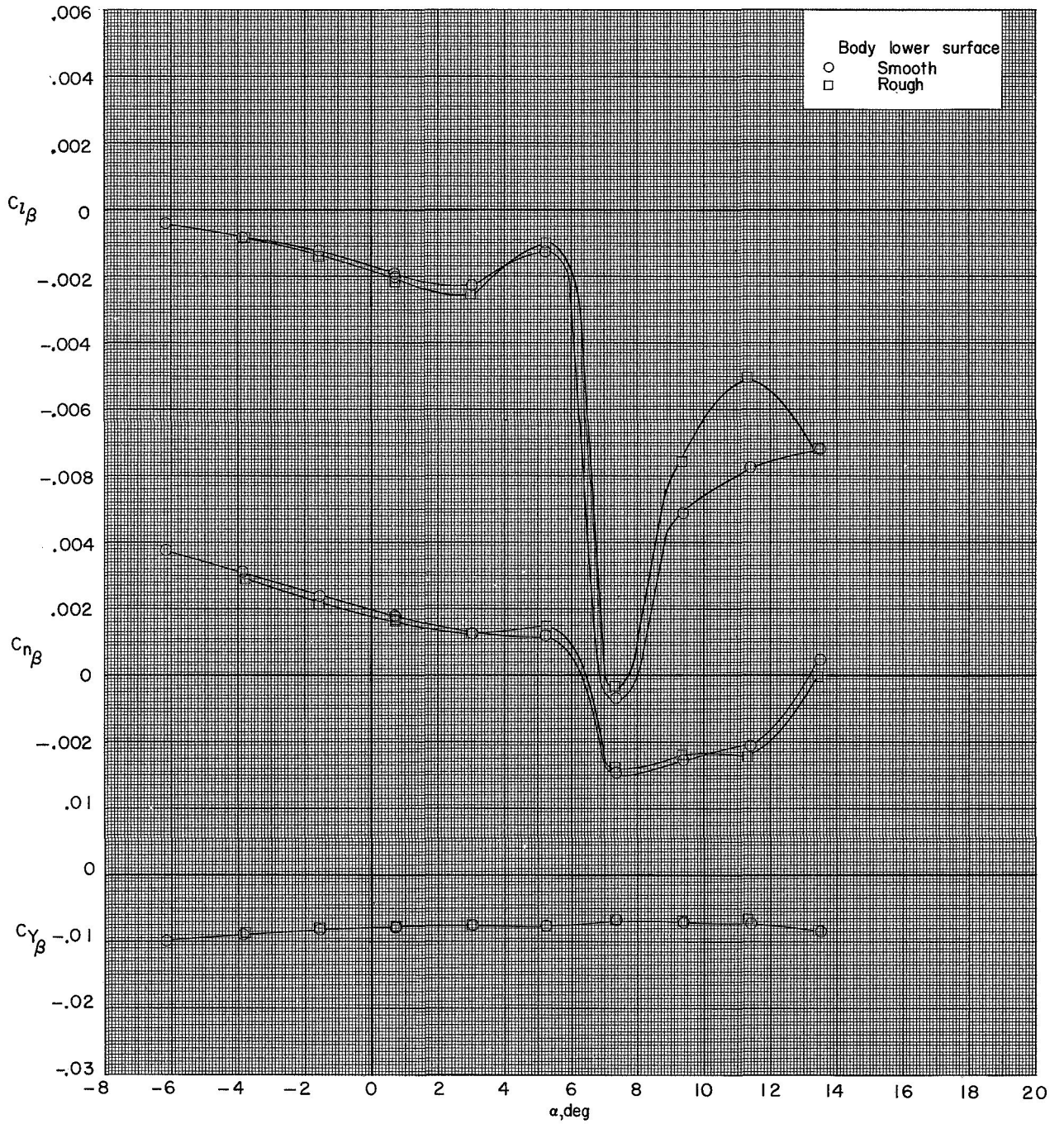

(b) M = 0.60.

Figure 16.- Continued.

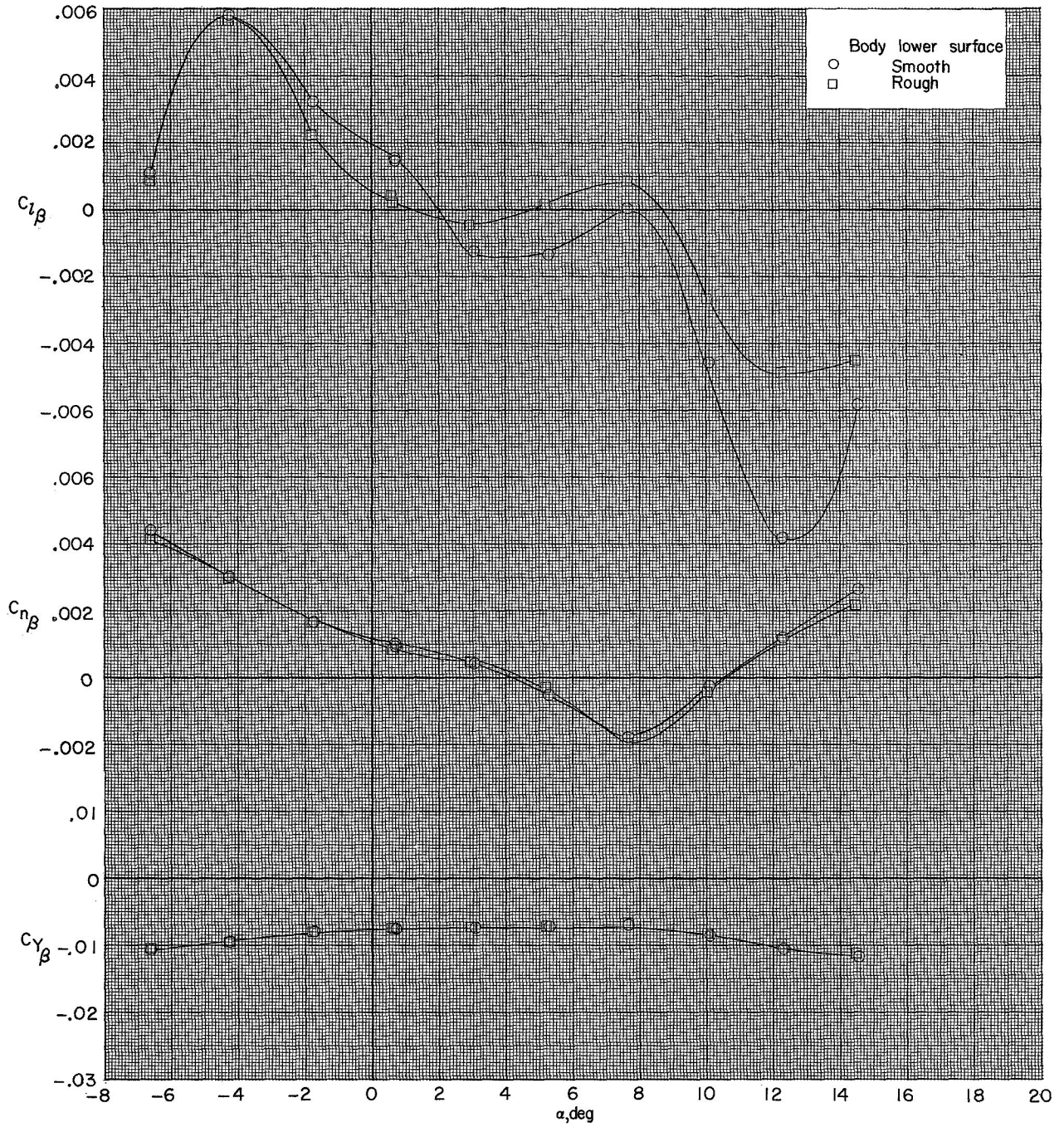

(c) M = 0.80.

Figure 16.- Continued.

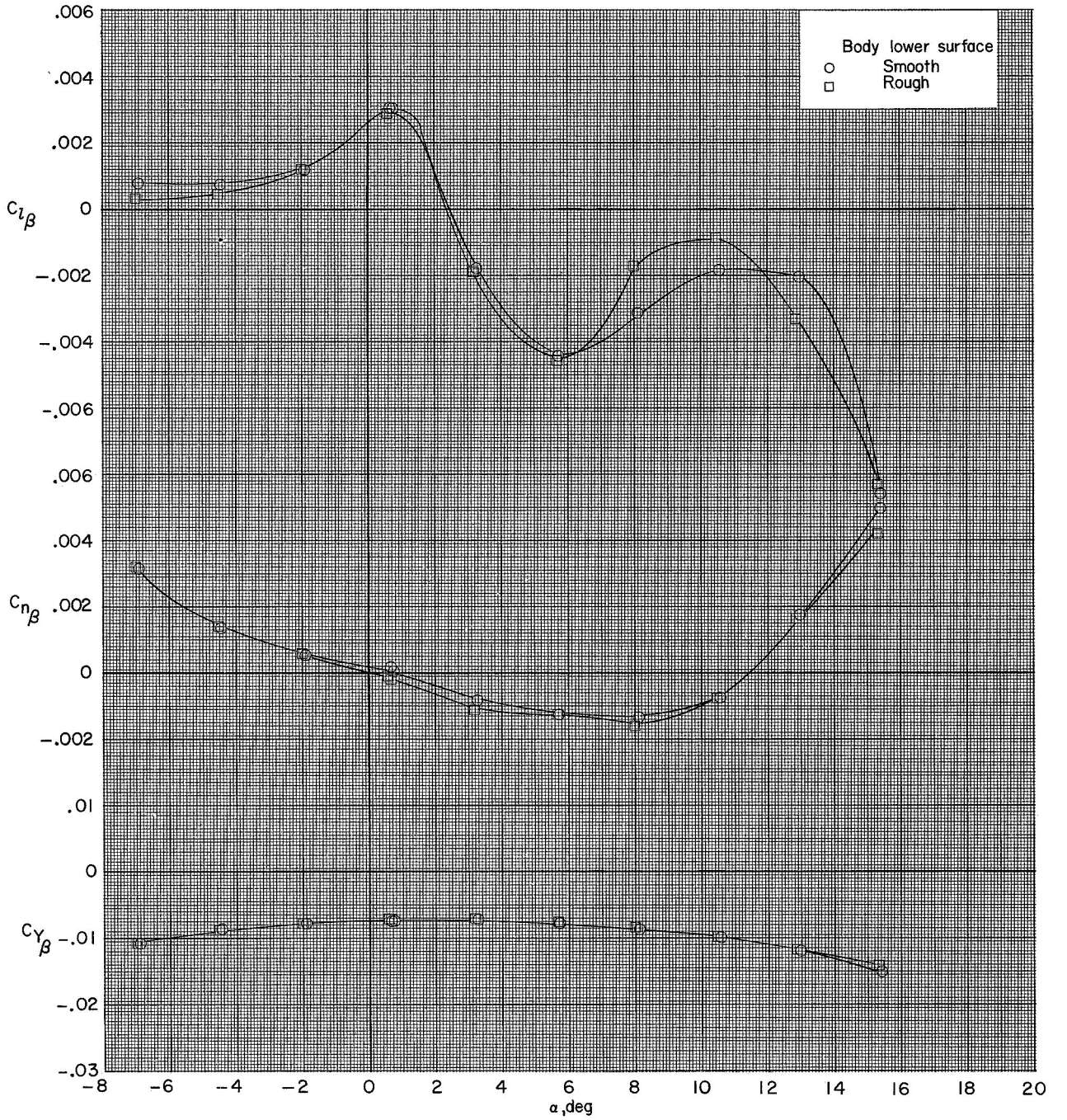

(d) M = 0.90.

Figure 16.- Concluded.

NATIONAL AERONAUTICS AND SPACE ADMINISTRATION
WASHINGTON, D.C. 20546

OFFICIAL BUSINESS

FIRST CLASS MAIL

POSTAGE AND FEES PA
NATIONAL AERONAUTICS
SPACE ADMINISTRATIO

POSTMASTER: If Undeliverable (Section
Postal Manual) Do Not Re

"The aeronautical and space activities of the United States shall be conducted so as to contribute . . . to the expansion of human knowledge of phenomena in the atmosphere and space. The Administration shall provide for the widest practicable and appropriate dissemination of information concerning its activities and the results thereof."

—NATIONAL AERONAUTICS AND SPACE ACT OF 1958

NASA SCIENTIFIC AND TECHNICAL PUBLICATIONS

TECHNICAL REPORTS: Scientific and technical information considered important, complete, and a lasting contribution to existing knowledge.

TECHNICAL NOTES: Information less broad in scope but nevertheless of importance as a contribution to existing knowledge.

TECHNICAL MEMORANDUMS: Information receiving limited distribution because of preliminary data, security classification, or other reasons.

CONTRACTOR REPORTS: Scientific and technical information generated under a NASA contract or grant and considered an important contribution to existing knowledge.

TECHNICAL TRANSLATIONS: Information published in a foreign language considered to merit NASA distribution in English.

SPECIAL PUBLICATIONS: Information derived from or of value to NASA activities. Publications include conference proceedings, monographs, data compilations, handbooks, sourcebooks, and special bibliographies.

TECHNOLOGY UTILIZATION PUBLICATIONS: Information on technology used by NASA that may be of particular interest in commercial and other non-aerospace applications. Publications include Tech Briefs, Technology Utilization Reports and Notes, and Technology Surveys.

Details on the availability of these publications may be obtained from:

SCIENTIFIC AND TECHNICAL INFORMATION DIVISION

NATIONAL AERONAUTICS AND SPACE ADMINISTRATION

Washington, D.C. 20546